In vivo characterization of an oncolytic virus for the treatment of pancreatic cancer

Von Divi-Sophie Sofiya Ba Trung

Inaugural-Dissertation zur Erlangung der Doktorwürde
der Tierärztlichen Fakultät der Ludwig-Maximilians-Universität
München

In vivo characterization of an oncolytic virus for the treatment of pancreatic cancer

von Divi-Sophie Sofiya Ba Trung

aus Versailles

München, 2024

Aus dem Zentrum für Klinische Tiermedizin der Tierärztlichen Fakultät

der Ludwig-Maximilians-Universität München

Lehrstuhl für Physiologie

Arbeit angefertigt unter der Leitung von

Univ.-Prof. Dr. Thomas W. Göbel

Angefertigt an der Klinik und Poliklinik für Innere Medizin II

Klinikum Rechts der Isar der Technischen Universität München

Mentor

PD Dr. rer.nat. Jennifer Altomonte

Gedruckt mit Genehmigung der Tierärztlichen Fakultät

der Ludwig-Maximilians-Universität München

Dekan:	Univ.-Prof. Dr. Reinhard K. Straubinger, Ph.D.
Berichterstatter:	Univ.-Prof. Dr. Thomas W. Göbel
Korreferent:	Univ.-Prof. Dr. Johannes Hirschberger

Tag der Promotion: 6. Juli 2024

À ma famille

I. TABLE OF CONTENTS

II. ABBREVIATIONS

%	Per cent
APC	Antigen-presenting cells
BET	Bromodomain and extraterminal domain
BRD	Bromodomain
CAF	Cancer associated-fibroblast
CCL5	CC-Chemokin-Ligand-5
CDK9	Cyclin-dependent kinase 9
CDKN2A	Cyclin-dependent kinase inhibitor 2A
DAMPs	Damage associated molecular patterns
DC	Dendritic cell
ECM	Extracellular matrix
EZH2	Enhancer of zeste2
FGF2	Fibroblast growth factor 2
HDAC	Histone deacetylase
HN	Hemagglutinin-neuraminidase
HPAI	High pathogenic avian influenza
HSV	Herpes simplex virus
i.p.	Intraperitoneal
i.v.	Intravenous

IFN	Interferon
IL	Interleukine
IP10	Interferon-gamma induced protein 10 kD
it.	intratumoural
KLRG1	Killer cell lectin-like receptor G1
KRAS	Kirsten rat sarcoma virus
LDLR	Low density lipoprotein receptor
LSEC	Liver sinusoidal endothelial cell
MDSC	Myeloid-derived suppressor cell
MHC	Major histocompatibility complex
mL	Milliliter
MMP8	Matrix metalloproteinase 8
MOI	Multiplicity of infection
NDV	Newcastle disease virus
NK cell	Natural killer cell
NKG2D	Natural killer group 2, member D
NKT	Natural killer T cell
OV	Oncolytic virus
PAMPs	Pathogen associated molecular patterns
PD-1	Programmed cell death-1

PDAC	Pancreatic adenocarcinoma
PD-L1	Programmed cell death 1 ligand 1
PPR	Pattern recognition receptors
p.o.	Per os
PRC2	Polycomb repressive complex 2
RIG-I	Retinoic acid inducible gene 1
RLN	Relaxin
RXFP1	Relaxin family peptide receptor 1
SHH	Sonic hedgehog
SMAD4	Mothers against decapentaplegic homolog 4
SPAM1	Sperm adhesion molecule 1
T-reg	Regulatory T-cell
TAA	Tumour associated antigen
TGF-β	Transforming growth factor-β
TLR	Toll-Like receptors
TME	Tumour microenvironment
TP53	Tumour suppressor protein 53
VSV	Vesiculostomatitis virus
µL	Microliter

III. LIST OF FIGURES

IV. LIST OF TABLES

1. INTRODUCTION

Pancreatic adenocarcinoma (PDAC) is one of the most aggressive cancers, and its diagnosis almost automatically implies a dramatically shortened life expectancy, classically of under 5 years[1] for the patients. This cancer tends to be discovered at an advanced stage at which surgery is no longer an option, and its resistance to available therapies, including radio- and chemotherapy, and highly metastatic phenotype, makes it a formidable opponent. Though some improvement has been achieved with combination therapies, there is still an urgent need for new approaches.

Immunotherapies have been a growing field of interest in cancer research. The principle is to educate the immune system to target exclusively cancer antigens, whilst sparing healthy cells. Oncolytic viruses work in this way, through their specific affinity for cancer cells, which they can infect and lyse while replicating, thereby releasing tumour antigens, turning immunologically cold tumours into hot ones[2]. Talimogene laherparepvec (T-VEC), a modified herpes simplex virus that is Food Drug Administration- and European Medicines Agency-approved for the treatment of nonresectable metastatic melanoma[3], is the best example of a successful, widely recognized oncolytic virus therapy. A novel hybrid virus, VSV-NDV, generated in our lab has been shown to be able to selectively infect cancerous cells, reprogram the immune-suppressive tumour microenvironment, and improve survival in an orthotopic liver cancer model. The was therefore speculated that it could represent an interesting candidate for investigation in other solid cancer types, including PDAC.

As PDAC research advances, light is being shed on the intricate role of the tumour microenvironment in the development and resistance mechanisms of this disease. Cancer-associated fibroblasts (CAFs) constitute one of its most important cell populations and are essential in regulating the tumour dynamics. The extracellular matrix of the tumour, directly supported by secreted factors from CAFs, has now become an important therapeutic target.

Due to the extreme complexity of PDAC, it is likely that a combination therapy, rationally designed to target multiple aspects of the tumour and tumour microenvironment (TME), could offer the most promising potential to address this aggressive and challenging malignancy. Various small molecule inhibitors, amongst which epigenetic inhibitors, are currently under examination as potential adjuvant therapies, as the numerous registered clinical trials[4] prove. Among them, bromodomain inhibitors sparked the interest of our group for its potential ability to synergize with VSV-NDV.

In this work, the efficacy of oncolytic VSV-NDV was investigated in pre-clinical *5.1.1.1* and *in vivo* studies for its ability to mediate direct tumour cell and CAF killing, as well as to modulate the TME and mediate systemic antitumour immune cell responses. Furthermore, the potential of VSV-NDV as a vector to express extracellular matrix degrading proteins for targeting the PDAC stroma was explored, as well as the potential synergies figure 13of oncolytic virotherapy with bromodomain inhibitors.

2. LITERATURE REVIEW

2.1. PANCREATIC ADENOCARCINOMA

2.1.1. The cancer

Pancreatic cancer is the 12th most common cancer worldwide and was the 7th cause of cancer-related death in 2020, according to the international agency for research on cancer (GLOBOCAN project). Pancreatic ductal adenocarcinoma (PDAC) represents 90 % of all pancreatic malignancies with 24% of the patients surviving over one year and only 9% for five years post-diagnosis[5]. Its incidence continues to rise worldwide, especially in highly developed countries[1,6], and it is expected to become the second leading cause of cancer related death in the United States of America by 2030[7].

Established risk factors for PDAC include aging, obesity and diabetes type 2, smoking, alcoholism and family history with susceptibility to certain gene mutations[89]. Indeed, classical key driver genes have been identified to facilitate the development of PDAC tumours, namely the oncogenic KRAS (Kirsten rat sarcoma virus) mutation with a 77% occurrence, and many loss-of-function mutations such as CDKN2A (cyclin-dependent kinase inhibitor 2A) with 63%, TP53 (tumour suppressor protein 53) with 22%, SMAD4 (Mothers against decapentaplegic homolog 4) with 16% for instance[8,10].

The biological hallmarks of PDAC tumours have been identified as follows[8]:

- Tumour plasticity and heterogeneity:
- Desmoplastic, hypoxic, immunosuppressive microenvironment
- Metastasis formation
- Therapy resistance.

Various treatment options are currently available for PDAC patients, depending on the disease stage at the time of diagnosis: surgical resection, chemotherapy, radiotherapy and palliative care[11]. Unfortunately, most patients are presented with

metastases or very advanced disease, preventing them from undergoing surgery, and out of the operated patients, only 20% survive after five years[12]. Thus, most patients are offered chemotherapy, with Gemcitabine often in combination with Nab-Paclitaxel, which was considered standard of care for decades[13], despite progressive drug-resistance. Another widely prescribed therapy is the multi-drug FOLFIRINOX regimen, with a combination of fluorouracil, leucovorin, irinotecan and oxaliplatin, which was recently deemed more efficient than Gemcitabine with Nab-Paclitaxel, with a survival prolongation by two months and fewer post-treatment hospitalizations[14]. For patients with non-metastatic disease, adjuvant radiotherapy in combination with surgery or chemotherapy (to sensitize radioresistant tumours[8,15]) can be strongly recommended[8,16], depending on the stage.

In the end, therapeutic success remains limited, with multiple evolving resistances encountered during treatment[15], due to the specific challenges of the PDAC tumour microenvironment.

2.1.2. The tumour microenvironment

Tumours have been described as “wounds that do not heal”[17] and the development of the tumour microenvironment (TME) bears many similarities to the healing process. In fact, wound healing stimulates the recruitment and activation of fibroblasts, which start producing an extracellular matrix (ECM) with excessive amounts of collagens, fibronectins, laminins and hyaluronan. There is also immune cell infiltration, new vascularization, and local cell plasticity[18,19] , similarly to tumours. In the case of PDAC, though, the TME can represent up to 90 % of the tumour volume[20] and is known to build a desmoplastic, mechanical barrier around the tumour cells, preventing sufficient vascularization, thus limiting access for drugs or efficient immune infiltration[21]. It also shapes a tolerant and immunosuppressive milieu by recruiting myeloid-derived suppressor cells, regulatory T-cells, tumour-associated macrophages, and only few, dysfunctional Natural Killer (NK) and T-cells[22]. Due to these features, PDAC tumours are known

as immunologically “cold” lesions. Figure 1 proposes a representation of normal pancreatic tissue compared to its altered cancerous version.

The stroma comprises different cancer-associated fibroblast (CAFs) subpopulations, mostly derived from pancreatic stellate cells, reprogrammed tissue resident fibroblasts or tumour infiltrating mesenchymal cells[23]. It has been demonstrated that CAFs can act either as tumour-promoters or tumour-suppressors and evolve together with cancer cells, adapting their behaviour through paracrine signalling[23]. Hence, various therapies target the ECM and the CAFs. One such strategy involves depletion of the stroma: with Losartan, an antifibrotic leading to the decompression of the blood vessels and improved patient survival[24] ; or PEGylated recombinant human hyaluronidase PH20 in combination with the classical nab-paclitaxel and gemcitabine (phase III trial)[25], or modified FOLFIRINOX (phase IB/II)[26]. The phase III trial did not improve overall survival, but the combination with modified FOLFIRINOX enabled a reduction of the treatment time. Another approach consists in reprogramming the tumour promoting CAFs into a quiescent state with calcipotriol (a vitamin D3 analog) and gemcitabine for instance, which successfully extended the life span of KPC mice, whilst impairing the efficiency of their cytotoxic T-cells[27]. The last strategy is to impede the signalling pathways in CAFs: for example, a CXCL12 inhibitor managed to slow down tumour growth and improved the infiltration of cytotoxic T-cells[28] ; transforming growth factor-β (TGF-β) is also targeted in combination with nab-paclitaxel and gemcitabine in an ongoing phase II trial[29].

In the end, despite all the current therapeutic approaches, the risk of recurrences remains very high, which highlights the need for new treatment options[30].

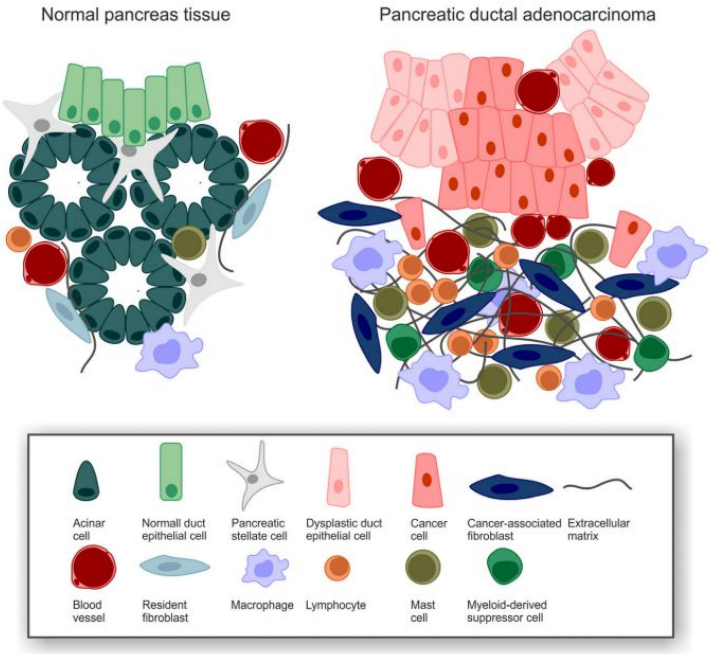

Figure 1: Pancreatic ductal adenocarcinoma with desmoplasia. The stroma is mostly composed of CAFs, immune cells and rich extracellular matrix. From *Orth M. et al, 2019*.

2.2. IMMUNO-ONCOLOGY

2.2.1. The immune system in general

To introduce the immunogenic properties of oncolytic viruses, some essential aspects of the immune system are reviewed here.

The immune system has 3 functions: protect the organism against foreign threats, clear damaged or dead tissue to promote a healthy milieu for healing, recognize and neutralize cancerous cells. The identification of non-self-proteins is carried out by to pattern recognition receptors (PPRs) localized on immune cells, such as toll-like receptors (TLRs), RIG-1 receptors, or C-lectin receptors, which bind to typical damage- or pathogen associated molecular patterns (DAMPS or PAMPS) expressed only by microbes[31]. The immune system articulates 2 arms, the innate and adaptive immune systems, working together to fulfil these tasks.

In case of aggression or injury, the innate or inborn immune system provides the fastest response. The first line of defense involves the physical barriers: the skin and mucous membranes. Second, if a pathogen crosses through, its spread will be hindered by macrophages in tissues, which will secrete cytokines (IL-18) and present antigens to the adaptive immune system, as well as attract the neutrophils to help with the phagocytosis. Other essential early phase agents are innate lymphoid cells, the natural killer cells (NKs), specialised in directly destroying membranes of virally infected or cancerous cells through the release of cytotoxic perforin and granzyme, which they recognize because of their low-levels of MHC-I receptors. They can also kill cells indirectly by producing interferon (IFN)-γ, tumour necrosis factor (TNF)-α or by stimulating the macrophages. IL-12 and IL-15 from dendritic cells (DCs) or monocytes also contribute to their activation[2]. Non-cellular factors from the innate immune system include interferons (IFN), produced by cells infected with RNA viruses, to prevent the infection of their neighbouring uninfected cells. Various cytokines are secreted by innate myeloid immune cells (neutrophils, macrophages and dendritic cells) to orchestrate the communication between all immune cells, and for the stimulation of the adaptive immune system[32].

The adaptive or acquired immune system include cell mediated and humoral components. The humoral, or antibody mediated immunity, rests on lymphocytes targeting specific tumour antigens (molecules or structures able to induce an adaptive immune reaction). Lymphocytes are divided into two families, depending on their prime maturation site during childhood: either the thymus (T-Lymphocytes), or the bone marrow (B-Lymphocytes). After being generated by bone-marrow stem cells, they migrate to mature and divide in secondary or peripheral lymphoid organs, such as the lymph nodes and the spleen, where they get activated by antigens (clonal selection). Mature lymphocytes are then released into the blood stream and circulate between lymphoid organs, to heighten their chance of encountering their specific antigen. B-Lymphocytes differentiate mostly into plasma cells for antibody protein secretion; the rest become memory cells, able to remain dormant for years until the next encounter with the specific pathogen. The antibodies' role is to prevent antigens from entering into the hosts' cells by

binding with them, to create antibody-antigen complexes for phagocytosis, and to stimulate the innate immune system.

The cell mediated adaptive immunity focuses on the T-cells and is of utmost importance for combatting viral infections, cancerous cells or intracellular pathogens. In contrast to the humoral response, cytotoxic T-cells (CD8+) need direct contact with their target. T-cell recognition of its target is dependent on antigen presentation by MHC-I and MHC-II molecules. Indeed, viruses manipulate the host's cell machinery to sustain their replication, potentially leading to the cell's death upon release of their progeny. The infected cells will then express some viral proteins, bound to their MHC-I complex. Once T-cells bind to the antigen, they release of perforin and granzyme to damage the target cell membrane and can also induce apoptosis and stimulate further activation by secreting IFN-γ, TNF-α and IL-2[33]. On the other hand, helper T-cells (CD4+) take mostly a regulatory function: only antigen presentation via MHC-II cells (macrophages, B-lymphocytes and especially dendritic cells) can trigger them to produce cytokines such as IFN-γ, which encourages the priming and stimulation of further humoral cells.

2.2.2. Immune functions of the spleen and the liver

The spleen carries out multiple functions, such as haematopoiesis, red blood cell clearance and the tasks of a secondary lymphoid organ. All cells enter via the blood stream, and, as explained by *Louis S. et al, 2019*[34], it is the place where antigen-presenting cells (APC) are most likely to meet with naïve lymphocytes. Roughly, the architecture of the spleen encompasses the white and red pulp, separated by the marginal zone. The connections between the pulps are named bridging channels.

In the red pulp, the spleen maintains and controls its red blood cell population and houses resident innate cells, such as NKs, neutrophils, dendritic cells, monocytes and macrophages. The white pulp is the space where naïve and memory T-cells can meet with the APCs, initiating the adaptive immune response. However, the immune effector function and antibody production happens in the red pulp, before

release into the blood stream. The spleen also hosts a specific subset of dendritic cells, the plasmacytoid DCs, able to recognize viruses. This leads in particular to massive secretion of IFN-1 and IL-12 and -18, which enhance the antiviral immune response, activate NK cells and promote effector CD8+ T cells and the differentiation of CD4+ T cells into T-helper 1 cells [35].

The liver is a major organ, characterized by its unique blood supply: on the one hand, fresh blood from the hepatic artery accounts for about 25%, on the other hand, blood from the portal vein, coming from the abdominal organs, provides around 75%. The liver is responsible for various tasks, such as the metabolism of sugar, proteins and fats, the neutralization of toxins, the storage of vitamins, and the synthesis of blood clotting factors for instance. Because portal vein blood isn't filtered by the spleen or lymph nodes, the liver also has an immunosurveillance function: indeed, it should be able to tolerate proteins derived from the microbiota or regular food intake, but also to recognize and neutralize pathogens. Immunosurveillance is facilitated by the slower blood flow in its core, which allows for maximum contact between pathogens and immune cells[36]. As usual, the immune functions of the liver can be divided into the innate and adaptive response.

As reviewed by Kubes et al, 2018[37], the innate immunity of the liver relies on many mechanisms and cell types. The Kupffer cells (resident macrophages) have an antigen-presenting function, can activate T-cells, and phagocyte activated, senescent neutrophils. The liver hosts the most important population of NK cells in the body[38,39] . These are important for cytokine secretion and targeted killing of cells that do not express normal self-molecules, like cells hosting viruses, or tumour cells. Invariant NK-T cells, with a CD4+ CD8+ profile (also present in the spleen and lungs), are involved in most of the immune responses in the liver, under a Th1 phenotype. These cells have a strong effector potential and can secrete IFN-γ. Classically as well, the recruitment of neutrophils, monocytes, T-helper cells of type 1 and 2, but also the regulation of inflammation by limiting the secretions complete the immune answer.

The balance between immune activation and immune tolerance is essential within the liver, as it should differentiate between pathogen-derived antigens and harmless proteins. Hence, the "default setting" in the liver is set on immunotolerance, or immune "hypo-responsiveness". As such, liver sinusoidal endothelial cells (LSECs) assume an APC function, activating CD8+ and CD4+ cells, while expressing PD-L1 and IL-10 at the same time: in the end, these effector cells can proliferate but not directly kill the cells within the liver[40–42]. Along similar mechanisms, the myeloid and plasmacytoid dendritic cells (pDCs) of the liver are less efficient at priming than in other tissues, and the pDCs also constitutively express PD-L1[37,43,44]. In contrast, other inflammatory cytokines can modulate the cells towards a more responsive state if required, such as the IFN-γ from CD11+ NK1.1+ DCs[45]. Hepatocytes also assume an antigen-presenting function with MHC-I and II complexes.

2.2.3. The immune response to cancer and viruses

As explained before, the immune system defence is primarily based on the distinction between self and non-self antigens. However, tumours are not foreign and can be defined as a "proliferation of cells that have managed to escape endogenous mecanisms"[46] through multiple genetic alterations and the loss of regulatory functions.

Many strategies enable immune evasion for cancer cells. Amongst others, there is the immunoediting strategy. In solid tumours especially, the high rate of mutations produces numerous variants, some of which ultimately survive and avoid detection thanks to irregular signalling[47]. Additionally, the abundance of neoantigens can exhaust the immune response. Also, the TME plays a decisive role in the shaping of immune evasion. Not only does the TME constitute a physical barrier protecting the tumour from the immune system, it also hosts more than 50% of non-neoplastic cells (hence not targeted by the immune system) involved in signalling, the secretion of ECM modelling enzymes, or the production of soluble factors and vesicles, which support tumour growth and metastasis[48]. Typically, expression of

PD-L1 in the TME acts as an "immunostat" by driving the down-modulation of T cells[49].

Immunosuppression has a protective function for the body, as it limits self-harming through excessive defence (typically in the liver). All immune responses rely on an interplay between (co-)stimulatory and inhibitory signals. The TME has a disrupted balance in these signals in order to promote further tumour growth. Classically, it uses cytokines like TGF-β or IL-10, attracts suppressive cells such as regulatory T cells (Treg), or myeloid-derived suppressor cells (MDSCs) and activates immune checkpoints[50] (such as PD-L1 or anti-CTLA4). The hypoxic TME also creates poor conditions for the high metabolism of cytotoxic T cells, altering their performance[51].

Finally, further mistakes may occur in the cancer immunity cycle, impairing its response. The tumour antigens or tumour associated antigens may not be recognized by the immune system if the genes expressed by the cells resemble silenced genes from the embryonal development phase. The immune environment can upregulate the T reg cell activity, or the immune infiltration of the tumour is limited by the vascularization in the case of desmoplastic PDAC, the microenvironment promotes a a non-inflammatory state, non-supportive of the diapedesis through cytokines and chemotractants.

The immune mechanisms awakened by OVs strongly resemble those used against cancer. Indeed, when a virus enters a body, it infects cells according to its tropism. The viruses are then identified by the PRR on innate cells: the free circulating virions are phagocytosed and neutralized, while some viruses manage to enter cells, where they can hide more easily, manipulating their MHC-I expression. IFN-I signalling is initiated, although these pathways are often disrupted in cancer, especially in KRAS-driven cancers[52], giving the virus more time to spread at first. Then, the cells of the adaptive immune system learn to remember and target the viral antigens, which is called immune interference. On the one hand, the immune reaction to the virus when it infects cancerous cells is positive, as it releases tumour antigens, mediates inflammation, and triggers adaptive anti-tumour immunity. On

the other hand, an early viral clearance impedes the efficiency of posterior administrations[53]. A way around this obstacle is the use of OVs primarily unknown to the host for treatments, which is why OVs derived from animal viral pathogens are ideal due to the lack of pre-existing immunity in humans.

2.2.4. Relevant markers for flow-cytometry analysis

In order to analyse the mice immune answer to the treatment during our kinetics experiment, flow cytometry analysis was used on the extracted and prepared organs, to observe which cell populations were present at the different time points of the kinetics experiments. To facilitate the analysis of the results (see chapter 4.3.9.), the functions of the markers used in the various organ panels are revised below.

CD69 is upregulated in T-cells activated by a dendritic cell: this in turn downregulates the expression of S1PR1, which enables the T-cell to remain in and proliferate within the lymphoid organ. In NK cells, CD69 enhances cytotoxic activity[54]. In tumours, the presence of CD69 on T cells regulates their effector function and controls their exhaustion[55].

Granzymes are serine proteases contained in the cytoplasmic granules of T- and NK cells. More specifically, they are pro-proteases which cause apoptosis, once in the cell[56]. While granzyme A triggers a caspase-independent apoptosis-like pathway[57], granzyme B complementarily starts a real caspase-dependent cell apoptosis, widening the spectrum of target cells[58].

NKG2D is present on NKs and activated murine CD8+ T-cells and is a lectin-like receptor, which binds to MHC class I-like molecules from infected, cancerous and damaged cells, fulfilling the functions of a sensor. It activates these immune cells and enhances their effector functions[5659].

Interferon-gamma (IFN-γ) is secreted by NK cells to activate the phagocytosis of macrophages, stimulates dendritic cells and regulates the differentiation of T-helper

cells into a pro-inflammatory type[56]. It is also produced by CD4+ T helper 1 cell type 1 (Th1), CD8+ T cells, B cells, NKT cells, and APCs, as reviewed in ref [60].

Programmed Cell Death 1 (PD-1) is an inhibitory receptor expressed transiently by activated B-, T- and myeloid cells. When they bind to Programmed Death Ligands 1 and 2 (PD-L1 and 2) of tumours cells for instance, it suppresses the CD8 effector function[56]. More precisely, it leads to T cell exhaustion and apoptosis, while reducing the apoptosis of regulatory T cells.

Killer cell lectin-like receptor G1 (KLRG1) is a receptor found on NK and T cells. As reviewed by Gründemann et al[61], its expression is upregulated during pathogenic infections: most effector cells are indeed KLRG1 positive. These T cells have shown normal function, little proliferation and a short life-span, which means that they are reaching the end of their differentiation stage. These observations were also made in NK cells, which is why KLRG1 is often used as a senescence marker.

2.3. ONCOLYTIC VIRUSES

2.3.1. History of oncolytic viruses

One of the most attractive features of oncolytic viruses (OVs) is their ability to selectively infect and lyse tumour cells through replication. This is allowed by some altered signalling pathways specific to tumour cells, while healthy cells are able to protect themselves against infection or at least replication[62]. For instance, the onco-selectivity of vesicular stomatitis viruses (VSV) has been linked to downregulated expression of interferon type 1 (IFN type I)[63], and herpes simplex virus 1 (HSV-1) takes advantage of abnormalities in the protein kinase R activation[64].

As depicted in Figure 2 from *Lauer et al (2022)*, oncolytic viruses damage tumours through multiple mechanisms. First, OV infection leads to direct tumour cell lysis, which releases additional virus particles that can infect additional cancerous cells. Secondly, dying tumour cells release their antigens which can be taken up and

presented by newly matured APCs that are stimulated by the virus infection, leading to a systemic adaptive immune response against the cancer. Finally, the immune suppressive mechanism of the TME becomes altered, leading to inflammation, immune stimulation, and reduced angiogenesis[65]. In fact, the crosstalk between the TME and tumour cells has been shown to sustain OV infections: when tumour cells secrete transforming growth factor β (TGF-β), CAFs are reprogrammed to become more sensitive to infection and prone to produce fibroblast growth factor 2 (FGF2), itself affecting the retinoic acid inducible gene 1 (RIG-1) expression in cancer cells, leading to less effective viral defence mechanisms[66].

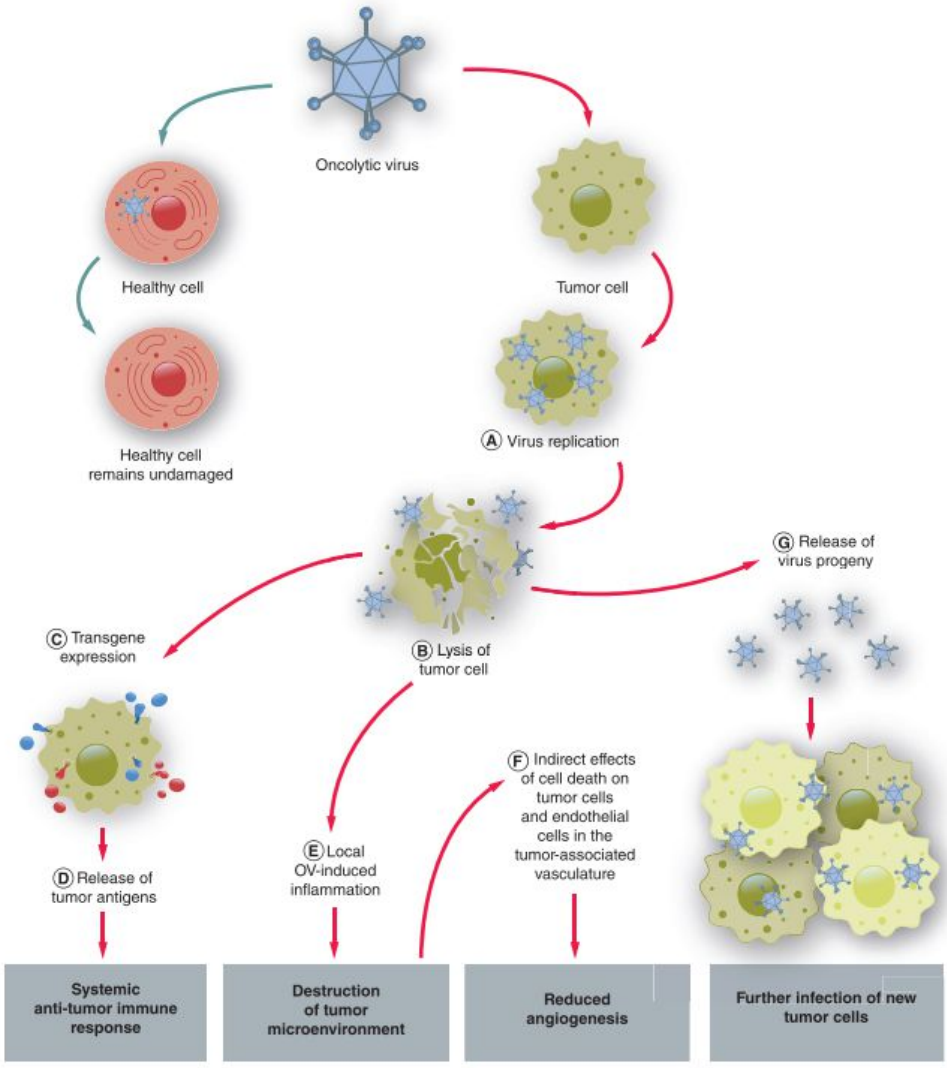

Figure 2: The different mechanisms of action of oncolytic viruses**.** From *Lauer et al, 2022*.

Many virus families have shown such promise for oncolytic virotherapy, that their efficiency, very often as recombinant platforms, was or is being assessed in clinical trials. To name only a few, herpes simplex viruses (HSV) and adenoviruses represent more than half of the OV-based clinical trials, followed by vaccinia virus, reovirus, vesicular stomatitis virus, polio virus, parvovirus and Newcastle disease virus (NDV) for example[65]. For pancreatic cancer, viral monotherapies with HSV, adenovirus or reovirus, as well as combinations from other viruses with chemo- and/or immunotherapies are being tested. Two delivery routes were favoured for these trials, namely intravenous and intratumoural[67].

So far, four oncolytic viruses were approved for human therapy worldwide: Rigvir®, an unmodified picornavirus, for treatment of melanoma in Latvia, Georgia and Armenia in 2004 (taken off the market in 2019); Oncorine® (Onyx-015), an engineered adenovirus (H101) for the treatment of head and neck cancer in China in 2005; Imlygic®, a recombinant herpes simplex virus 1 for metastatic melanoma therapy, in the US and Europe, in 2015 ; more recently in 2021, Delytact®, another modified HSV1, received conditional and time-limited approval for the treatment of malignant glioma or primary brain cancers[65,68].

In veterinary medicine, lots of progress was made in the recent years, with the passage to *in vivo* trials: starting in 2013, an adenovirus was tested intratumourally in melanoma ; in 2014, the Lasota strain of NDV was injected both intratumourally and intravenously in dogs for cutaneous lymphoma, and regression was observed ; in 2018, an extensive study on the use of the intravenous route was conducted and concluded for the safety of recombinant VSV-IFNb-NIS in dogs afflicted with anal adenosarcoma, lymphoma or multiple myeloma, with beneficial effects on regression. Later that year, a recombinant Myxoma virus was tested intratumourally on dogs with soft tissue sarcoma and deemed safe as well. Two years ago in 2021 recombinant HSV M032 was injected intratumourally and was able to elicit a systemic anti-tumour response to glioma; the same virus injected intracranially could also extend the survival of dogs operated for glioma[68].

2.3.2. Challenges of delivery

The efficacy of oncolytic therapy depends directly on the access to the tumour site. Concerns about biosafety are decisive for the choice of the application route, if negative systemic effects of the virus are to be expected. Furthermore, a pre-existing immunity against the virus, in the case of prior exposure, severely limits the efficacy of intravenous applied virus therapies.

The easiest application route for tumours located on the surface is intratumoural (it.). This route is considered to be the most efficient for the direct oncolytic effects, but might be too invasive for deep seated tumours located in the abdomen or intracranially, where ultrasound- or CT-guided injections or stereotactic surgery are required. Furthermore, in the case of metastatic disease, it is not feasible to directly inject small or micrometastatic tumours distributed in multiple sites of the body. The main advantage of intratumoural application is the delivery of a high, exact concentration of virus particles on-site, which allows for a better comparison with *in vitro* simulations, and almost no off-target effects. Repeated treatments may be easy to perform for accessible tumours. Abscopal effects with i.t. injections were also reported on distant tumours in a melanoma mouse model[69].

Diverse OVs were applied via i.t. application in PDAC therapy in clinical studies. For instance, in 2018, in Japan, a phase 1 dose-escalation study was performed with unresectable PDAC patients. HF10, a spontaneously mutated herpes simplex virus 1 (HSV-1), has demonstrated a potent antitumour effect with minimal adverse effects, in combination with Gemcitabine[70]. The same year, in Spain, an adenovirus encoding for human hyaluronidase, VCN-01, was combined with chemotherapy[71]. Treatment was well tolerated and stabilized the tumours.

More elegant with regards to the clinical application, is the intravenous route (i.v.). The difficulties encountered with this route are nonspecific uptake, blood stability with retained infectiousness, actual access to the tumour if the vascularization is disturbed on-site[72], and viral clearance by the host's immune system. This systemic type of delivery also calls for a high selectivity of the viruses for cancer cells, as

some of them are able to cross the brain-blood barrier, which can be used for central nervous system afflictions, but also raises neurotoxicity concerns[73]. Strategies to improve intravenous delivery include: the coating of viruses with polymers targeted to the tumours and/or to protect them from immune system recognition, the normalization of the vasculature, or increasing the blood pressure through exercise during the delivery[72,74]. The first clinical trial for pancreatic cancer treatment via intravenous route was made for VCN-01 with hyaluronidase, the adenovirus armed with hyaluronidase mentioned for intratumoural applications. The results of this study, where it was implemented alongside chemotherapy, were encouraging and demonstrated sufficient safety[75].

Another feasible way to deliver viruses is the intraperitoneal route (i.p.). It enables resorption of larger quantities than intravenously, is ideal for accessing abdominal organs, and is easy to implement. In 2006, a pancreatic cancer study involving a chimeric HSV2 compared treatment via three treatment routes: i.t. with subcutaneous tumours, i.v. and i.p. with orthotopic tumours. The best results were obtained via the i.p. route with 75% tumour eradication and prevention of local metastases[76].

Some other routes are used more marginally, with little relevance for pancreatic cancer, for instance: intrathecal delivery (in the spinal cord, for central nervous system tumours), limb perfusion, aerosol, and intrapleural[77].

2.3.3. Introducing VSV-NDV

2.3.3.1. Vesicular stomatitis virus (VSV)

The Vesicular stomatitis virus is a single stranded negative sense RNA-virus belonging to the *Rhabdoviridae* family, hence its bullet shape, and to the order

Mononegavirales, with a genome of approximately 11kb in length. A virion is constituted by a nucleocapsid and an envelope.

As schematically represented below in Figure 3 from *Liu G. et al, 2021*, the genome of VSV comprises five proteins: the nucleoprotein N, the phosphoprotein P, the matrix protein M, the glycoprotein G and the large protein or polymerase L. The G protein enables attachment to the low-density lipoprotein receptor (LDLR) and entry into the cell, through clathrin-actin mediated endocytosis. Under acidic endosomal conditions, the G protein undergoes conformational changes and becomes hydrophobic, allowing the penetration of its fusion loops into the endosomal membrane. The fusion between the virus and host cell membranes lets the nucleocapsid into the cell cytoplasm, where transcription and replication can take place, under the lead of the L and P proteins. Newly synthetized nucleocapsids are condensed via the M protein, forming nucleocapsid-M protein complexes, acting as adaptors for the budding of the virions at G-protein rich sites[78].

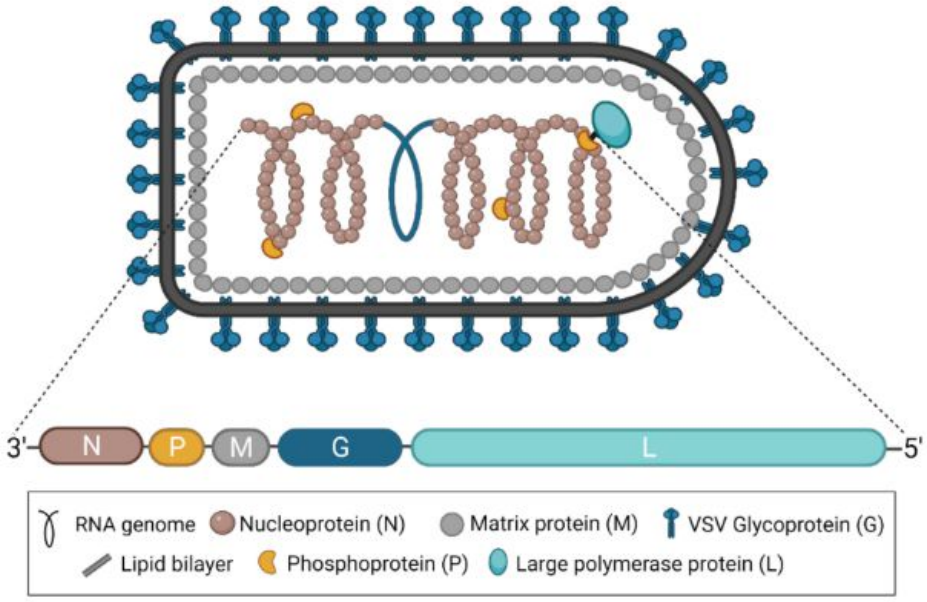

Figure 3: Schematic representation of a VSV particle with its 5 encoded genes, including the glycoprotein on the surface and envelope. From *Liu G et al, 2021*.

VSV stems from the animal kingdom, where it infects primarily hoofed animals, namely horses, cattle and swine, rarely lamas or humans. Infections of the natural host are characterized by blisters found in oral mucosa, feet and mammary area. Typical for the infection are also fever, transient viremia, anorexia due the discomfort in the mouth area, and lameness. Animals commonly recover within a three weeks period[78]. The clinical representation of VSV resembles the symptoms of the foot and mouth disease, caused by a Picorna virus.

Humans in direct contact with these infected animals can also contract the disease, in the form of a mild flu-like illness with possible oral lesions[79]. Despite the interest in this virus, some transmission mechanisms still need to be elucidated, but evidence suggests biting arthropods as serving vectors[80].

The replication process of VSV with final lysis of the infected cells is known for its rapidity and efficacy as an oncolytic virus, and together with the broad tropism of the virus, explains the interest for its implementation as on oncolytic platform. Studies also demonstrated VSV's ability to induce CD8+ T cells against tumour antigens post-lysis[81] and a better infiltration of immune cells, especially NK cells and neutrophils[82,83]. It also infects endothelial cells, causing a reduction of the vascularization of the tumour[84,85]. But despite all its advantages, reported cases of neurotoxicity and off-target effects in mice, rats and also non-human primates[63] have led to safety concerns surrounding the development of VSV as a clinical agent.

2.3.3.2. New castle disease virus (NDV)

The Newcastle disease virus is a single stranded, non-segmented RNA virus with negative polarity, belonging to the avian *Paramyxoviridae* family, and just like VSV, to the *Mononegavirales* order. It has a spherical shape and its genome is about 15,2 kb long. As depicted in Figure 4, NDV comprises six genes in a highly preserved order: N for the nucleocapsid protein encoding gene, a phosphoprotein (P), a matrix protein M, a fusion protein F on the envelope, a hemagglutinin-neuraminidase protein HN and a large protein or polymerase L. Noticeably, the

RNA of the P gene can be edited to express a V or W protein, responsible for the immune modulation of the host[86]. The F and HN proteins are both surface glycoproteins: first, HN recognizes and binds to the sialic acid receptors present on the host cell membrane, while F mediates fusion of the viral envelope with the cell membrane. In this process, the F protein is cleaved by proteases from the host: the exact site is relevant for the pathotype of the NDV strain, namely lentigenic (avirulent), mesogenic (intermediate) or velogenic (virulent)[87]. Once in the host cell cytoplasm, an active ribonucleoprotein (RNP) complex consisting of the viral genome associated to the N and P proteins and RNA-polymerase is formed for the replication and transcription[88]. The new RNA then forms a complex with the N, P and L proteins, forming the nucleocapsid, which is finally assembled by the M protein and both surface proteins HN and F, allowing budding[89].

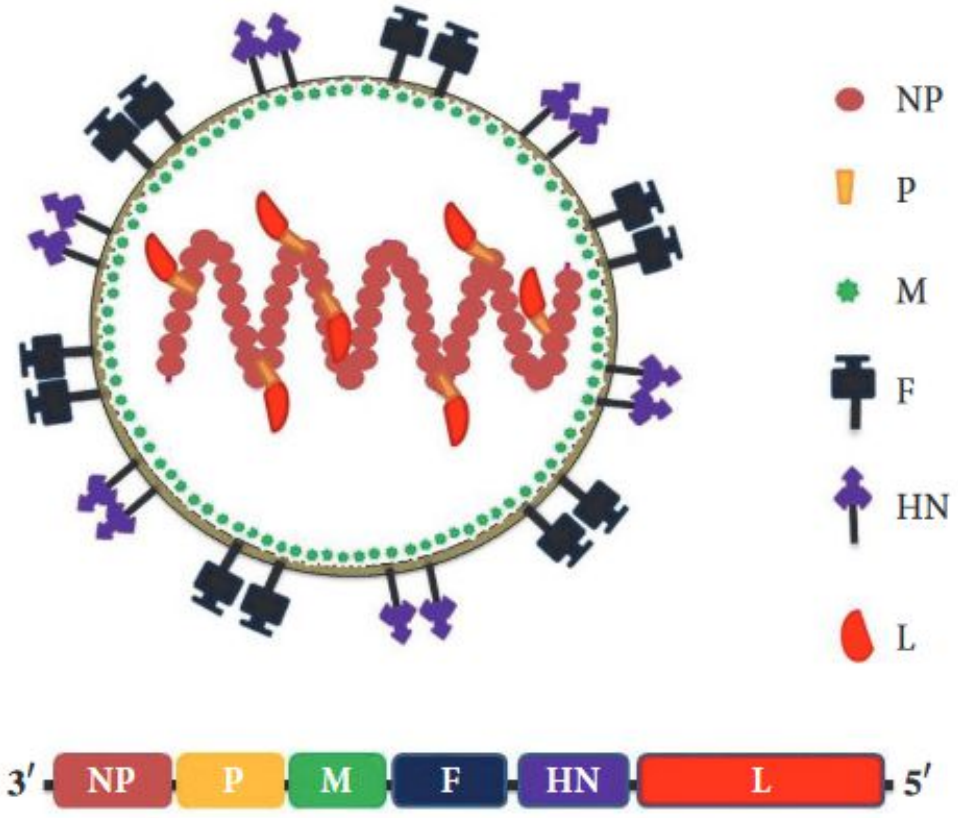

Figure 4: Schematic structure of a NDV particle, with its 6 main viral proteins: nucleoprotein (NP), phosphoprotein (P), matrix protein (M), fusion protein (F), hemagglutinin-neuraminidase (HN) and polymerase protein (L). From *Bello et al, 2018*.

The Newcastle disease is endemic in many Asian, African and American countries, and can have devastating effects in poultry herds, with a mortality of up to 90%[90]. In fact, wild birds like cormorants or pigeons can also cause outbreaks. Indeed, depending on the pathotype of the strain, infections can run different courses and display different symptoms. The strains can be classified as follows, sometimes with overlap: the highly virulent viscerotropic velogenic strain, linked to intestinal haemorrhages; the neurotropic velogenic strain, highly lethal due to respiratory and nervous system symptoms; the mesogenic strain with rare respiratory and nervous symptoms and low mortality; the lentogenic strain with mild to subclinical airways symptoms; the asymptomatic, subclinical enteric strain[91]. Furthermore, a drop in egg production is often observed. The velogenic strains are listed as highly pathogenic and the disease must be reported to the World Organisation of Animal Health for monitoring. The importance of correct identification of the strain is understandable to prevent further spread of the disease, and differentiate it from other devastating agents, such as HPAI (high pathogenic avian influenza).

The virus spreads directly from bird to bird, either vertically, or through aerosols and excretions, if they come in contact with mucous membranes from the respiratory or digestive tract, or the eye. Vaccination can protect birds from clinical symptoms, but not from shedding virulent viruses after exposure. Indirect contamination through equipment, water or food for example is also possible[90]. Avian paramyxoviruses are able to infect humans exposed to high viral loads, typically causing self-limiting conjunctivitis and mild flu-like symptoms[92]. However, human to human transmission hasn't been reported[92].

The fact that NDV is emerging as an oncolytic platform is due to four main characteristics. First, similarly to VSV, it targets cancer cells, deficient in IFN signalling for its replication and lyses them, while leaving healthy cells unharmed[93]. Second, it was shown to trigger apoptosis (via expression of IFN-α, IFN-β, CCL5 and IP10)[94], which was contradicted by *Koks et al*., who reported no signs of apoptosis, but immunogenic cell death and necroptosis[95]. Third, due to the expression of the F protein, it is able to build syncytia (multinucleated giant cells), hence a potentially enhanced intratumoural spread[96]. Fourth, like VSV, it was

shown to elicit antitumour immunity and infiltration in directly injected and abscopal tumours[97].

2.3.3.3. Recombinant VSV-NDV and variants

According to *Lin et al, 2023*, the valued qualities in an OV candidate are: tumour specificity, an efficient infection with replication in tumour cytoplasm, safety/security for the host, the promotion of anti-tumour immunity, a way of overcoming the tumour immunosuppressive milieu, and last but not least, a good balance between the immunity directed against the virus and the tumour. Some of the methods used to reach these goals are anti-angiogenesis, metabolic modulation and degradation of the TME[98].

As mentioned earlier in this chapter, wild-type VSV and NDV offer many of these properties:

- tumour specificity, with the selectivity for cells with deficient IFN1-signalling
- recruitment of innate and adaptive immune cells with anti-tumour immunity demonstrated in numerous studies
- inflammation in the TME and modulation of the vascularization
- limited pre-existing immunity against NDV and VSV in humans, as they are not natural hosts, and most humans have limited exposure to these viruses.

However, each of these viruses have safety concerns associated with them. Back in 1969, Sinkovics' study with VSV and a neurotropic variant of NDV in a mouse model of sarcoma reported slower tumour growth, but also the death of several mice due to encephalitis[99]; since then, other groups showed similar off-target effects[100,101]. Equally, an outbreak of NDV is an environmental concern and an economic threat for the poultry industry.

Genetic engineering held the answer to these challenges, and in 2018, recombinant VSV-NDV (mostly abbreviated as VSV-NDV in this work) was reported to eliminate the safety risks inherent to both parent viruses, while enhancing their

direct oncolytic effect and immune stimulating properties[102]. As Figure 5 shows, the hybrid virus used in this work is based on a vesicular stomatitis virus backbone, in which its glycoprotein (G) was replaced by NDV surface proteins: hemagglutinin-neuraminidase (HN) and a modified F protein for enhanced fusion[102].

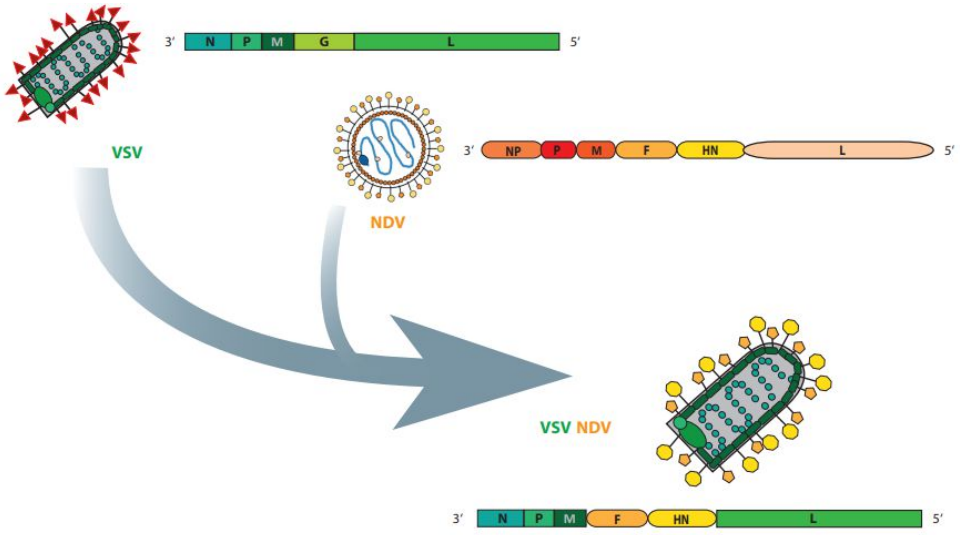

Figure 5: Schematic representation of rVSV-NDV and its parent viruses, VSV (vesicular stomatitis virus) and NDV (Newcastle disease virus). The endogenous G protein of VSV was replaced by the F and HN from the NDV envelope in the hybrid virus construct.

Many advantages are expected from these modifications. To start, the cell tropism changes, improving safety: through the deletion of the VSV-G protein and its replacement with the NDV-HN surface protein, the hepato- and neurotoxicity from wild-type VSV[103] is reduced, while NDV phase I/II trials highlight its safe profile[104,105]. Second, the hybrid virus should not pose a threat to the poultry industry, since its added proteins originated from NDV/F3aa(L289A), a mesogenic strain, knowing that highly pathogenic strains possess both virulent HN and F proteins[106]. Furthermore, the NDV-P protein is also lacking in this construct, hence the impossibility to express any V protein, which is responsible for the antagonism of IFN-signalling in birds, leading to pathogenic effects[107]. Third, the ability to form

syncytia (see Figure 6): on the one hand, the primarily intratumoural spread of the virus limits the exposure of healthy cells, on the other hand, it protects the viral particles from humoral immune responses[108], which offers the virus more time before viral clearance onset. On top of that, the F/3aa(L289A) protein used in the recombinant virus has a leucine-to-alanine substitution, which leads to greater syncytia than the wildtype F protein[109]. Concurrently, dying syncytia produce a lot of exosome-like vesicles, able to recruit and activate dendritic cells more efficiently than other cell death types. The following cross-presentation and antitumour response are more potent than with non-fusogenic viruses[110].

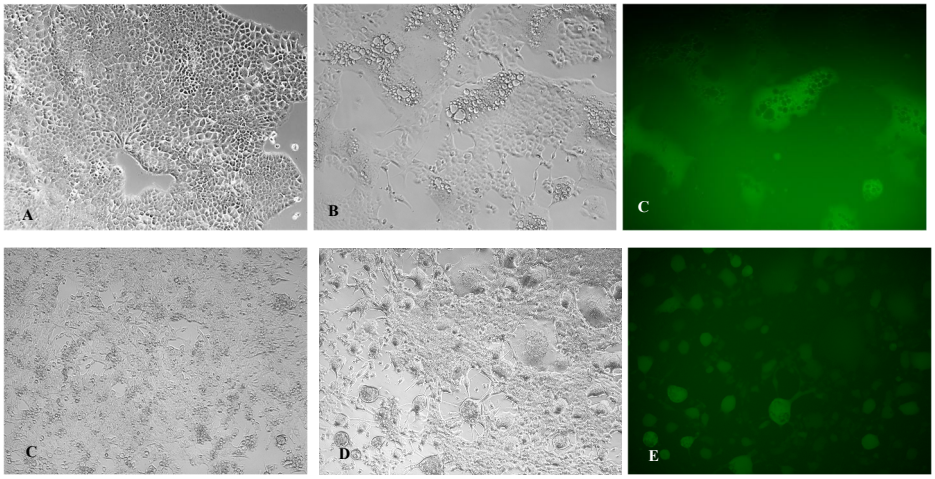

Figure 6: Syncytia formation in cells infected with a variant of VSV-NDV expressing GFP, MOI 1. (A) uninfected R211 cells (B & C) infected R211 cells, 48 hours post-infection, in bright field or GFP (D) uninfected B191-KO5 cells (E & F) infected B191-KO5 cells, 24 hours post-infection, in bright field or GFP.

On the down-side, the virus showed an attenuated replication *in vitro*. However, with lower titres than its parent viruses, it managed to reach sufficient levels of cytotoxicity *in vitro* and even extended the life-span of mice with an orthotopic hepatocarcinoma model, via systemic delivery[102].

2.3.3.4. Virus variants targeting the extracellular matrix

One of the advantages of rVSV-NDV, is that it can encode a therapeutic transgene, allowing the creation of armed variants. It has been recognized that the localized expression of some therapeutic genes was safer than their systemic administration, as their action directly within the tumour tends to reduce the systemic side-effects[111,112].

In the case of PDAC, the abundant TME is a major obstacle to the efficiency of any therapy, including OVs, which is why many groups have utilized virus engineering strategies to address this problem[113]. Three such viruses were engineered in our group, with the aim of degrading the collagen-rich extracellular matrix of PDACs, via different mechanisms of action. Their genomic structure is visible in Figure 7.

The first variant, VSV-NDV-SPAM1 expresses the human sperm adhesion molecule 1, a hyaluronidase (also named PH-20). Hyaluronidase has been previously used to digest the hyaluronic acid of the cumulus-oocyte matrix, to enable the entrance of the spermatozoids[114]. Hyaluronidase has also been used in OV therapy, for example the adenovirus VCN-01, which was tested in PDACs. In a first concluded phase 1 dose escalation study (NCT02045589), this modified adenovirus was successful in degrading tumour stroma, hereby stabilizing lesions, and reducing its stiffness. Hyaluronidase was detected in patients' blood[71]. These good results led to another phase 1 trial (NCT02045602), where VCN-01 was tested intravenously, in combination with nab-paclitaxel and gemcitabine, in patients with advanced PDAC[75]. Again, the virus was able to replicate in the tumours, elicit a systemic immune response, turn cold tumours into hot ones, while further demonstrating acceptable safety levels. Currently, recruitment is ongoing for a phase 2b trial (NCT05673811), where metastatic pancreatic cancer will be treated with nab-paclitaxel and gemcitabine with or without VCN-01[115].

The second variant of VSV-NDV expresses a gene for MMP8, a collagenase that is able to break down collagens type I, II and III, as was similarly utilized in the modified adenovirus, AdMMP8[116]. In this case, an *in vivo* trial in BxPC3 xenografts showed that a non-replicating AdMMP8 injected intratumourally, along with a

wild-type Adenovirus, was able to slow tumour growth and reduce its collagen deposition, compared to the controls.

The third variant, VSV-NDV-Relaxin2, could be compared to YDC002, an adenovirus engineered for the expression of Relaxin as well. In fact, this hormone peptide acts as both a collagenase and a down-regulator of the expression of ECM components, preventing fibrosis in tissues[117]. YDC002 has only been tested intratumourally in a murine xenograft model *in vivo*, and, alongside with Gemcitabine, it inhibited tumour growth by inducing apoptosis and attenuated the deposition of collagens I and IV, elastin and fibronectin, giving access to previously highly desmoplastic tumours[118].

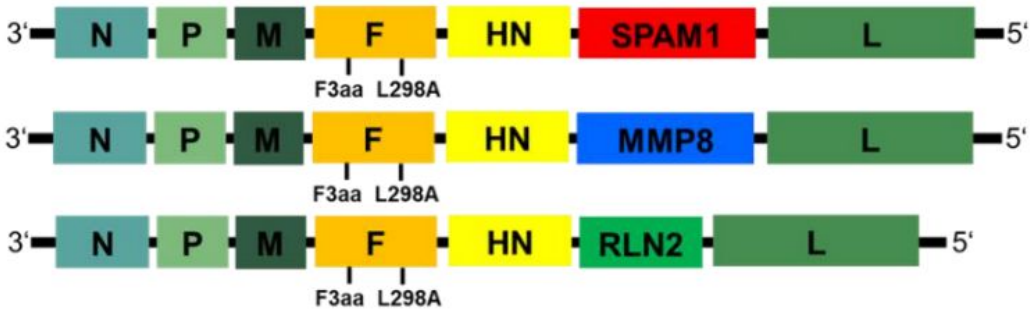

Figure 7: Schematic illustration of the genomes of VSV-NDV-SPAM1, VSV-NDV-MMP8 and VSV-NDV-RLN2. Transgenes are inserted as additional transcription units between the hemagglutinin-neuraminidase (HN) and large polymerase (L) genes.

In summary the three viruses had been engineered to express transgenes that were shown to be effective in PDAC in other OV constructs.

2.4. SMALL MOLECULE INHIBITORS

2.4.1. Trametinib (MEK inhibitor)

Trametinib is a selective MEK1 and MEK2 inhibitor, approved under the trade name Mekinist® in Europe[119] and in the US, for the treatment of metastatic melanoma and non-small cell lung carcinoma, in combination with dabrafenib, a BRAF inhibitor. As reviewed by Eser et al, 2014[120], the KRAS pathway and its downstream RAF-MEK1/2-ERK1/2 pathways are classically activated in PDAC tumours. This explains the enthusiasm for MEK inhibitors in PDACs: currently, there are 9 ongoing registered trials (on clinicaltrials.gov) for PDAC using Trametinib, out of 16 in total. On the oncolytic virus side, it was tested in combination with T-VEC and improved cytotoxicity of melanoma cells *in vitro*, as well as prolonged survival *in vivo* and enhanced T cell activation, even more with the use of anti-PD-1 antibodies[121]. Another group investigated the combination of vaccinia virus with Trametinib and observed enhanced replication through STAT3 activation and downregulation of antiviral sensing mechanisms (including interferon regulatory factor 3) in an ovarian cancer model[122]. In China, Zhou et al reported in 2021 that the MEK inhibitor allowed for a better replication of a herpes simplex virus 1 in BRAF mutated tumour cells, by downregulation STAT1 and PKR expression. As mentioned before, the results were also improved by the use of PD-1 antibodies[123].

2.4.2. HDAC-Inhibitors (Panobinostat und Entinostat)

Histone deacetylases (HDAC) are enzymes which can modulate chromatin between "open" and "closed" forms, regulating epigenetic gene expression; non-histone proteins can also be affected by hypo-acetylation. HDAC inhibitors are broken down into four categories, after their resemblance to yeast structures: hydroxamates (like Panobinostat), short-chain fatty acids, cyclic tetrapeptide, and benzamides (like Entinostat)[124]. HDAC inhibitors have been investigated thoroughly in the last years for their capacity to reverse some of cancers' pathologic overexpression of

genes[125]. However, their efficacy in PDACs seems to be self-limiting so far, as they may as well downregulate tumour promoting as tumour suppressing functions[124].

As reviewed by Singh et al in 2016[126], Panobinostat was shown to suppress angiogenesis, mediate apoptotic pathways and induce cell cycle arrest in PDAC cells[126]. Moreover, this molecule, under the brand name Farydak®, is an American Food and Drugs Administration (FDA) and European Medicines Agency (EMA) approved drug for the treatment of resistant or recurring multiple myeloma[127]. It can be administered orally or intravenously. It is characterized by a prolonged hyperacetylation of proteins, which enables a reduced frequency of administration thus less side-effects such as thrombocytopenia[126]. Another ongoing phase 1b study is testing the compound on different types of solid tumours, including local and metastatic PDACs, in combination with other drugs[128]. When combined with an Herpes Simplex Virus 1 (HSV-1), Panobinostat enhanced its viral replication and cytotoxicity, by downregulating IFN-β and the antiviral immune response, while upregulating the PD-L1 expression of glioma and squamous cell carcinomas[129].

Entinostat benefits from a long half-life (between 33 and 52 hours), which makes it a good candidate for trials. Indeed, it was tested for PDACs, in a phase 1 trial: in combination with chemotherapy (13-cis-retinoic acid), it was well tolerated and offered a 6 month stabilization of one patient[130]. The inhibitor was found to increase apoptosis by sustaining the oncolytic activity and viral replication of VSVΔ51 (a natural variant of VSV) in solid tumours, by dampening the IFN response, *in vitro* and *in vivo*, similarly to Panobinostat. This combination also showed a decrease in the antiviral response of the host, leaving the antitumoural response unscathed[131]. The IFN modulation also helped other virus types, namely Vaccinia and Semliki Forest virus, replicate faster in breast, lung, or melanoma cancer lines[132].

2.4.3. EZH2-Inhibitor (Tazemetostat)

Tazemetostat is an enhancer of zeste2 (EZH2) inhibitor. EZH2 is known for promoting cancer cell proliferation, and the epithelial to mesenchymal transition.

Tazemetostat is an enzyme, a histone methyltransferase, part of the PRC2 complex (polycomb repressive complex 2), itself linked with chromatin compaction and transcription regulation[133]. Tazverik® is an EZH2 inhibitor, approved in Europe and the USA for the treatment of diffuse large B-cell lymphoma[134].

2.4.4. Bromodomain inhibitor (JQ1 and AZD5153)

The bromodomain and extraterminal domain comprises four proteins: BRD2, 3, 4 and BRDT (bromodomain testis-specific protein), each of them containing two separate bromodomains. They can interact with acetylated histone tails and act as epigenetic regulators[135]. As reviewed by *Shi et al, 2014*[136], BRD4 has an associated complex made of P-TEFb, a heterodimer made of cyclin-dependent kinase (CDK9) and a subunit promoting Polymerase II elongation. BET inhibitors inhibit transcription and demonstrated tumour growth reduction in numerous models. The downregulation of the oncogenic c-MYC gene is believed to play a role in these anti-cancerous properties[137,138]; cell cycle arrest was also observed with both JQ1 and AZD5153[139,140]. Potent anti-inflammatory effects of BET inhibitors were also reported *in vivo*[141].

JQ1 is a pan-BET inhibitor bromodomains of the BET family. Tested *in vivo* in PDAC tumours, JQ1 caused higher levels of DNA damages than the control and reduced the expression of repair proteins, ad was thus used to sensitize these tumours to another compound[142]. However, its short half-life in plasma (around 1 hour) disqualifies JQ1 for clinical applications in humans.

Unlike JQ1, AZD5153 is a bivalent BET inhibitor, as it can bind to the proteins of both bromodomains at the same time, via two acetyl lysine mimicking halves, which enhances its selectivity and potency[138] . It also benefits from a longer half-life of 6 hours in plasma. AZD5153 was shown to induce apoptosis, increase the expression of cleaved-caspase 3 and PARP (poly-ADP ribose polymerase), while inhibiting the expression of c-MYC in colorectal cancer *in vivo*[140].

Finally, in preliminary data from a phase 1 dose escalation study (NCT03205176), orally administered AZD5153 was deemed safe in patients with relapsed or refractory solid (including ovarian, breast or pancreatic) tumours or lymphoma[143].

3. AIMS OF THIS PROJECT

As explained, PDAC is a disease with a difficult prognosis. Since immunotherapies are making great progress in cancer treatment, this work aims to determine whether our oncolytic hybrid virus could fill in the gap for efficient therapies in challenging solid tumours like PDAC. Furthermore, due to the complexity of cancer, we propose that only a combination therapy will have sufficient efficacy to go further to clinical trials.

In this project, the effects of the virus *in vitro* and in an orthotopic mouse model were investigated to determine the potential of the virus as a monotherapy and its mechanism of action in the TME and systemic immune system. The aim of the treatment was, not only to target cancer cells, but also an important subgroup of cells present in the tumour stroma, the cancer-associated fibroblasts. This defined the baseline for VSV-NDV's effects.

The ability of VSV-NDV therapy to target the tumour stroma was attempted to be augmented by the development of three specifically engineered viruses that express extracellular matrix-degrading proteins, to address the complex TME in PDAC more efficiently. Again, these viruses were first characterized *in vitro* before their implementation *in vivo*.

Finally, small molecule inhibitors were investigated as an adjuvant therapy, to determine whether these compounds could enhance the oncolytic virus therapy and provide with an even more efficient therapeutic outcome.

4. MATERIAL AND METHODS

4.1. MATERIAL

Table 1: general laboratory equipment

Centrifuge 5910R	Eppendorf AG, Hamburg, Germany
Centrifuge 5424	Eppendorf AG, Hamburg, Germany
Ultracentrifuge Optima XL-100K	Beckman Coulter, Brea, USA
CO2 incubator Cell Vios 160i	Thermo Fisher Scientific Inc., Waltham, USA
Counting chamber Luna	Logos Biosystems, Gyeonggi-do, South Korea
Mr. Frosty™ freezing container	Thermo Fischer Scientific Inc., Waltham, USA
Multichannel 50, 300 µl	Corning, New York, USA
Multipette M4	Eppendorf AG, Hamburg, Germany
Nanodrop Objectives LSM700 5, 10, 20 x	Zeiss, Oberkochen, Germany
GloMax® Discover Microplate Reader	Promega, Fitchburg, USA
Thermomixer compact	Eppendorf AG, Hamburg, Germany

Vortexer REA X	Heidolph Instruments, Schwabach, Germany
Water bath GFL 1086	Lauda-GFL, Burgwedel, Germany
ChemiDoc XRS+ Imager	Biorad Laboratories Inc., Hercules, USA
Thermocycler Peqstar	VWR, Radnor, USA
Nanodrop lite spectrometer	Thermo Fischer Scientific inc. Waltham, USA

Table 2: reagents used for cell culture

Accutase	Sigma-Aldrich
DMEM low glucose, low pyruvate	Biowest
DMEM/F-12	Gibco
DMEM GlutaMAX	Gibco
DPBS	Pan Biotech
Fetal calf serum	Serana
Penicillin-Streptomycin	Pan Biotech
Trypsin EDTA	Pan Biotech

Table 3: Consumables used for cell culture

75cm2 Cell Culture Flask	TPP Techno Plastic Products AG, Schaffhausen, Switzerland
Tissue culture plate, 24/96-wells	TPP Techno Plastic Products AG, Schaffhausen, Switzerland
Cellstar tubes, 15/50 mL	Greiner bio-one, Kremsmünster, Germany
Reaction Tubes 1,5/2 mL	Eppendorf AG, Hamburg, Germany
0,5-10µL pipette	Eppendorf Research
2-20µL pipette	Eppendorf Research
20-200µL pipette	Eppendorf Research
100-1000µL pipette	Eppendorf Research
Combitips advanced 5/10mL	Eppendorf AG, Hamburg, Germany
Pipet tips, 10/20/200/1000 µL	Sarstedt AG & Co. KG, Nümbrecht, Germany
Filter tips, 1000µL	Clear Line
Serological pipet, 5/10/25/50 mL	Greiner bio-one, Kremsmünster, Germany

Tip one RPT, Pipet tip 10µL RNAse, DNAse, DNA and pyrogen free	StarLab
RPT Filter tips, 20µL	StarLab
Universal Fit Pipet Tips, 200µL	Corning

4.2. *IN VITRO* EXPERIMENTS

4.2.1. Cell culture

The cell lines used for all experiments were maintained in a HeraCell incubator, at 37°C, 90°C humidity and 5% CO2. The cell lines were passaged when they reached a confluency of 80-90%. The cell lines and their culture media are listed below in Table 4.

Table 4: list of the used cell lines and their culture medium

Cell line	Type	Medium	Supplements
CKP530202	Murine PDAC	DMEM high glucose	10 % FBS 1 % Pen/Strep
CKP110299	Murine PDAC	DMEM high glucose	10 % FBS 1 % Pen/Strep
R211	Murine PDAC	DMEM high glucose	10 % FBS 1 % Pen/Strep
B191	Murine PDAC	DMEM high glucose	10 % FBS 1 % Pen/Strep

PSN1	Human PDAC	RPMI 1640 + GlutaMAX	10 % FBS 1 % Pen/Strep
Bx-PC3	Human PDAC	RPMI 1640 + GlutaMAX	10 % FBS 1 % Pen/Strep
PSC 806/810	Murine cancer associated fibroblasts	50% DMEM/F-12™, DMEM low glucose, low pyruvate	20% FBS 1% Pen/Strep
FB 704F3	Murine cancer associated fibroblasts	50% DMEM/F-12™, DMEM low glucose, low pyruvate	20% FBS 1% Pen/Strep
PSC3 Prrx1	Murine cancer associated fibroblasts	50% DMEM/F-12™, DMEM low glucose, low pyruvate	20% FBS 1% Pen/Strep
HEK-293T	Human embryonic kidney cells	DMEM	8% FBS
BHK-21	Hamster kidney fibroblasts	PEM	4mM Pyruvat 8mM Glutamin
Co-cultures PDAC and CAFs	Ratio 1 PDAC for 3 CAFs	50% DMEM/F-12™, DMEM low glucose, low pyruvate	5% FBS 1% Pen/Strep

AGE1.CR	Muscovy Duck retina	DMEM F12	10% FBS 1% Pen/Strep

4.2.2. Virus production

4.2.2.1. Virus stock production from existing master banks

The production method of the VSV-NDV, -GFP, -SPAM1, -MMP8 and -RLN2 used during this doctorate has evolved over the years, which is why some viruses were produced in adherent cultures of AGE1.CR (subsequently referred to as AGE1), an adherent cell line (*in vitro* work, route finding and dose finding survival), while some virus stocks (the ones used for kinetics, ECM-survival, AZD5153 survival) were produced in BHK-21 cells adapted to suspension culture.

For the production in AGE1, the cells were plated on 15 cm dishes and infected at an MOI of 0,0001 of the respective virus masterbank. After 48 hours, the virus-containing medium was then clarified by centrifugation (500 rcf, 5 minutes) to remove floating cells and debris, and the supernatant was collected.

The cell monolayers were then incubated with 0,001% Triton X in PBS and scraped and collected into 50ml Falcon tubes. The cell lysates were then vortexed (1 minute), sonicated for 3 minutes, and vortexed again to release cell-associated virions. To remove cell debris, another centrifugation (1000 rcf, 5 minutes) of this lysate was performed. This supernatant was combined with the collected cell medium and processed further by ultracentrifugation.

All the supernatants were then subjected to ultracentrifugation (25 000 rpm, 4 °C, 1 hour) to separate and concentrate the virus into the pellet. These pellets were then resuspended in 1mL of PBS, the aggregates dispersed through a 20G needle with syringe and gently layered over a freshly prepared sucrose gradient (60%, 30% and 15% sucrose in PBS) for ultracentrifugation (same conditions as before). The virus band (between 60 and 30% sucrose) was then collected with a 20 needle into a 3 ml

syringe, re-suspended in PBS with another needle and syringe and subjected to a last cycle of ultracentrifugation.

The concentrated virus stocks were aliquoted and stored at -80°C until titration by TCID50 assay and further use.

The steps for the production of viruses from BHK-21 cells in suspension culture were the same as previously described, without the cell lysis steps. BHK-21 cells were progressively adapted to a PEM suspension medium. On the day of the infection, the cell numbers were calculated, and $2x10^6$ cells in 750mL were infected with the masterbank from the needed virus at an MOI of 0,0001. After 48 hours, the content of the flask was centrifuged at 1000rcf for 15 minutes, the cell pellet discarded and the supernatant saved for further processing.

4.2.2.2. ECM-degrading viruses

Several recombinant "armed" versions of rVSV-NDV, expressing extracellular matrix-degrading viruses were previously engineered, rescued and characterized in human PDAC cell lines.

The first variant expresses the sperm adhesion molecule 1 (SPAM1), a hyaluronidase, and was amplified from RNA isolated from human testis tissue by RT-PCR. The second variant's cDNA was extracted from the metastatic breast adenocarcinoma cell line MDA-MB-231 (ATCC HTB-26) and expresses a collagenase, MMP8 (matrix metalloproteinase 8). The third vector expresses a hormone, Relaxin2, which was obtained from T-47D (ATCC HTB-133), an infiltrating ductal carcinoma of the breast cell line.

The transgenes were expressed as additional transcription units between the genes expressing hemagglutinin-neuraminidase (HN)) and large polymerase (L). Recombinant vectors were rescued by an established method of reverse genetics[144].

4.2.3. *In vitro* infections

4.2.3.1. Viability and cytotoxicity assays

Cell viability was determined using the Promega CellTiter-Glo® Luminescent Cell Viability Assay. It quantifies the ATP contained in metabolically active, viable cells, upon lysis, which is why it was used as an end-time point assay.

After infection of the cells, the supernatant was discarded to remove the dead cells, and replaced by an equal mixture of resuspended reagent and cell medium, both at room temperature. The plate was then placed on a shaker at 300 rpm for 12 minutes, for the cell lysis. After careful removal of remaining air bubbles, the luminescence was measured by the GloMax® Discover Microplate Reader. The final values were calculated as a percentage in relation to the uninfected wells.

The CytoTox 96® Non-Radioactive Cytotoxicity Assay was used to quantify the amount of LDH (lactate dehydrogenase), a cytosolic enzyme released upon cell lysis, in the supernatant. Therefore, aliquots of supernatant could be collected for measurement at multiple time-points over the course of an experiment. The samples were collected and transferred to a 96-well plate and frozen at -80°C to enable a single reading at the end of the experiment.

The thawed supernatant was mixed with an equal volume of resuspended reagent and left to react for 30minutes. After incubation, the reaction was interrupted with a stopping solution and the absorbance measured by the plate reader. All results were calculated as a percentage in relation to a maximum release control, which was a well of lysed, untreated cells.

4.2.3.2. Half maximal effective concentration (EC50)

In our case, the EC50 assay was used to help determine which concentration of virus was sufficient for killing half of a cell population at 72 hours post-infection. The cells were seeded in flat, white-walled, transparent-bottomed 96 well plates

and infected in half-logarithmic concentrations of virus (MOI from 0,0001 to 10) 24 hours after seeding. Cell viability was determined by CellTiter-Glo assay as described above after 72 hours. In experiments involving the use of an inhibitor, the inhibitor was added to the medium 6 hours post-seeding, and the infection and cell viability analysis was performed as described.

4.2.3.3. TCID50 and growth curves

Growth curves were plotted as a function of virus titre measurements performed using the medium collected from infected cell lines at 0, 16, 24, 48 and/or 72 hours post-infection.

The cells were seeded in 24-well plates on day 1 and infected on day 2, exactly 24 hours after seeding. Before the infection, the supernatant was carefully aspirated from the wells, saved, and replaced by a low volume of 300 µL of virus diluted in PBS containing magnesium and calcium for a one-hour infection. Next, the PBS was aspirated, and the wells washed twice with a 700 µL of PBS, to remove the excess of virions which was not taken up by the cells. The saved supernatant was then transferred back into the original wells and the first sample for TCID50 was taken (time-point 0 hour) and frozen at -80°C for a later titration. Further sampling was performed at defined time-points.

The 50% tissue culture infective dose (TCID50) assay was performed in order to quantify infectious virus titres. Serial dilution of the collected sample are prepared in quadruplicate and added to a monolayer of virus-sensitive AGE1 cells. 72 hours later, the plates were assessed by microscopy for signs of infection, and the results are analysed using the Spearman & Kärber algorithm, in order to determine the concentration of infectious virus particles in each sample.

4.2.3.4. Co-culture experiments

4.2.3.4.1. Conditioned media experiments

To create the conditioned media, the cells were plated in 6-well plates for 72 hours. The supernatants were then collected, centrifuged for 5 minutes at a speed of 500 RCF, passed through a 0,2 µm strainer, and frozen at -80°C, as schematized in Figure 8.

After seeding the cells with 600 µL of fresh medium in 24 well plates for the experiment, 600 µL of conditioned media was added: this ensured the delivery of necessary nutrients during the experiment, while exposing the cells to the secreted factors released by the other cell line.

The infection took place 24h post-seeding: the mixed supernatant was collected and kept aside for the infection at MOI 1 of VSV-NDV-GFP to take place in a low volume of PBS with calcium and magnesium, for one hour. The well was then washed twice with PBS, and the saved conditioned media put back into the corresponding well.

Aliquots of supernatant were collected from each well at time-points 0, 24, and 48 hours, and a final cell viability assay was performed at the end of the experiment. Figure 9 summarizes the experimental design of this experiment.

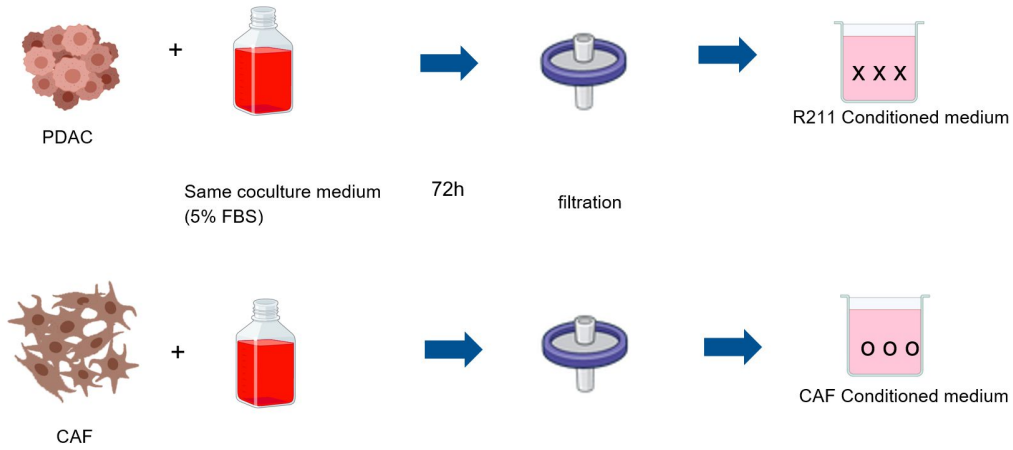

Figure 8: Preparation of conditioned media. *Created with Biorender.com*

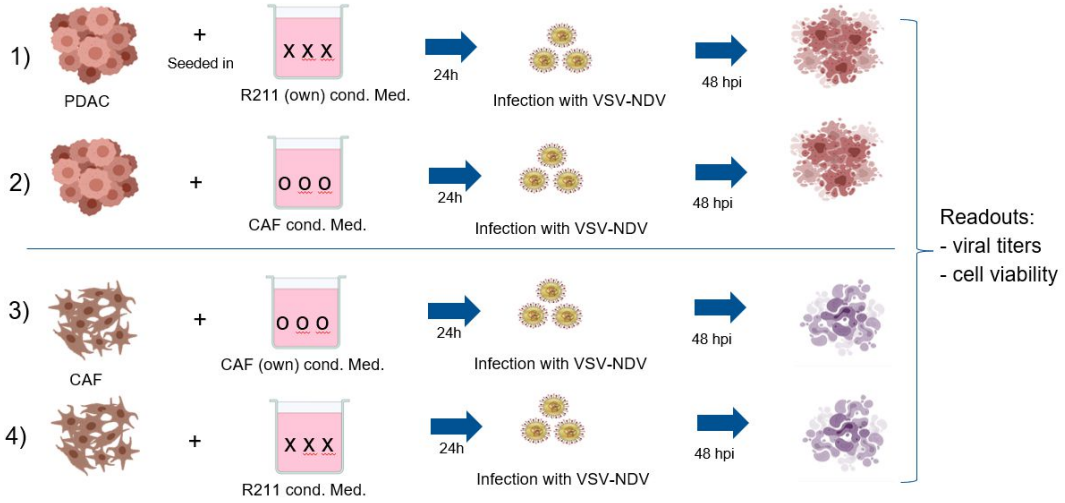

Figure 9: Experimental design for the conditioned media experiments**.** *Created with Biorender.com*

4.2.3.4.2. Direct coculture experiment

In this experiment, the cell lines were each cultured within their own medium, until the splitting day. Then, the cells were trypsinized, resuspended into the 5% FBS coculture medium and seeded at a ratio of 1:3 (PDAC:CAF). When inhibitor was included, it was added 6 hours post-seeding. The infection, sample taking and cell viability assay were done similarly to the conditioned media experiment. Figure 10 sums up the different conditions of this experiment.

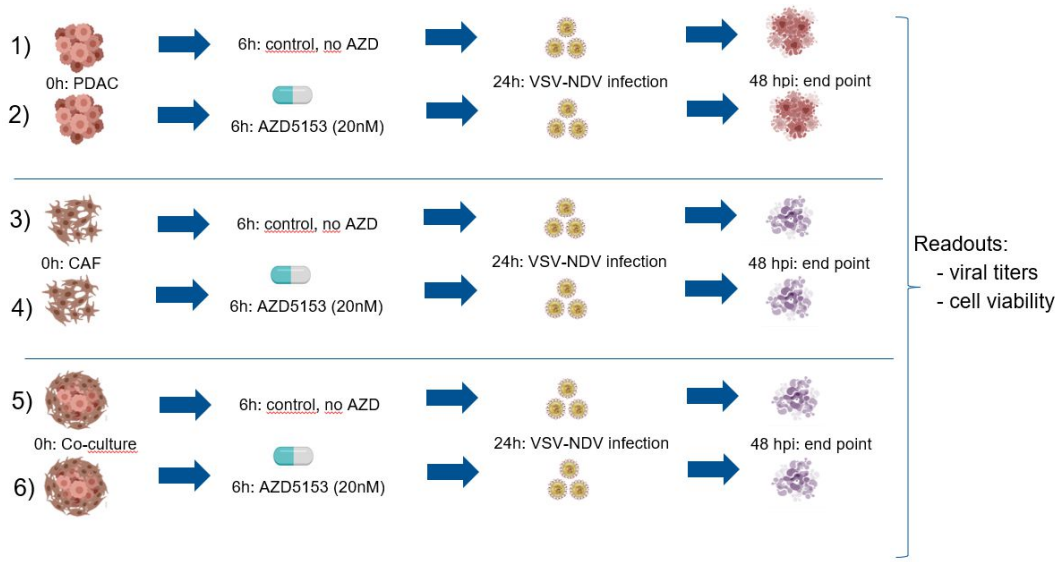

Figure 10: Experimental design for the direct co-culture experiments. *Created with BioRender.*

4.2.3.5. Inhibitors

The inhibitors were always added 6 hours post-seeding to the medium of the cells. The subsequent infections would take place normally as described for each individual experiment.

4.2.4. Microscopy

All the microscopic images were captured with the microscope Axiovert 40CFL and the objectives LSM700 5, 10, 20 x from Zeiss.

4.2.5. CRISPR-Cas9

Two murine PDAC cell lines, B191 and R211, were engineered to generate a Bromodomain 4 knock-out, in order to confirm the mechanism of action of the AZD5153 inhibitor.

The process can be divided into three steps: first, the preparation of the guides, second, the production of the lentivirus and third, the transduction of the cells.

The primers for human BRD4 [145] were:

Forward GAGCTACCCACAGAAGAAACC

Reverse GAGTCGATGCTTGAGTTGTGTT

After adaptation on ChopChop®, the following sequences of oligonucleotides were ordered by Eurofins:

Forward1: 5'- CACCGGATTTCTCAATCTTGTCCCA -3'

Forward2: 5'- CACCGTGTCTACGGAGAGCGGCCCT -3'

Forward3: 5'- CACCGTGGGATCACTAGCATGTCTA -3'

Reverse1: 3'- AAACTGGGACAAGATTGAGAAATCC -5'

Reverse2: 3'- AAACAGGGCCGCTCTCCGTAGACAC -5'

Reverse3: 3'- AAACTAGACATGCTAGTGATCCCAC -5'

The oligos were prepared with the master mix (respectively 1µL of forward and reverse primer, 1µL of T4 ligation Buffer (10x) from Thermofischer, 7 µL of distilled H2O) and placed in the thermocycler for annealing with T4 ligase, following a ramping down PCR protocol going from 95°C to 20°C at 0,1°C per second.

The guides were then ligated into the pLentiCRISPRv2 plasmid, according to the *Sanjana N. et al* [146]protocol, at the restriction site BsmBI.

The three plasmids were subsequently sent to Eurofins for validation through Sanger sequencing, using their U6_fwd primer: 5'-GAGGGCCTATTTCCCATGATTCC-3'.

For the second phase, HEK-293T cells were transfected at a 4:2:1 ratio, respectively, with: the transfer vector pLentiCRISPRv2 (Addgene #52961), the viral packaging psPAX2 (Addgene #12260) and the viral envelope pMD2G expressing a VSV-G surface receptor (Addgene #12259), and the pooled combination of all 3 BRD4 plasmids. After 72 hours of incubation, the supernatant containing the lentiviruses was collected, spun down, filtered and stored at -80°C.

For the last step, the transduction, the lentivirus solution at MOI 1 was added with polybrene at a concentration of 8µg/mL to the PDAC cell line, in its medium and left overnight. The following morning, the edited cells were selected through the addition of puromycin at a concentration of 5 µg/mL for B191 and 10 µg/mL for R211.

Surviving single cell colonies were then picked manually under a microscope and cultured individually.

After sufficient expansion, the selected knock-out candidates were first analysed by Western-blot for the expression of BRD4, followed by PCR and eventually sent to Eurofins for Sanger sequencing validation. The results were finally analysed with the help of Synthego ICE Analysis tool (v3)[147].

4.2.6. BCA assay and Western Blot

To detect the Bromodomain protein 4 in the edited cell lines, Western blots were performed.

The cells were lysed on ice using RIPA lysis buffer containing protease inhibitor (Roche Complete® protease inhibitor cocktail) and phosphatase inhibitor (Roche PhosSTOP®), followed by sonication and centrifugation (15 min, 16000x g, 4°C). The protein concentration was measured from the supernatant (cleared lysate) with the BCA assay Kit from Pierce® against their pre-diluted BSA standards (Thermo Fischer). The bicinchoninic acid assay relies on two reactions: the reduction of Cu^{2+} to Cu^{+}, proportional to the protein amount present in the solution and its subsequent

chelation with bicinchoninic acid, which results in the purple colouring of the solution. The absorbance of the samples (at 749 nm) is compared to the standard curve established with the known solutions to obtain a value.

20µg of total protein was mixed with 6x Laemmli protein loading dye and denatured at 95°C for 5 minutes. Proteins were separated using SDS-Polyacrylamide gel electrophoresis alongside the ROTI® Mark TRICOLOR as molecular weight reference. Electrophoresis was conducted at 85 Volts for 30 minutes at the beginning and elevated to 110 Volts for a remaining 1,5 hour.

For protein transfer, the wet blotting method was used (80 Volts, 1 hour, with ice cooling of the buffer). Unspecific binding sites were blocked using 5% non-fat dry milk in TBS-T (Tris buffered saline with 0,1% Tween-20), at room temperature for at least one hour.

After this step, the membrane was briefly rinsed with dH_2O and then incubated with the primary antibody (Rabbit anti-BRD4 recombinant monoclonal antibody [BL-151-6F11] from Novus Biotechne, for human or mouse BRD4) diluted at 1:1000 in 2,5% BSA in TBS-T at 4°C overnight.

To remove the unbound antibodies, a six times 10 minute wash cycle in TBS-T followed, preparing the membrane for the incubation with the HRP coupled secondary antibody (AB 10015282 from Jackson Immunoresearch), at a 1:10 000 dilution in 2,5% BSA in TBS-T for at least one hour.

Finally, the membrane was washed again 6 times, prior to the detection reaction (ECL Prime Western Blotting Detection Reagent®) from GE Healthcare Amersham. The visualization of the protein bands was carried out with the ChemiDoc XRS+ imager and ImageLab software from Biorad.

4.2.7. DNA isolation, Polymerase Chain reaction (PCR) and sequencing

To further validate the BRD4 CRISPR knockouts, DNA sequences covering the sgRNA binding and cas9 cut sites were amplified using polymerase chain reactions and Sanger sequencing, as described below.

Firstly, the DNA had to be isolated from the edited single cell clones: after a PBS wash, cells were incubated with DNA extraction buffer containing proteinase K for at least 10 minutes at 57°C, followed by heat inactivation of the enzyme at 95°C for 10 min.

Secondly, the DNA had to be precipitated by adding 0,7x Volumes of 100% isopropanol and incubating for a minimum of 15 minutes at room temperature. The tube was then centrifuged (13000 rpm, 10min). The DNA precipitate was then washed with 70% ethanol, centrifuged again and the purified, air-dried DNA pellet was then resuspended in nuclease free water and incubated at 50°C for 15 minutes to help solubilization.

Two pairs of primers flanking the sgRNA binding sites on exon 3 were designed to amplify the CRISPR cas9 cut sites:

BRD4_Exon3_1_fwd: 5'- TACTGCCCCTCATCACCAAGCC -3'
BRD4_Exon3_1_rev: 3'- AGGCCCTGTCCAGATGGCTACT -5'

BRD4_Exon3_2_fwd: 5'- TCTTTGGAATCTGCAGCCAGGGT -3'
BRD4_Exon3_2_rev: 3'- ACCATCTCACCAGCCCTCCTGT 5'

The detailed thermocycler protocol for the BRD4 edited cell lines was:

Start at 95°C for 15 minutes (polymerase activation), then 95°C for 30 seconds (denaturation or separation of the strands through heat), 60°C for 30 seconds (annealing of the primers to the template), 72°C for 60 seconds (elongation of the targeted sequences with free nucleotides), 30 times repetition and finally 10 minutes at 72°C.

After this amplification, a 5µL aliquot of the PCR products was mixed with 6x loading DNA dye (New England Biolabs) and separated on a 2% Agarose gel containing Midori Green Advance DNA stain® (Nippon Genetics) for half an hour at 120 Volts. The resulting primers should yield a 563 bp (exon 3_1) and 595 bp (exon 3_2) product in the wildtype, unedited sample, and smaller fragmented products if the CRISPR/cas9 gene editing of BRD4 was successful. The DNA gel was imaged using the BioRad imager with the ImageLab Software.

The remaining PCR product (30µL) was purified using QIAquick PCR clean up kit® from Qiagen. DNA was eluted in 40µL nuclease free water and the DNA content was measured on a Nanodrop spectrophotometer (ThermoFisher). 10 ng of the purified PCR product were sent for Sanger Sequencing (Eurofins genomics) using the same forward primer as for the PCR reaction. Mutations covering the exon 3 of BRD4 were validated and compared to the reference sequence using Benchling online software.

4.3. ANIMAL EXPERIMENTS

4.3.1. Animal facility

All animal experiments were conducted in agreement with protocols approved by the institute's Center for Preclinical Research and the regional government commission for animal protection (Regierung von Oberbayern, Munich, Germany.) File numbers: ROB-55.2.2532.Vet_02-18-148 and ROB-55.2.2532.Vet_02-22-48.

The mice (C57/BL6J) were held under specific pathogen free conditions, in SafeSeal Next Greenline IVC cages from Tecniplast Typ GM500 with HEPA filters, at a density respecting the EU directive 2010/63. Each cage was furnished with red polycarbonate houses, bedding material (autoclaved cotton) and chewing wooden sticks (Select fine from Ssmiff). Food pellets (Nr 1324 from Altromin international) and autoclaved water were offered ad libitum during the whole experiment.

Finally, the wellbeing of the mice was assessed visually by the animal care keepers, on a daily basis.

4.3.2. Cells preparation for the implantation

An aliquot of R211 cells was thawed 14 days before the operation day and split regularly upon reaching a confluence of around 90%. The cells were last split 48h prior to the implantation in order to reach a confluence of approximately 85%.

On the implantation day, supernatant was discarded and the cells were washed with PBS. After removal of the PBS, the cells were incubated at room temperature in Accutase® from Sigma-Aldrich, until detachment from the flask. The process was stopped by adding PBS and centrifuging at 500g for 5 minutes at room temperature. The cell pellet was resuspended in PBS again and centrifuged the same way, for a total of three wash cycles. The cells were then counted and resuspended in PBS in order to reach a concentration of 2500 cells per µL and placed on ice.

4.3.3. Experimental design

All *in vivo* experiments were performed on immunocompetent 7 to 8 weeks old male immunocompetent C57/BL6J mice (Janvier Labs, Le Genest-Saint-Isle, France), after at least one-week acclimation period following their arrival.

4.3.4. Orthotopic implantation of PDAC cells

Inhalation anaesthesia was administered with isoflurane (induction with 3%, maintenance with 1,5%). Ointment was applied onto the eyes to prevent against dehydration. Analgesia was covered by the administration of metamizole (200mg/kg p.o.) and buprenorphine (0,05mg/kg sc.) 30 minutes prior to surgery, followed by buprenorphine every 8 hours over 36 hours (ROB-55.2.2532.Vet_02-

18-148); or buprenorphine sc. (0,1mg/kg sc.) and meloxicam sc. (5mg/kg sc) every 12 hours, over 36 hours (ROB-55.2.2532.Vet_02-22-48).

The left flanks of the animals were shaven to facilitate the visualisation of the spleen and to avoid fur from entering the surgical opening. The left flank subcostal incision was chosen to access the abdominal cavity and allow the extracorporealization of part of the spleen and pancreas. Using an atraumatic ring forceps, the caudal part of the spleen was delicately placed extra-abdominally on a sterile gauze compress. The exposed pancreatic tail was then held with a fine-tipped forceps, while the cells (in 10 µL of PBS) were injected with a Hamilton syringe. The injection canal was created as long as possible carefully avoiding major vessels, to prevent leakage. Afterwards, the pancreas was gently returned to its original location in the peritoneum. Two layers of sutures were applied with resorbable suture material (Ethicon coated Vicryl® V303H): one with the peritoneum and muscle layer, one with the subcutaneous and cutaneous layers.

4.3.5. Magnetic resonance imaging (MRI)

For magnetic resonance imaging to visualize tumours, the mice were anesthetized using isoflurane as described in the previous section. The animal was then placed in a dStream wrist coil and imaged with the NanoScan® PET/MRI 3 Tesla from Mediso. The temperature of the bed and the breathing frequency of the mice were monitored with the Multicell Gui v2.5b software and sensors on the bed. The images were locally visualized in Nucline NanoScan® (version 3.04.025.0000) for control and exported under DICOM format. The MRI images were then analysed with ITK-Snap (Version 3.8.0)[148] software, and the volume of the tumours was calculated (with the segmentation tool of the program, with manual contouring of the tumours) in order to evenly distribute the mice between the experimental treatment groups. The mice showing exclusively intraperitoneal tumours were excluded, as well as outliers (displaying tumours at least 3 times bigger than the group's average).

Due to technical issues, two experiments had to be conducted without the possibility to scan all or some of the animals. In these cases, manual palpation under isoflurane for muscle relaxation was performed, and the animals were randomized according to these findings. The day 1 of the kinetics experiment was randomized exclusively through palpation, and half the mice of the AZD5153 survival experiment were randomized solely through palpation (the other half was scanned and palpated).

4.3.6. Preparation of the virus

The viruses, stored at -80°C, were thawed and diluted in PBS on the day of each injection, to reach a dose of either $1*10^7$ TCID50 (infectious virions) or $1*10^8$ TCID50 per mouse. The preparation was kept on ice until injection.

The injection volumes differed according to the chosen route: intravenously, each mouse received 100 µL; intraperitoneally, each mouse was given 400 µL.

4.3.7. Preparation and administration of AZD5153

The aliquot of AZD5153 was purchased from MedChemExpress (Nr: HY-100653A). After complete dilution in DMSO to reach a concentration of 34mg/mL, the vehicle (filtered 0,5% CMC-Na) was added to reach a concentration corresponding to 30 mg/kg of AZD5153 per mouse. For reasons of compound stability, the premixed vehicle with DMSO or vehicle with DMSO and inhibitor were frozen in Falcon tubes, at -20°C. Each week, a new pre-dosed Falcon was thawed and stored in the fridge for use during that week.

The doses of AZD5153 in vehicle or DMSO in vehicle were administered 3 times each week by oral gavage, starting on day 0, over a period of 21 days. Each mouse received 200 µL for each dose.

4.3.8. Survival experiments

After randomization through imaging, the mice received 4 injections of virus or PBS via the tail vein at the following time-points: day 0 (starting one day post imaging), day 3, day 7 and day 14. The well-being of the mice was evaluated at least two times a week with the aid of scoring sheets, and they were sacrificed upon reaching the end-of-experiment criteria.

The experiment with oral gavage of AZD5153 is described in 5.3.3.

4.3.9. Kinetics experiment and flow cytometry

The animals were implanted with tumours, scanned and randomized as described for the survival experiment. At the defined time points (day 1, day 4, and day 8) post-treatment, animals from each treatment group were sacrificed for tissue analysis.

The extracted spleens were minced and mashed through a 100 µm strainer, put in solution with Red Blood Cell lysis buffer (Biolegend) for 10 minutes, the reaction stopped with PBS, centrifuged for 5 minutes at 500g and plated for staining.

The other organs, namely livers, pancreatic lymph nodes and tumours required more preparation steps before the staining. First, they were minced and digested with either 0,063mg/mL collagenase (livers) or 0,02mg/mL liberase (PDAC tumours) for 30 minutes at 37°C, then filtered through a strainer (30 µm for the lymphnodes, 100µm for the rest). The resulting mass was washed twice with PBS and pelleted by centrifugation. A percoll gradient was prepared, and the samples were layered in the upper 40% layer. After centrifugation, the band between the 40 and 60% layer, containing the immune cells, was gently isolated, washed twice in PBS, repelleted and finally plated for further staining.

The extracted immune cells were plated and stained using FcR Blocking Reagent (mouse) from Miltenyi Biotech for 30 minutes, followed by incubation at room

temperature with one or more antibodies, washed again and analysed in the CytoFlex platform. The antibodies used, the detection fluorochrome, manufacturer, and dilution are listed in Table 5.

The flow-cytometry graphics and analysis were conceived in collaboration with Sonja Glauss, using the FlowJo™ v10.8 Software (BD Life Sciences).

Table 5: List of antibodies used for flow-cytometry.

Target	Product	Fluorochrome	Manufacturer	Dilution
CD3	Clone REA641	FITC	Miltenyi	1:300
CD8a	53-6.7	PE	Biolegend	1:300
CD4	GK1.5	PerCP	Biolegend	1:300
NK-1.1	PK136	APC	Biolegend	1:300
CD11c	N418	Brilliant Violet 421	Biolegend	1:300
KLRG1	2F1/KLRG1	PE/Dazzle 599	Biolegend	1:300
CD279		Brilliant Violet 605	Biolegend	1:300
CD69	H1.2F3	PE/Cyanine 7	Biolegend	1:300
F4/80	BM8	APC/Cyanine7	Biolegend	1:300
Viobility		405/520	Biolegend	1:300
CD49b	DX5	PB	Sony	1:300
CD69	H1.2F3	Brilliant Violet 605	Biolegend	1:300
NK-1.1	PK136	Brilliant Violet 650	Biolegend	1:200
NKG2D	CX5	PE/Dazzle 599	Biolegend	1:300
Granzyme A	3G8.5	PE	Biolegend	1:300
CD11b	M1/70	PerCP/Cyanine 5.5	Biolegend	1:300

IFNgamma	XMG1.1	PE/Cyanine 7	Biolegend	1:800
CD49a	REA493	FITC	Miltenyi	1:300
CD3e	145-2C11	APC/Cyanine7	Biolegend	1:300
CD19c	1D3/CD19	APC/Cyanine7	Biolegend	1:300

4.4. STATISTICAL ANALYSIS

Data were analyzed using GraphPad Prism 10 (GraphPad Software, San Diego, CA). When experiments were repeated, means and standard of errors (SEM) were plotted, otherwise means and standard deviations were shown.

Data was analyzed for normal distribution by Shapiro-Wilk test, and statistical significance was determined by two-way anova or unpaired t-tests (flow cytometry). All survival experiments were plotted using Kaplan-Maier survival curves and analysed by logrank-test.

A confidence interval of 95% was applied to determine significance. Hence, p values under 0,05 were considered statistically significant, according to this rule: * $p < 0.05$ (significant), ** $p < 0.01$ (very significant), ***$p < 0.001$ and **** $p < 0.0001$ (extremely significant).

5. RESULTS

5.1. *IN VITRO* EXPERIMENTS

Preliminary tests were conducted *in vitro* in order to characterize the oncolytic virus and combination therapies in mouse PDAC cell lines prior to testing them *in vivo*.

5.1.1. Infection of PDAC cells

5.1.1.1. Comparison of VSV-NDV with its parent viruses

Two mouse CKP pancreatic adenocarcinoma cell lines were infected with VSV, NDV and VSV-NDV *in vitro*, to compare virus replication kinetics. As can be seen in the pictures (Figure 12 and 14), only NDV and VSV-NDV were forming syncytia. Two concentrations were used for each virus: MOI 1 (one virus particle per seeded cell) and MOI 0,1 (1 virus particle per 10 seeded cells), to demonstrate possible dose-dependent effects. For the cell viability and cell toxicity assays,

Figure 11 presents the data produced by the infection of CKP530202 cells by CellTiter Glo and LDH assays of cell viability, and the TCID50 method of quantifying infectious virus titres.

In CKP530202 cells, the cell viability decreased over 72 hours for all conditions: in general, the higher the MOI, the lower the viability of the cells. In this assay, at the end time-point, VSV at an MOI of 1 resulted in the lowest value, followed by VSV-NDV at MOI 1, VSV-NDV at MOI 0,1 then VSV at MOI 0,1 and finally NDV at MOI 0,1 and NDV at MOI 1. Only VSV was clearly causing more damage to the cells in an MOI dependent manner; for the other viruses, the differences were subtler. There was a slight increase in viability for NDV0,1 at 48 hours, negligible considering the error bars.

As expected, cell cytotoxicity increased over time, with more toxicity observed in higher MOIs. Again, VSV had the most potent effect of all 3 viruses on this cell

line, followed by NDV and VSV-NDV at 48 hours, but with more cell death from VSV-NDV than NDV at 72 hours.

The growth curves depicted a dose-related replication, with higher viral MOIs producing more viral particles in VSV and NDV than in VSV-NDV, where there was barely any replication to be seen. The VSV replication began very powerfully for MOI 1, reaching its peak after 24 hours, and maintaining its level over time, while MOI 0,1 followed a steadier course, finally catching up with MOI 1 at 48 hours, and almost overhauling it at 72 hours post-infection with 10^9 TCID50/ml. NDV replications were less impressive, reaching a peak concentration of 10^5 TCID50/ml. VSV-NDV, on the other hand, barely replicated in this cell-line, and just maintained its starting concentration of maximum 10^1 TCID50/ml.

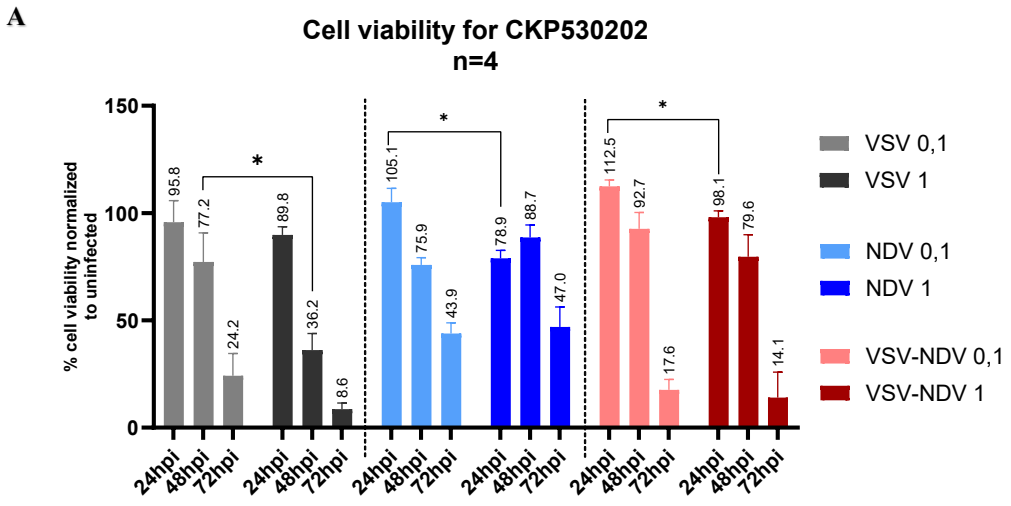

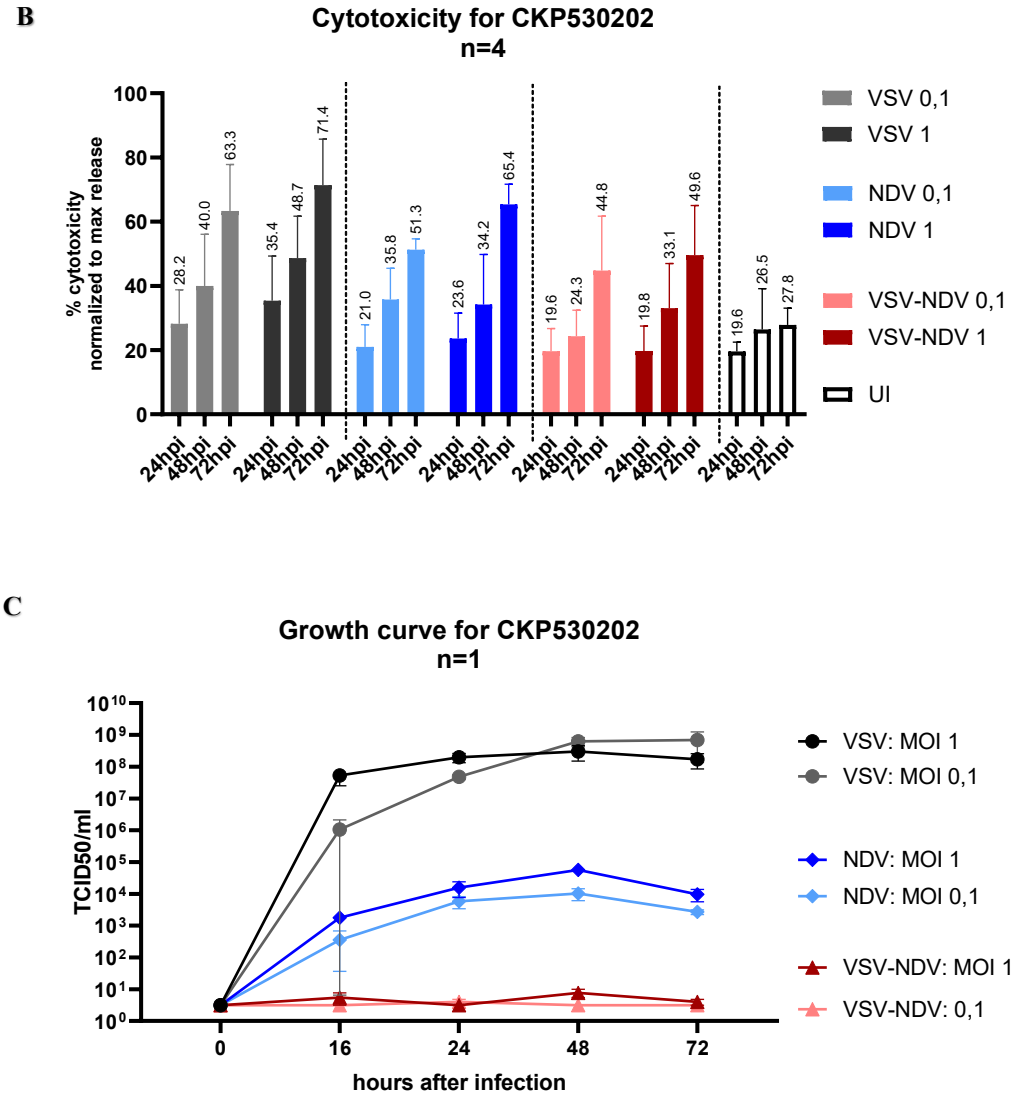

Figure 11: Comparison of VSV-NDV, VSV and NDV infection at different time points, with two different MOIs, in the murine PDAC cell line CKP530202**.** (A) Cell viability was measured by Cell Titer Glo in the adherent viable cells, after removal of the supernatant. Results were normalized to the uninfected cells. Represented are standard error of the mean results (B) Cytotoxicity was measured via LDH concentration in the supernatant of infected. Results were normalized to a maximum release control. Represented are standard error of the mean results (C) Growth curves demonstrate replication of the viruses in supernatants at 0, 16, 24, 48 and 72 hours post-infection, as determined by TCID50, with standard deviations.

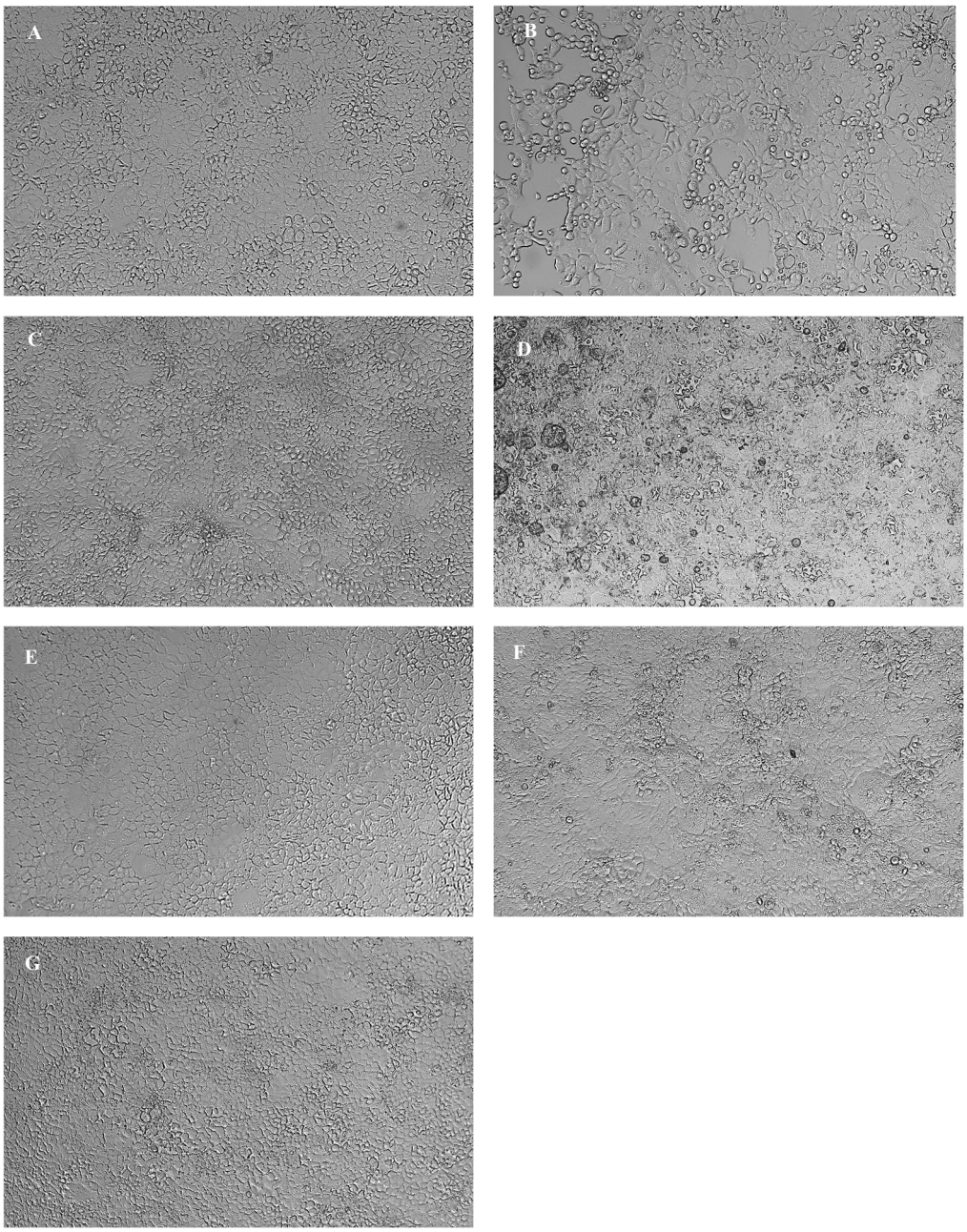

Figure 12: Microscopic pictures of the CKP530202 cell line at 48hpi (10x). (A) VSV: MOI 0,1 (B) VSV: MOI 1 (C) NDV: MOI 0,1 (D) NDV: MOI 1 (E) VSV-NDV: MOI 0,1 (F) VSV-NDV: MOI 1 (G) Uninfected.

For CKP110299, similar trends were observed, as shown in Figure 13. VSV was the virus decreasing cell viability the fastest in an MOI-dependent manner, while NDV and VSV-NDV were lagging behind. For the two fusogenic viruses, the cell

viability drop, linked to the viral concentration, was only visible at 72 hpi. In contrast to the CKP530202 line, VSV-NDV performed better than NDV at an MOI of 1 in these cells.

The cytotoxicity values also increased alongside the MOI and replication time for the viruses: VSV being the most oncolytic, followed by NDV and finally VSV-NDV. Interestingly, NDV infected cells died in a steadier fashion over time, than VSV-NDV infected ones, whose cytotoxicity factors suddenly rose at 72hpi. The cytoxicity of the control wells also increased over time to reach over 50%, which most likely signalled overconfluency of the cells.

The growth curves show a rather MOI-dependent replication, more marked for NDV and VSV-NDV than for VSV. VSV infected wells reached the highest titre of 10^9 TCID50/mL within 24 hours, with barely any difference between the two MOIs: when almost all cells are infected even at the lowest dose, there is little room for improvement. Both NDV MOIs peaked at a maximum value of 10^6 per mL, despite the advance of MOI 1 during the first 48 hours. VSV-NDV was again slower and replicated less, reaching a maximum of 10^6 TCID50 per mL for MOI1 48 hpi. Noticeably, NDV and VSV-NDV, both slower in replication show the greater difference dose-related difference, with an equalisation after 48 hpi for NDV. VSV-NDV 0,1 barely evolved from its starting value.

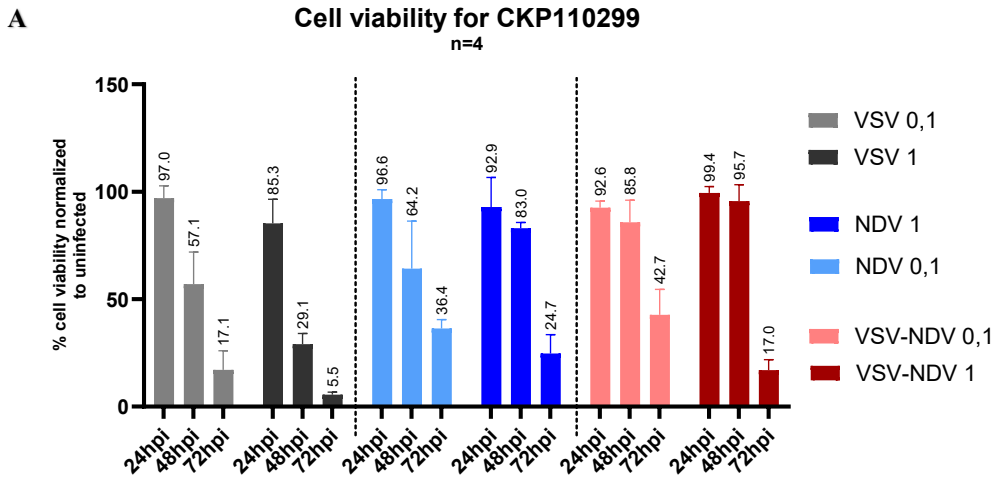

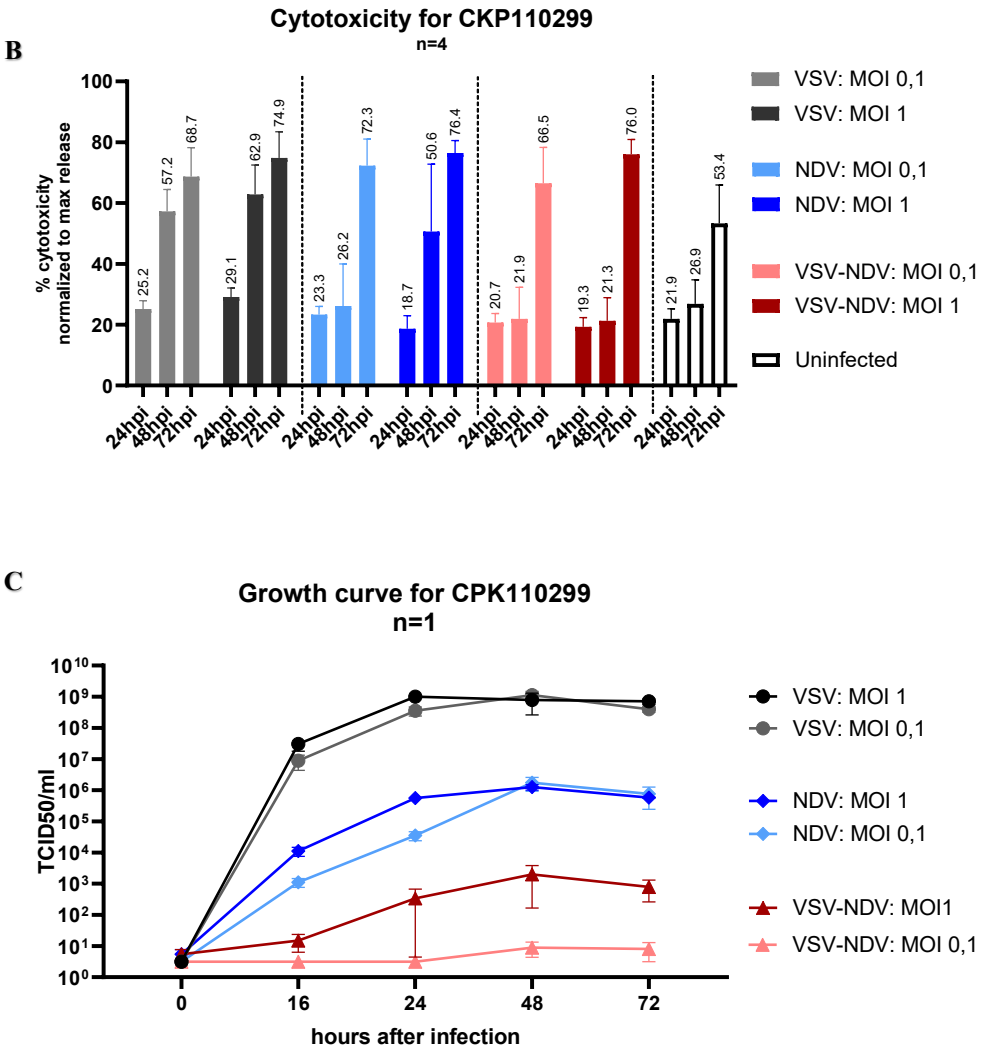

Figure 13: Comparison of VSV-NDV, VSV and NDV infection at different time points, with two different MOIs, in the murine PDAC cell line CKP110299. (A) cell viability was measured by Cell Titer Glo in the adherent viable cells, after removal of the supernatant. Results were normalized to the uninfected cells. Represented are standard error of the mean results (B) Cytotoxicity was measured via LDH concentration in the supernatant of infected. Results were normalized to a maximum release control. Represented are standard error of the mean results (C) Growth curves demonstrate replication of the viruses in supernatants at 0, 16, 24, 48 and 72 hours post-infection, as determined by TCID50, with standard deviations.

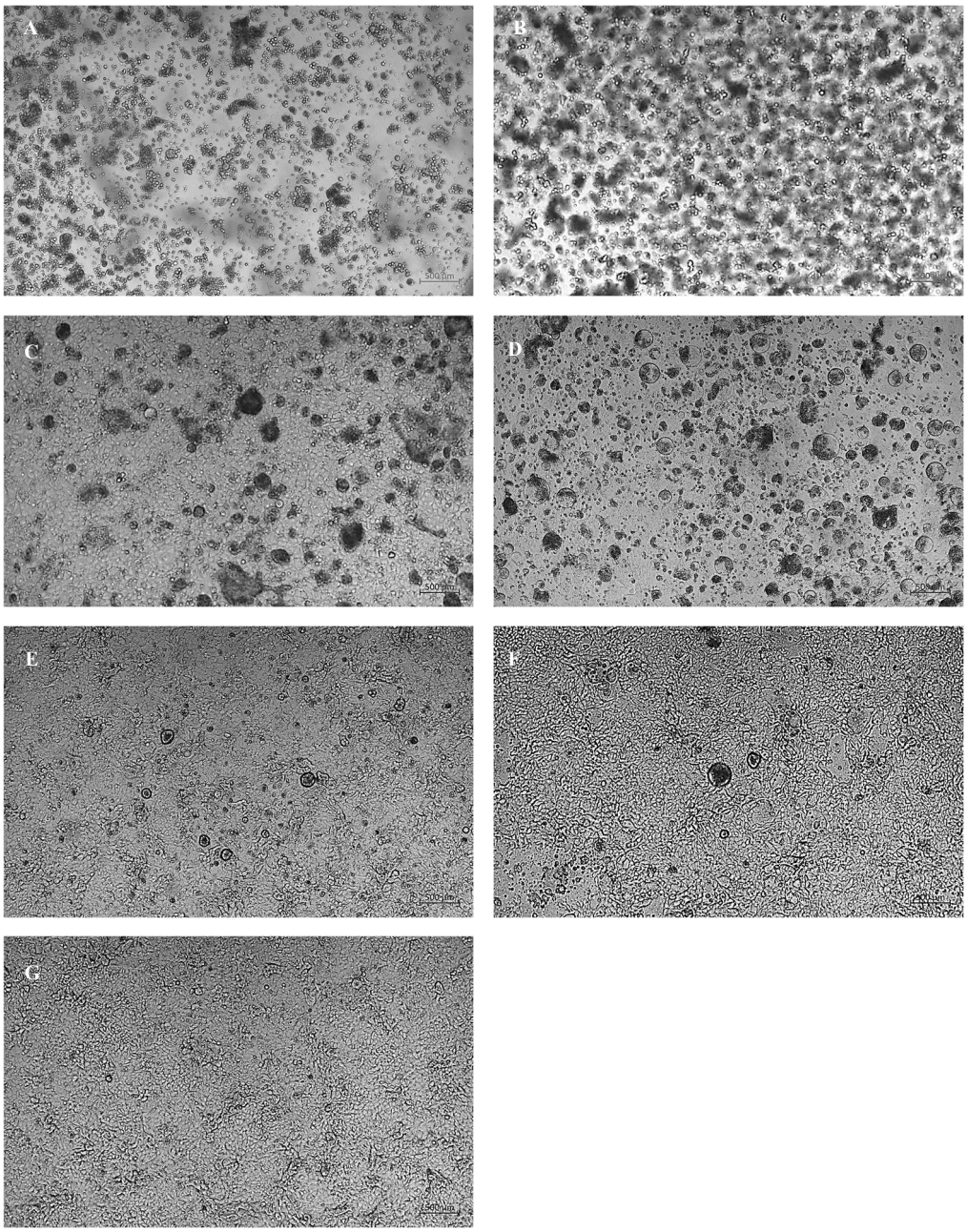

Figure 14: Microscopy of the infections at 72 hours post-infection for CKP110299**.** (A) VSV: MOI 0,1 (B) VSV: MOI 1 (C) NDV: MOI 0,1 at 72hpi (D) NDV: MOI 1 (E) VSV-NDV: MOI 0,1 (F) VSV-NDV: MOI 1 (G) uninfected cells.

Both PDAC cell lines showed similar responses towards the three viruses, CKP 110299 being slightly more susceptible to the hybrid virus than CKP530202. VSV proved to be the fastest virus to replicate and efficiently kill the cells, followed by NDV and VSV-NDV. The formation of syncytia probably slows down virus replication. The performance of VSV-NDV1 in CKP110299 demonstrated that the

virus doesn't need to reach concentrations as high as its parent viruses to exhibit efficiency, as was stated in a previous publication[102].

The hybrid virus therapy project required the use of a more susceptible cell-line, hence the following screening.

5.1.1.2. Testing cell lines with solely VSV-NDV

To test as many cell lines as possible, infection experiments were conducted in single wells of murine PDAC from different genetic backgrounds. Repetitions were only done for the more promising cell lines. The cells were seeded in 96 well plates, infected at decreasing MOIs and the results assessed visually by microscopy and by cell viability assay.

The cell lines tested and represented here can be divided into the following genetic background categories:

- KRAS driven, epithelial type: 8661, 8442, 9591, R211, S813, B191
- KRAS driven, mesenchymal type: 9091, 8513, 8028
- KRAS/Trp53 deleted, quasi-mesenchymal type: 13781
- KRAS/Trp53 mutated, epithelial type: 10232.

As can be seen in Figure 15, only R211, S813 and B191 were sensitive to VSV-NDV. Interestingly, these three cell lines share a similar genetic profile. In fact, out of five cell lines resembling R211 (the first susceptible cell line), four demonstrated sensitivity. However, it remains to be elucidated which genetic traits are responsible for a permissiveness to VSV-NDV and only a much larger screening could provide answers. The testing process was modified over time to finally assess cell viability at 72 hours post-infection, explaining the different time-points in the results.

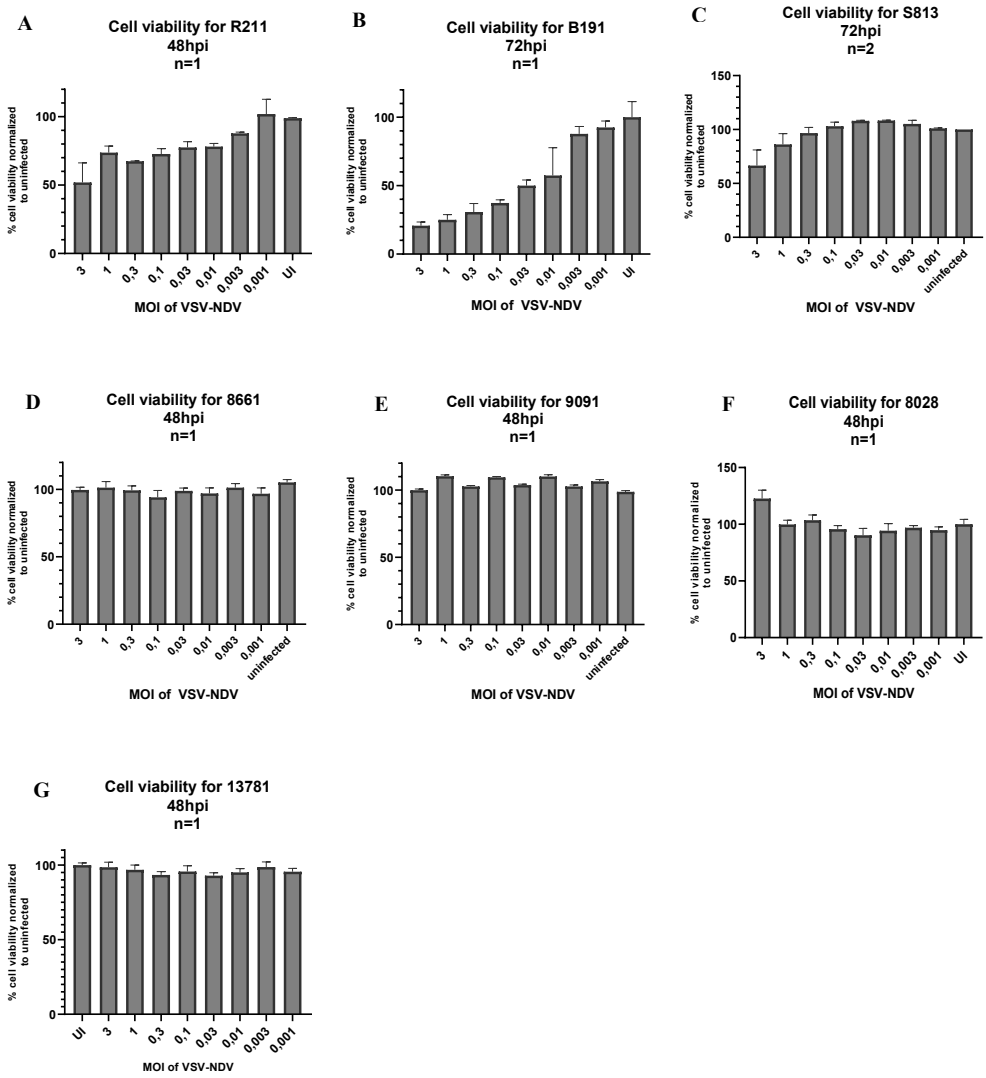

Figure 15: Infections of various murine PDAC cell lines with VSV-NDV, at MOIs between 3 and 0,001. Cell viability was measured by CellTiter Glo in the adherent viable cells, after removal of the supernatant. Results were normalized to the uninfected cells. (A-D) KRAS-driven cell lines of epithelial type: R211, B191, S813 and 8661. (E-F) KRAS-driven cell lines of mesenchymal type: 9091 and 8028. (G) KRAS/Trp53 deleted cell line of quasi-mesenchymal type: 13781.

In the end, R211 and B191 were selected for further studies. R211 stands as a moderately sensible cell line, and B191 as a sensitive cell line.

5.1.2. Cancer associated fibroblasts and extracellular matrix

5.1.2.1. CAFs experiments

The three cancer associated fibroblasts cell lines (CAFs) used in these experiments: PSC 806/10 (later called 806/10), PSC3 Prrx1 (later called PSC3) and FB 704F3 were isolated from mouse models genetically depleted of the transcription factor Prrx1, responsible for CAF plasticity, and remain constitutively activated[149].

Only one PDAC cell line was used, R211.

5.1.2.1.1. Conditioned media experiments

This experiment was designed in order to see if the factors secreted by cancer cells or CAFs under culture could mediate a crosstalk between the cell types, leading to effects on the infection of the other cell type.

Cell culture and experiment in 5% FBS

The cells were put under culture with a 5% fetal calf serum (FBS) coculture medium, so that the harvested supernatants also from 5% FBS conditions. This low FBS aimed at reducing potential interferences in the cell-to-cell communication.

As can be seen in Figure 16 A, the cell viability after infection of R211 cultured in PSC3-conditioned medium was lower than during a simple infection. The other experimental conditions did not show any significant difference in the infection potency, whether the cells were seeded in their own medium or in foreign conditioned medium. The measured viability of the PSC always remained very high.

In Figure 16 B, surprisingly, the viability drop observed for R211 in PSC3 did not correlate with a higher viral titre than for the R211 control (in its own medium). Indeed, none of the different conditions showed any significant effect on virus

titres. There was only a trend toward a better replication in PSC3 exposed to R211-conditioned medium.

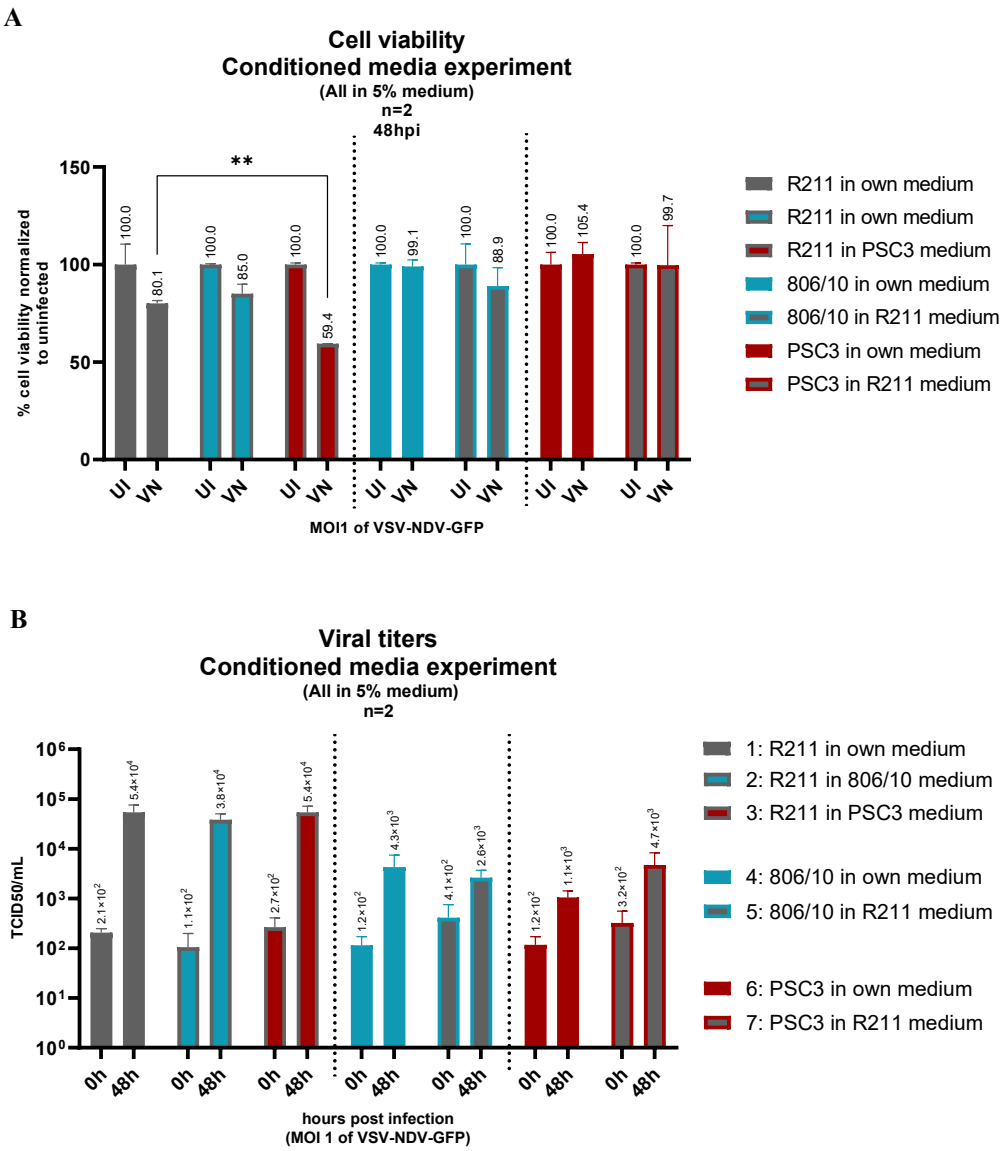

Figure 16: Comparison of the infections with the conditioned media, in PDAC or CAFs, all in 5% FBS medium (A) Cell viability assay by Cell titer Glo, on thehpi time-points (B) Evolution of the viral titres, calculated by TCID50, between the beginning and end of experiment (C) Growth curves demonstrate replication of the viruses in supernatants at 0, 16, 24, 48 and 72 hours post-infection, as determined by TCID50.

There were concerns about the low FBS culturing conditions of the cells, which may have impacted the experimental results by inducing stress. Therefore, this experimental set-up was aborted after the second repetition, to be repeated as follows, under “normal” cell culture conditions, and with low FBS medium used only during the experiment itself.

Normal cell culture, experiment in coculture medium

Fresh cells were thawed for this experiment and cultured in their “normal” respective medium. Once they divided normally, they were split, spun down and washed with PBS, before being resuspended in fresh 5% coculture medium. The same protocol as in 4.4.1.1 was then followed.

In these experiments (Figure 17 A), the cell viability assay showed no significant effect between the conditions. There was solely a trend for R211 cells in PSC3 medium, suggesting that secreted factors from PSC3 cells could sensitize R211 cells to VSV-NDV infection. As observed in the previous conditioned media experiment, the very high cell viability of the PSCs under infection wasn’t affected by the foreign conditioned medium.

As Figure 17 B demonstrated, the viral replication in all R211 conditions was relatively equal considering the error bars, and slightly higher titres for both cultures in CAF conditioned media. These results correlate with the viability assay. For PSC 806/10, titres were relatively stable between the conditions at 24 hours, but there was a feeble increase in the number of viral particles with the PDAC conditioned medium at 48 hours. For PSC3, the starting concentrations were much higher in the own medium than in the PDAC conditioned media, but over time the differences shrunk to a point where the differences were negligible, with the own media showing a lightly better replication.

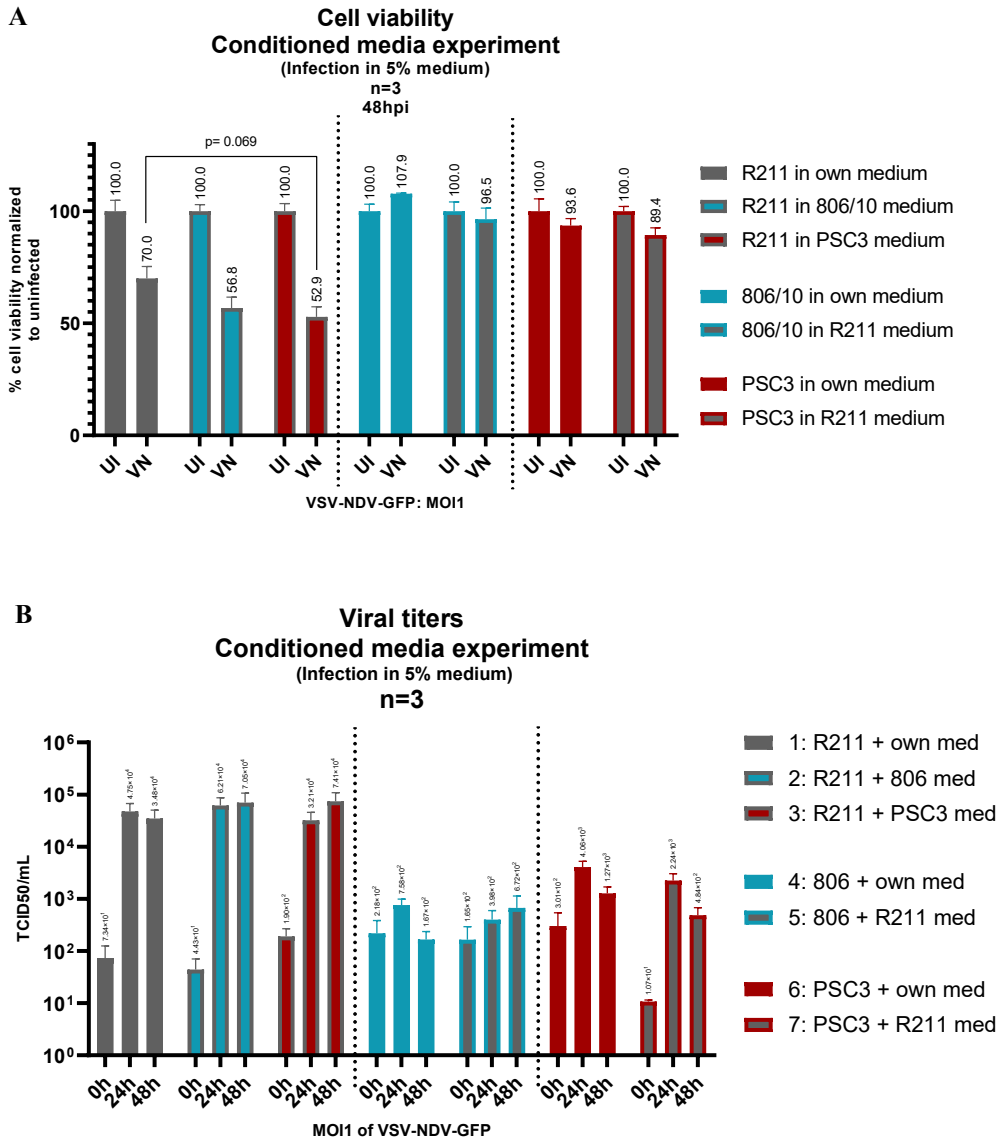

Figure 17: Comparison of the infections with the conditioned media, in PDAC or CAFs: the 5% FBS medium was used solely for the experiments (A) Cell viability assay by Cell titer Glo, at 48 hours post.infection, the end time-point (B) Evolution of the viral titres, calculated by TCID50, at 0, 24 and 48 hours post-infection.

The results of both conditioned media experiments suggested there might be some minor interactions between the PDAC cell line and the CAFs, but they were not entirely obvious. The set-up was designed as a "monologue", where only one cell type could "talk" to the other. Hence, it seemed logical to continue with the "dialogue" experiment, or the direct co-culture, in order to investigate whether direct cell-cell contact between tumour cells and CAFs might lead to a more profound impact on VSV-NDV replication.

5.1.2.1.2. Direct co-culture experiments

For this experiment, the same number of cells was seeded in all wells, monocultures (controls) or cocultures (ratio 1 PDAC for 3 CAFs). All cells were cultured in their classical conditions, until the start of the experiment, which took place in the 5% FBS coculture medium.

In Figure 18 A, the cell viability of the R211 PDAC cells under infection dropped to 68,8%, while the viability of the PSC806/10 and FB 704F3 remained relatively stable. The only CAF line showing susceptibility to infection was PSC3, with 88,6% viable cells remaining after 48 hours. The cocultures all showed some diminution of their viability under infection, and ranked as follows: R211 with PSC3 dropped in a synergistic, very significant manner to 49,9%, reaching the lowest viability of all conditions, while the cocultures with 704F3 and 806/10 attained titres that seemed to be an average of the values of their monocultures (higher than R211 alone yet lower than the CAFs on their own).

In Figure 18 B, the titres of the PDAC monoculture surged to $2x10^4$ after 24h and maintained this level until the end of the experiment. Both CAFs 806/10 and 704F3 saw their viral load sink over time, suggesting non-replication. On the other hand, PSC3, starting with higher levels than all the other conditions ($1x10^3$), let virus particles replicate until $3x10^3$, reaching their maximum at 24 hours post-infection, and dropped down to $4x10^2$. The titres in both 806/10 and 704F3 cocultures rose steadily, attaining similar titres of respectively $3x10^4$ and $2x10^4$ after 48 hours. Conversely, the viral titres in PSC3 coculture plummeted to $3x10^4$ (like the other co-cultures), but faster, after only 24 hours, before declining to $8x10^2$ at 48 hours. The reasons for this decline could be the exhaustion of uninfected cells, or a starting resistance mechanism.

In both experiments, 806/10 and 704F3 demonstrated analogous low infectability, which nevertheless didn't translate into lower viral titres. In comparison, the virus-sensitive PSC3 cell line allowed for a faster replication in mono- and coculture conditions, and displayed more lytic effects of the virus. It is unknown how the cell

ratios evolved over time with the different cell lines, so it is impossible to quantify its influence over the results.

Also, the mechanistics of this crosstalk remain a mystery, as the attempts to carry out both a FGF2 and TGF-β ELISAs failed.

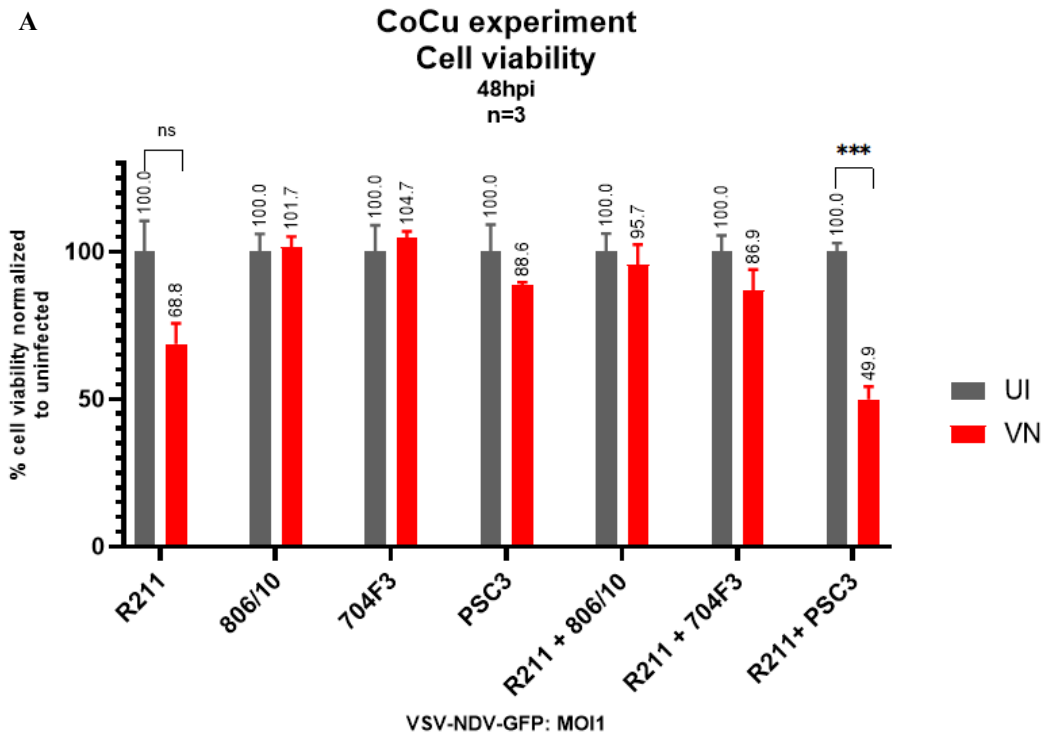

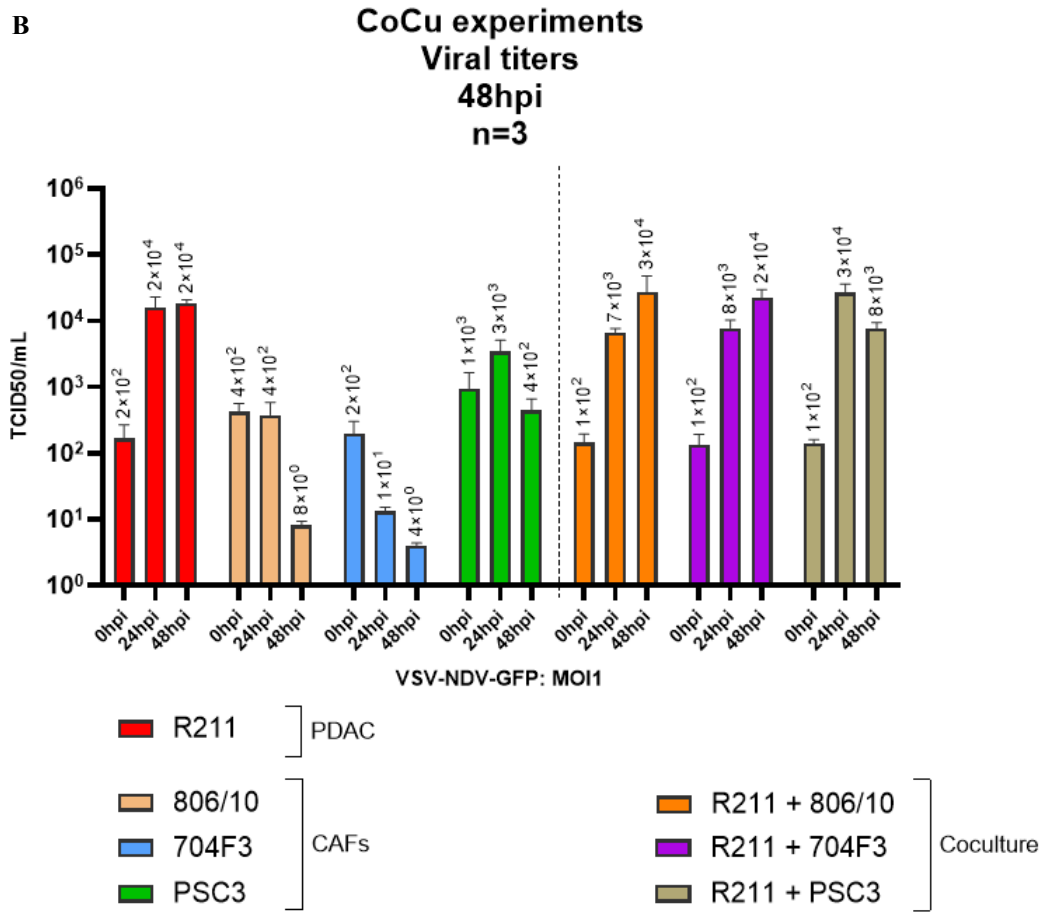

Figure 18: Comparison of the viral infection in PDAC and CAFs monocultures against their direct cocultures**.** (A) Cell viability assay by Cell titer Glo, at 48hpi, normalized to uninfected cells. The grey bars show the uninfected controls, the red bars their infected counterparts (B) viral titres at time-points 0, 24 and 48hpi, determined by TCID50.

5.1.2.2. ECM-degrading viruses

The three extracellular matrix degrading viruses (VSV-NDV-SPAM1, - MMP8 and -RLN2) developed for targeted PDAC therapy were tested *in vitro* on two murine PDAC cell lines, with cell viability assay as a quantifying tool.

As Figure 20 shows, the baseline infectivity of R211 with VSV-NDV gave an IC50 situated at MOI 3,47. Unfortunately, in this cell line, all three ECM-viruses failed to decrease its viability, which remained close to 100% independently of the MOI.

However, probably due to its higher sensitivity to the basic VSV-NDV virus (IC50 of 0,116), B191 showed more promising results, with VSV-NDV-MMP8 infection producing an IC50 of 2,51, although this is more than 20x more than that of VSV-NDV. The Relaxin2-producing virus only effectively decreased the viability of the cells at a very high MOI, and the activity of the SPAM1-expressing virus was negligible.

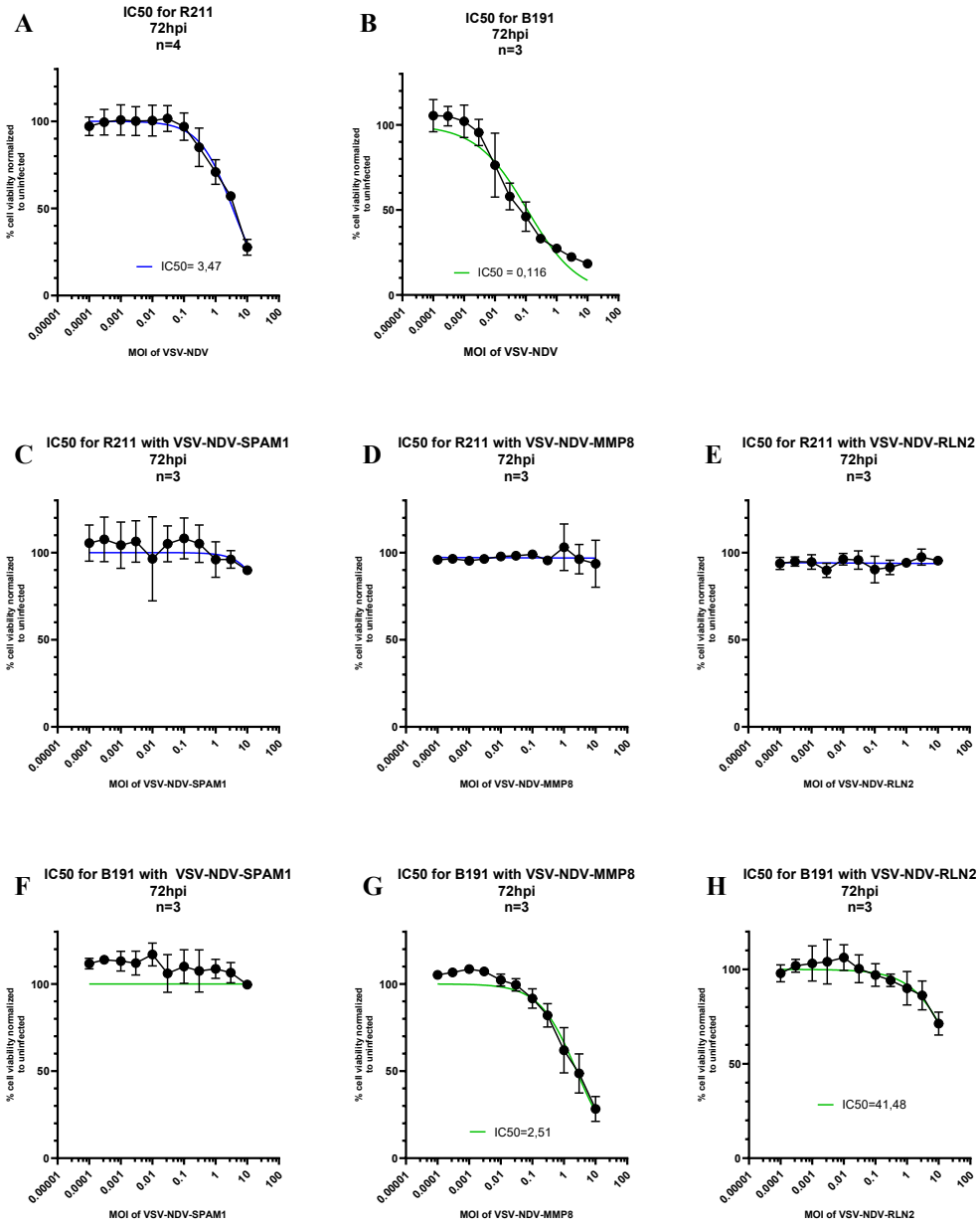

Figure 19: IC50 of the ECM-degrading viruses on the murine PDAC cell lines R211 and B191. (A) R211 with VSV-NDV (B) B191 with VSV-NDV (C, D, E) R211 with VSV-NDV-SPAM1, -MMP8, -RLN2 (F, G, H) B191 with VSV-NDV-SPAM1, -MMP8, -RLN2.

In summary, we determined that all three viruses were strongly attenuated in these two cell lines. But, as the literature review suggested, most viruses reaching the clinical trial stage involved the use of an adjuvant therapy.

5.1.3. Inhibitors

The aim of these *in vitro* experiments was to identify at least one inhibitor with an enhancing effect on VSV-NDV infections or its oncolytic effects in PDAC cells, at an innocuous concentration for the uninfected cells.

5.1.3.1. Inhibitor screening on murine PDAC cell lines

A multitude of experiments were performed on three murine cell lines with several different inhibitors, but for clarity, only selected examples are presented in this work. The concentrations chosen for each inhibitor in Figure 20 were the results of literature research and/or pre-testing. The cells were seeded, and 6 hours later inhibitor was added into the medium. 24 hours post-seeding the virus was added to the supernatant. After 48 or 72 hours, the efficiency of the inhibitor on the VSV-NDV-GFP infection at MOI 1 (for R211) or 0,1 (for B191) was assessed via CellTiter Glo assay, and sometimes the viral titres were calculated by TCID50 assay.

Trametinib, a MEK-inhibitor, was added at concentrations ranging from 1 to 50µM, in the medium of R211 cells, which were subsequently infected. There was a downhill trend in the viability of the infected and uninfected cells under increasing concentration of Trametinib, until the cells were so inhibited that the infection had little effect. The growth curve clearly showed that virus replication was more efficient in the absence of inhibitor. It was therefore concluded that Trametinib does not synergize with VSV-NDV treatment in R211 cells.

Panobinostat, an HDAC inhibitor, was also tested on R211 cells at concentrations ranging from 10 nM to 1 µM. Although it did not affect the viability of the cells at the lowest concentration, its effect started to be visible at 50nM on the uninfected

cells, and seemed to reduce the effects of the infection. At a concentration of 100nM, the viral infection did not cause any change in the viability, and at 1µM, the cells were dead, even in the absence of virus infection. In this one attempt, panobinostat did not enhance the infection and did not appear to be a good candidate.

Entinostat, an inhibitor from the same family, was tested on the same cell line at concentrations between 50nM and 10µM. Until 1 µM, there was no real inhibition of the uninfected cells, and at lower doses (50 and 100nM) there was no appreciable effect on virus replication. Strangely, there was no visible infection in the wells treated with 1µM. Suddenly, at 5µM, the inhibition had a stronger effect, so that the viability dropped to below 25%, regardless of the addition of virus. The same effects were observed at the maximal concentration of 10 µM. Entinostat did seem to provide any beneficial effects in combination with VSV-NDV infection.

Tazemetostat, an EZH2 inhibitor, was tested on two PDAC cell lines, at concentrations ranging from 10 to 50 µM. On R211, there was a rather progressive decrease in the viability of both inhibited conditions, except for 20 and 50nM, where the viability dropped lower than the infected control. In this single attempt, the data did not really suggest an enhanced infection under inhibition. Conversely, on B191, the same concentrations of tazemetostat demonstrated stronger effects. At 10-30 µM, there was apparently a synergy between the inhibitor and the virus, with a tremendous drop in viability, much lower than the control, despite a viability of the control close to 100%. At higher concentrations, the uninfected controls were under 100%. Interestingly, these promising results didn't translate into higher viral titres with the use of tazemetostat, indicating that we might simply be seeing an additive cytotoxic effect of the inhibitor plus the oncolytic virus.

JQ1, a bromodomain inhibitor, was tested at concentrations between 1 and 100 µM on the R211 cell line. From 1 to 10 µM, the inhibitor seemed to partially hinder the viral infection, with viability values slightly higher than that of the control. Only at 50 µM was the infection equivalent to the control value, while at 100 µM, the inhibitor had a substantial effect on cell viability when added in combination with VSV-NDV. The viral titres obtained at 72 hours post-infection were more or less

equivalent in the presence versus absence of virus at all inhibitor concentrations. JQ1 showed interesting results, but due to its reported short half-life in blood, it was decided to continue researching with another Bromodomain inhibitor, AZD5153.

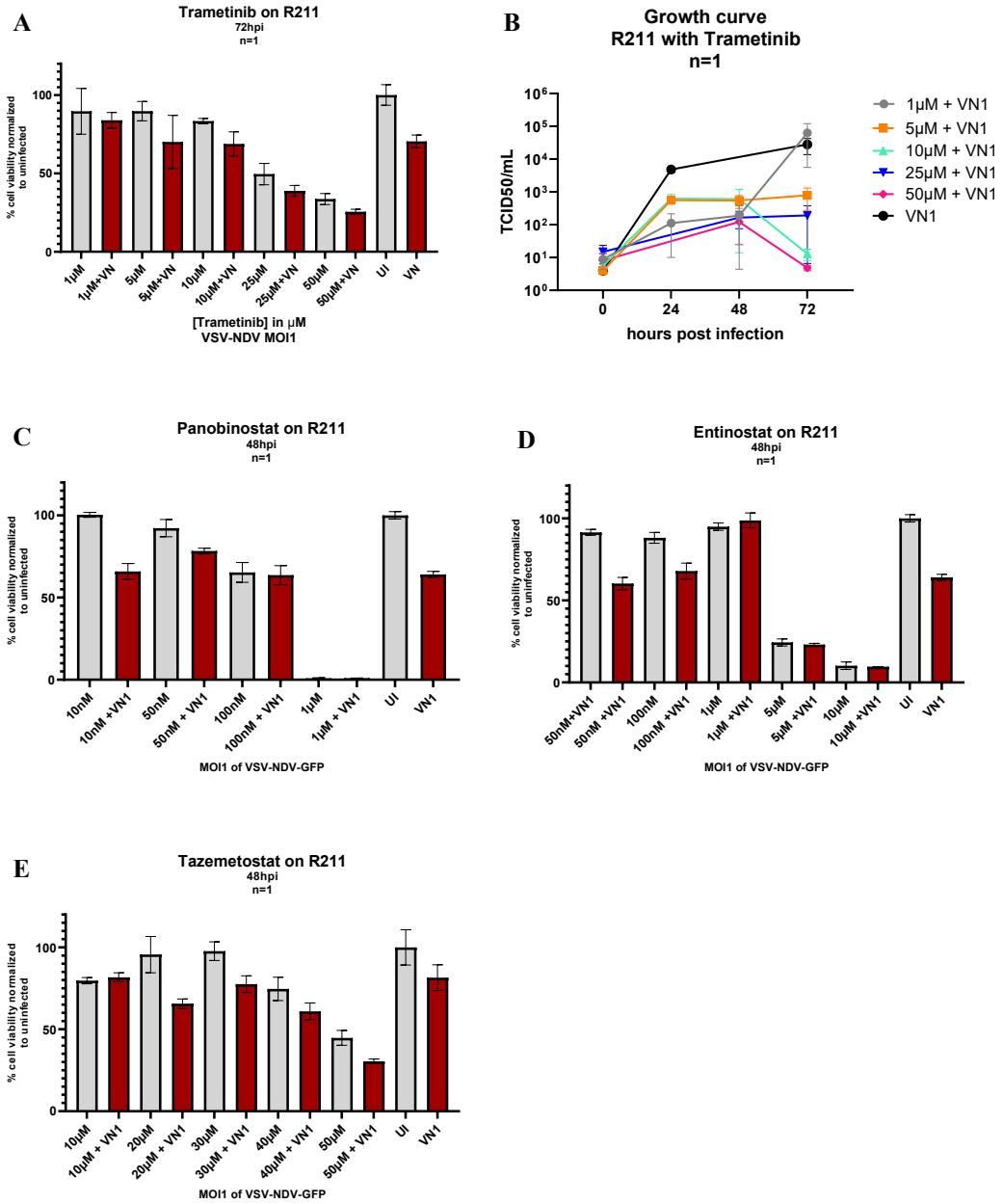

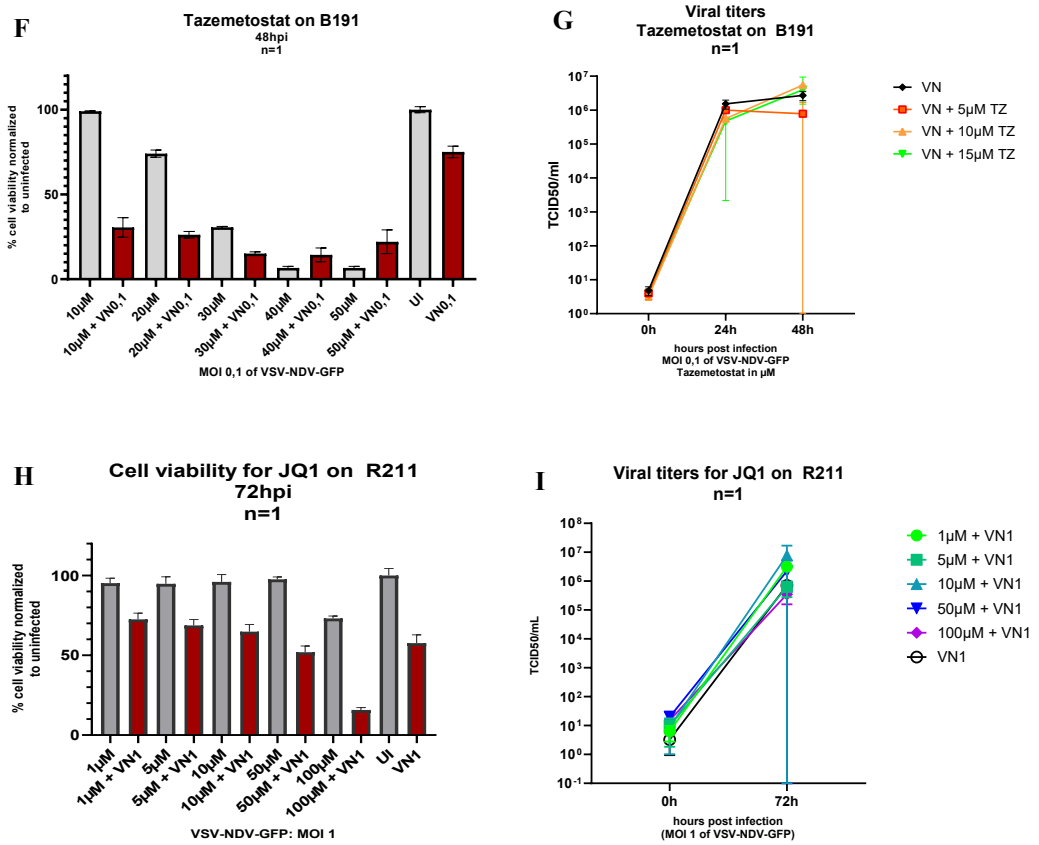

Figure 20: Cell viability assays and virus growth curves of two murine PDAC cell lines (R211 and B191) infected with VSV-NDV-GFP, with diverse inhibitors (A) R211 viability under concentrations of trametinib between 1 and 50µM (B) Growth curve for R211 with trametinib concentrations from1 and 50 µM (C) R211 viability submitted to concentrations of panobinostat comprised between 10 nM and 1 µM (D) R211 viability under concentrations of entinostat between 50 nM and 10 µM (E) R211 viability under concentrations of tazemetostat between 10 and 50 µM (F) Cell viability of B191 under tazemetostat concentrations between 10 and 50 (G) Evolution of the viral titres in B191's supernatant corresponding to F (H) R211 under concentrations of JQ1 between 1 and 100 µM (I) Evolution of the viral titres in R211's supernatant corresponding to H.

5.1.3.2. Bromodomain 4 inhibitor (AZD5153) on mouse PDAC cell lines

The bromodomain 4 inhibitor AZD5153 was tested on two different mouse PDAC cell lines: one moderately sensitive to VSV-NDV, R211 (around 75% of cell viability at MOI 1 of VSV-NDV GFP), the other one quite resistant, 13781 (around 95% cell viability at MOI 1).

The chosen concentrations for this experiment (from 10 to 40 nM) are in the range where the cell viability wasn't affected by the inhibitor's single action, but where heightened effects of the inhibitor and virus combination where expected.

In Figure 21, for both cell lines, the viability of the infected cells strongly decreased in comparison to the control when combined with the inhibitor, and remained rather stable between 10 and 40 nM. Only in 13781 did the viability of the uninfected cells start to decrease slowly when the inhibitor concentrations rose. Both growth curves revealed titres reaching higher values than the infection control at 24 hours, for an equalization of all conditions at 48 hours post-infection, independently of the original susceptibility of the cell line to VSV-NDV.

When the cells were exposed to AZD5153, viral replication was faster and more prolific, corresponding to a higher loss of cell viability, than with a single VSV-NDV-GFP infection. The 20nM concentration was selected to continue the experiments in R211, as it combined high virus titres, low cell viability, and the least impact on the uninfected inhibited cells.

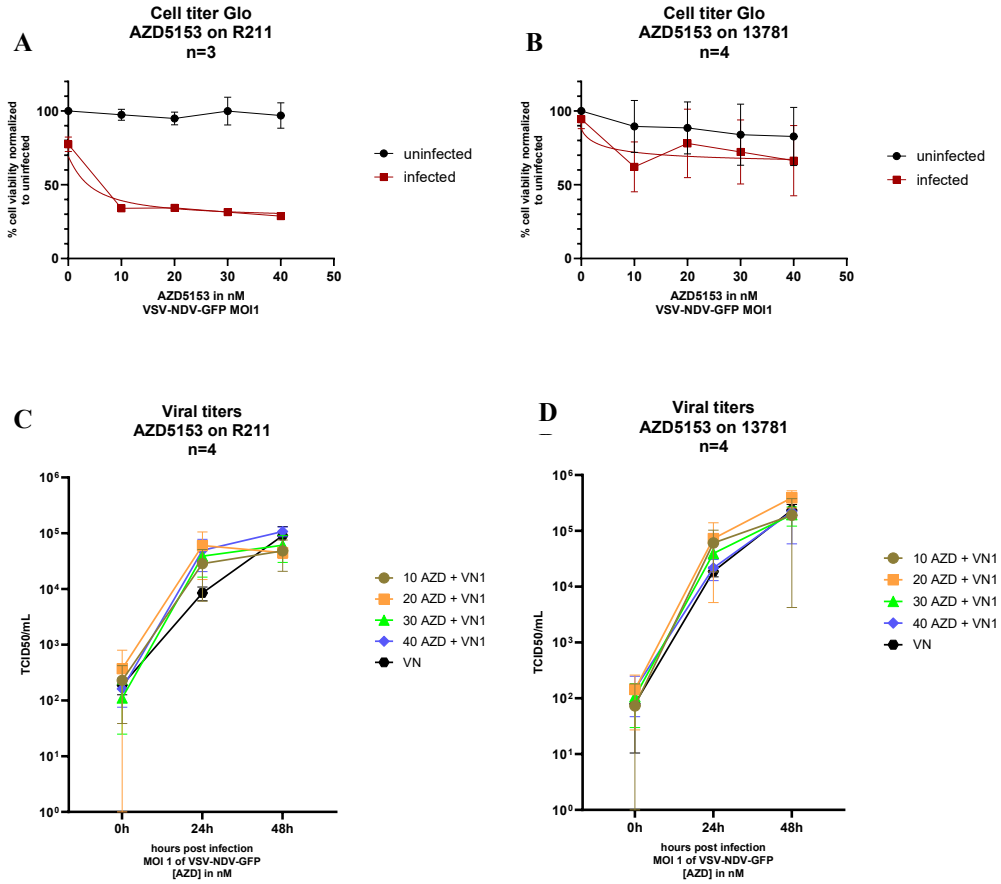

Figure 21: Effects of different AZD5153 concentrations on the cell viability and viral titres of two murine PDAC cell lines (A) Cell titer Glo for R211 with 0 to 50nM of inhibitor (B) Cell titer Glo for 13781 with 0 to 50 nM of inhibitor (C) rVSV-NDV growth curve in R211 cells under AZD5153 inhibition (D) rVSV-NDV growth curve in 13781 cells under AZD5153 inhibition.

Representative microscopic pictures of these experiments, taken at 48 hours post-infection, are shown in Figure 22, pointing out the contrast between single infections and infections with AZD5153. For the 13781 cell line, the application of the inhibitor alone did not show any effect, while there were slightly more damaged cells for the virus combined with the inhibitor, compared to the sole viral infection. Visually as well, for the R211 cell line, there was no difference when only the inhibitor was present in the medium of uninfected cells. However, the viral infection, which formed distinct syncytia, was potentiated by the presence of the inhibitor, as can be seen in H, where only few intact cells remained.

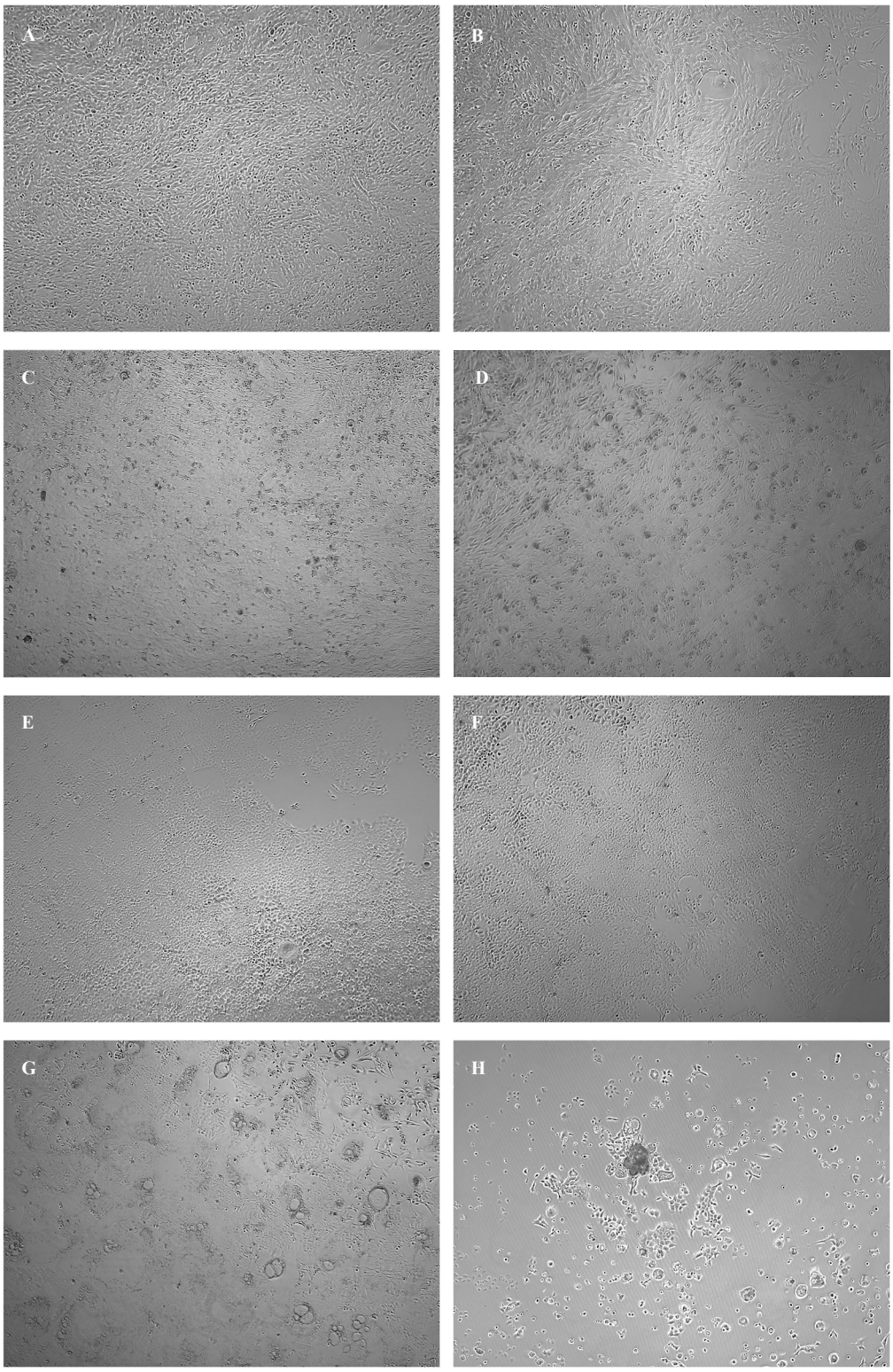

Figure 22: Microscopy of the cells at 48 hours post-infection with VSV-NDV-GFP, 10x. (A) 13781 uninfected (B) 13781 with 20nM AZD5153 (C) 13781 infected control (D) 13781 infected with 20nM AZD5153 (E) R211 uninfected (F) R211 with 20nM of AZD5153 (G) R211 infected control (H) R211 infected with 20nM of AZD5153.

5.1.3.2.1. AZD5153 in combination with different viruses and cell types

After the promising results obtained with the simple infections with VSV-NDV, further experiments were conducted with the attenuated ECM-degraded viruses (VSV-NDV-SPAM1, -MMP8, -RLN2), but also on other cell types, like human PDACs or a murine hepatocarcinoma cell line.

As can be seen for the PDAC cell lines B191 and R211 (in Figure 23), the addition of AZD5153 at a concentration of 20 nM led to much lower IC50 values, even with the attenuated ECM-degrading viruses. For both cell lines, the most powerful infection was obtained by VSV-NDV with AZD5153 input, followed by VSV-NDV-RLN2 under inhibition, and third, the basic VSV-NDV infection. Unexpectedly, the second-best ECM-degrading virus under inhibition was VSV-NDV-MMP8, despite the previous results of this variant in B191 without inhibition, where it performed better than VSV-NDV-SPAM1 and -RLN2 alone. Table 6 summarizes the IC50 values reached under the different conditions.

In two human PDAC cell lines (graphs G and H from Figure 23), Bx-PC3 and PSN1, both sensitive to VSV-NDV, there was a minimum improvement of the IC50 values under inhibition. On the contrary, in HPAFII (graph I from Figure 23), which is a virus-resistant cell line, the concurrent exposition to AZD5153 and VSV-NDV resulted in even higher viability values, which means that the cell multiplies faster in these conditions. The murine hepatocarcinoma cell line, RIL 175, also went from a high IC50 to a ten times lower value thanks to AZD5153.

A

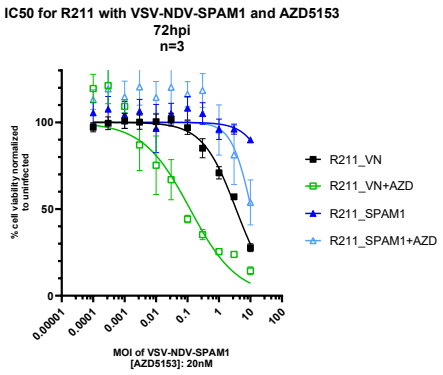
IC50 for R211 with VSV-NDV-SPAM1 and AZD5153
72hpi
n=3
% cell viability normalized to uninfected
MOI of VSV-NDV-SPAM1
[AZD5153]: 20nM
R211_VN
R211_VN+AZD
R211_SPAM1
R211_SPAM1+AZD

B

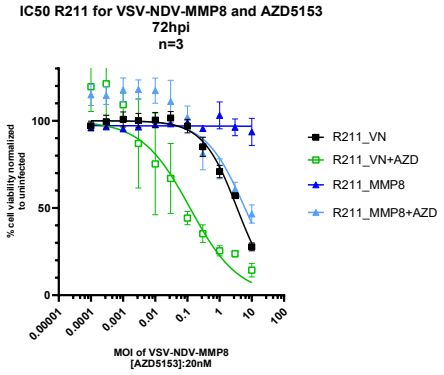
IC50 R211 for VSV-NDV-MMP8 and AZD5153
72hpi
n=3
% cell viability normalized to uninfected
MOI of VSV-NDV-MMP8
[AZD5153]:20nM
R211_VN
R211_VN+AZD
R211_MMP8
R211_MMP8+AZD

C

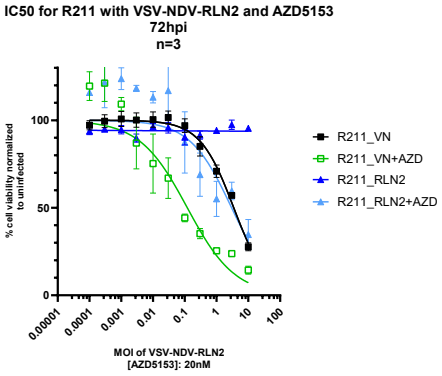
IC50 for R211 with VSV-NDV-RLN2 and AZD5153
72hpi
n=3
% cell viability normalized to uninfected
MOI of VSV-NDV-RLN2
[AZD5153]: 20nM
R211_VN
R211_VN+AZD
R211_RLN2
R211_RLN2+AZD

D

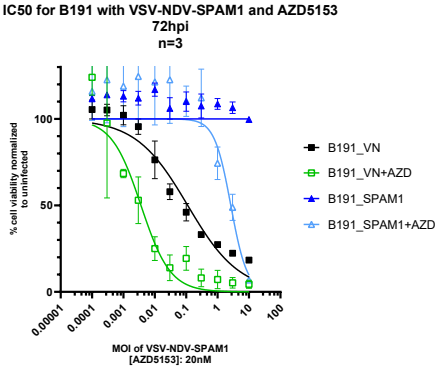
IC50 for B191 with VSV-NDV-SPAM1 and AZD5153
72hpi
n=3
% cell viability normalized to uninfected
MOI of VSV-NDV-SPAM1
[AZD5153]: 20nM
B191_VN
B191_VN+AZD
B191_SPAM1
B191_SPAM1+AZD

E

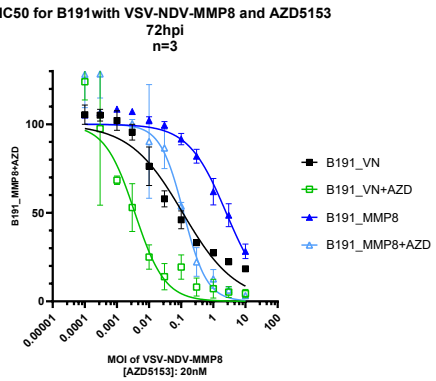
IC50 for B191with VSV-NDV-MMP8 and AZD5153
72hpi
n=3
B191_MMP8+AZD
MOI of VSV-NDV-MMP8
[AZD5153]: 20nM
B191_VN
B191_VN+AZD
B191_MMP8
B191_MMP8+AZD

F

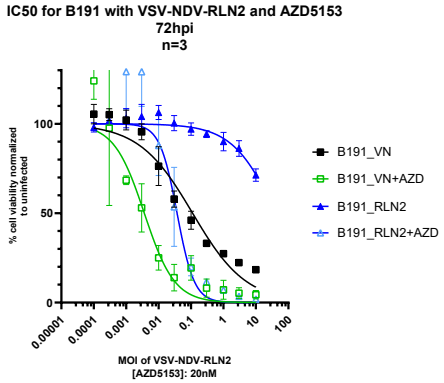
IC50 for B191 with VSV-NDV-RLN2 and AZD5153
72hpi
n=3
% cell viability normalized to uninfected
MOI of VSV-NDV-RLN2
[AZD5153]: 20nM
B191_VN
B191_VN+AZD
B191_RLN2
B191_RLN2+AZD

G

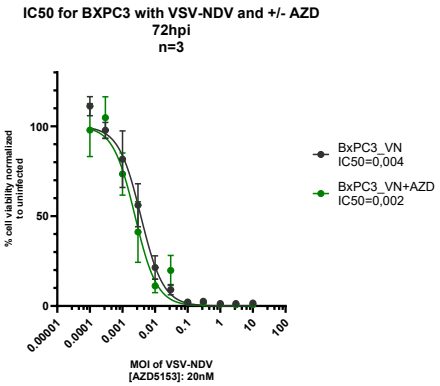
IC50 for BXPC3 with VSV-NDV and +/- AZD
72hpi
n=3
% cell viability normalized to uninfected
MOI of VSV-NDV
[AZD5153]: 20nM
BxPC3_VN
IC50=0,004
BxPC3_VN+AZD
IC50=0,002

H

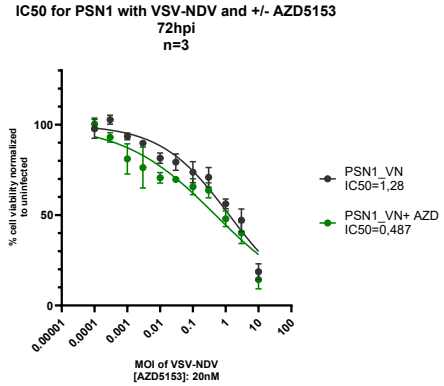
IC50 for PSN1 with VSV-NDV and +/- AZD5153
72hpi
n=3
% cell viability normalized to uninfected
MOI of VSV-NDV
[AZD5153]: 20nM
PSN1_VN
IC50=1,28
PSN1_VN+ AZD
IC50=0,487

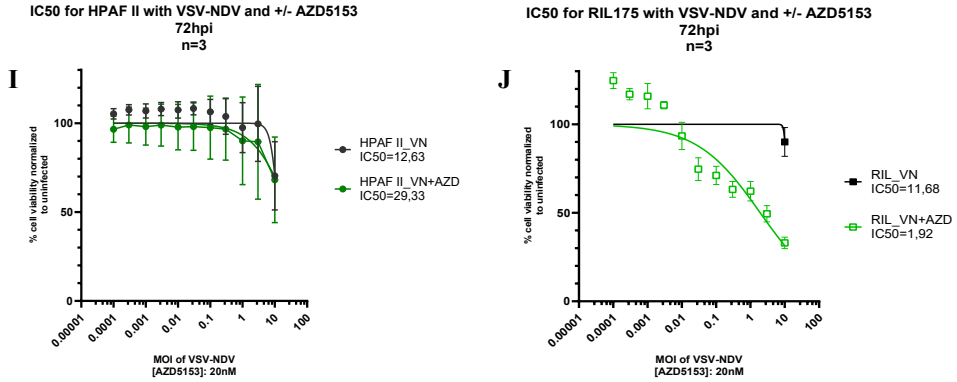

Figure 23: Comparing the IC50 of different viruses, with AZD5153, on different cell lines. (A to F) Basic and ECM-degrading viruses with or without inhibitors on 2 murine PDAC lines (G to I) Infections with VSV-NDV with or without AZD5153 on 3 human PDAC lines (J) infections with VSV-NDV with or without AZD5153 on a murine HCC line.

Table 6: Comparative table of the IC50 of R211 and B191 with different viruses and with/without AZD5153 inhibition.

IC50	AZD5153	VSV-NDV	VSV-NDV SPAM1	VSV-NDV MMP8	VSV-NDV RLN2
R211	without	3,47	76,48	no value	no value
	with 20 nM	0,12	10,72	6,09	2,98
B191	without	0,116	no value	2,52	41,48
	with 20nM	0,004	2,63	0,119	0,037

A minimum level of viral replication appeared necessary for the inhibitor to enhance the spread of VSV-NDV. Logically, when the cells were already very sensitive to the virus, there was not much difference when adding the inhibitor, as the virus did not spare many cells. However, the basal susceptibility of a cell line was not always a reliable predictor for the synergistic effect of AZD5153 on the infection, as HPAF-II and RIL 175, which had a similar IC50, demonstrated.

5.1.3.2.2. Effects of AZD5153 inhibition in PDACs and cancer-associated fibroblasts

The cell-dependent synergy observed between the viruses and the AZD5153 inhibitor on cancer cell lines motivated investigations to test whether cancer-associated fibroblasts, alone or in coculture with PDAC cells, would also be sensitized to the virus when exposed to AZD5153. The following experiments compare the infections of monocultures and combinations of R211 (PDAC) and three CAFs: the pancreatic stellate cells (PSC) 806/10, the fibroblasts (FB) 704F3 and the pancreatic stellate cells 3 Prrx1 (referred to as PSC3). The data is visible in Figure 24.

Luckily, the cell viability data corroborated this assumption for PSC3 in mono and coculture with R211. Indeed, this CAF line was the most infectible non-PDAC line, with a significant viability drop to 88,6% in response to virus treatment, reduced to 50% in combination with the inhibitor. On the contrary, single cultures of 806/10 and 704F3 were proven very resistant to VSV-NDV, with a maintained viability despite infection, and the viability drop observed in the combination of inhibitor plus virus can be attributed to the inhibition solely. The cocultures of 806/10 and 704F3 were slightly more infectible, probably due to the presence of PDACs, and also showed a decrease in viability when virus and inhibitor were combined, to levels comparable with a single PDAC infection. The PSC3 line showed more promising results, as it is more permissive to virus infection. The inhibition enhanced the virus action both in its mono- and coculture. The crosstalk between R211 and PSC3 allows for the most efficient single infection of all conditions (49,9% viability), and the addition of the inhibitor helped reach 31,3%, a value very similar to infected and inhibited R211. In fact, for all cocultures, the presence of PDACs, which are more susceptible to the virus than any CAFs, enabled a reduction of the viability during infection. Also, if 1 PDAC for 3 CAFs were seeded at the beginning of the experiment, the actual ratio between PDACs and CAFs was unknown at 48 hours post-infection, hence the influence of the PDACs on a better infectability over the results. In general, the cumulative effects of the inhibitor and of the viral infection resulted in lower viability results for all conditions.

Fitting to the cell viability data, the viral titres (Figure 24 B) also showed a slightly more efficient viral replication in the monocultures R211 and PSC3 than in the other monocultures: this was the same in the inhibited coculture titres. Indeed, in the combination group, there were significant increases in the titres of R211 monoculture at 24hours, in the coculture with 704F3, and in the coculture with PSC3, as well as at 48 hours, despite the decline for the PSC3 coculture. In 806/10 and 704F3 monocultures, the inhibition's only effect was a delay in the titres' decline over time (more exactly, inhibited 806/10 managed to maintain a low replication rate during the whole experiment). There was barely a difference in the 806/10 coculture with or without inhibition. Out of three CAF cell lines, 806/10 was the most insensitive to AZD5153, followed by 704F3. In R211, PSC3, 704F3 and PSC3 coculture, the presence of inhibitor apparently facilitated the viral replication, which reached higher values than uninhibited wells, and in shorter periods. Seemingly synergistic effects were observed only in treated R211 and PSC3 cocultures, while the other cocultures appear to show a bare combination of the results obtained by each cell line separately.

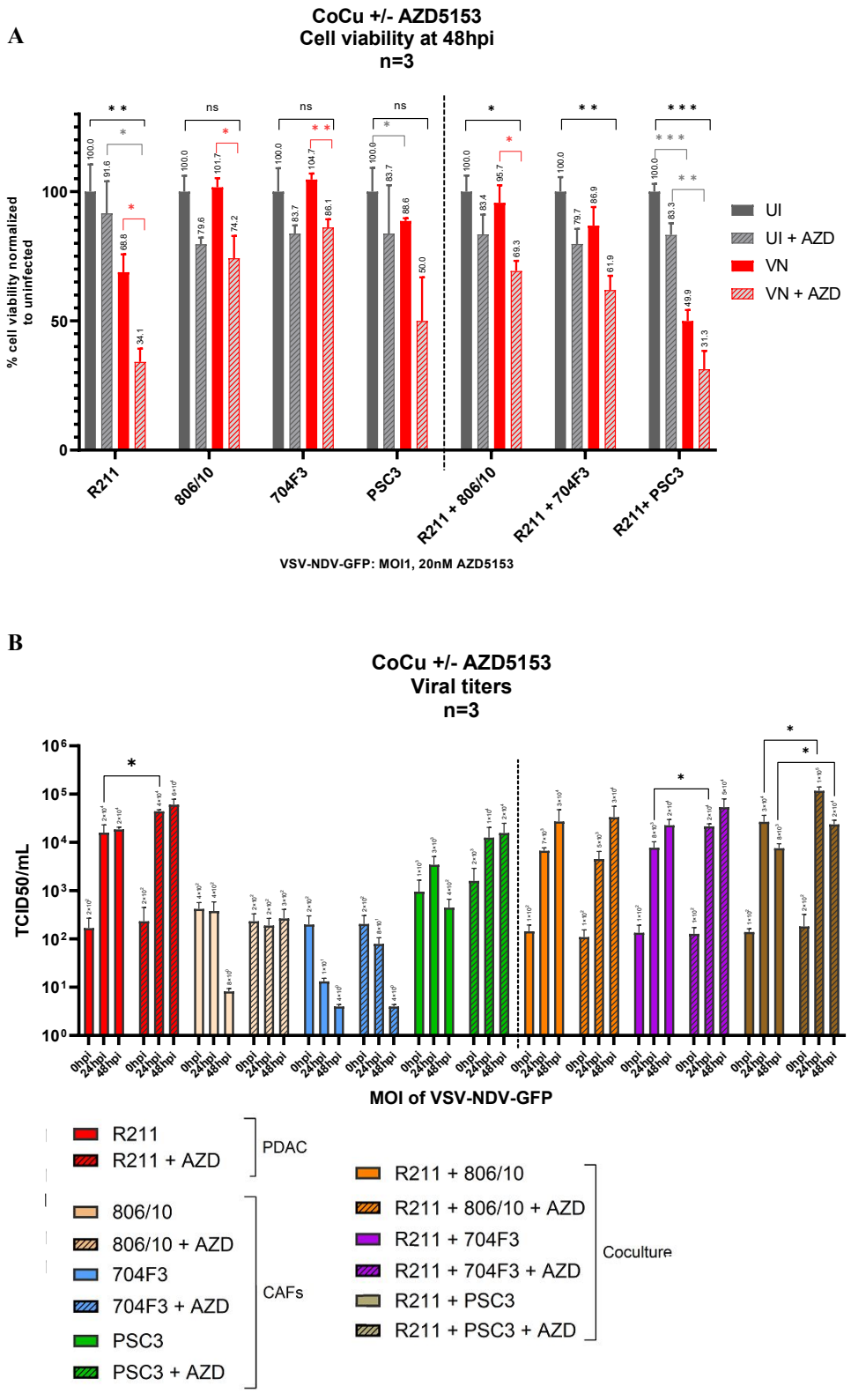

Figure 24: Comparison of the viral infection in PDAC and CAFs monocultures against their direct cocultures, with or without 20nM of AZD5153 (A) Cell viability assay by Cell titer Glo, at 48hpi, normalized to uninfected cells (B) viral titres at time-points 0, 24 and 48hpi, determined by TCID50.

5.1.3.2.3. BRD4 Knock-out cells

As a proof of concept that the observed effects were indeed due to the inhibition of the announced target, the bromodomain 4, the CRISPR-CAS9 method was applied on two PDAC cell lines, to produce knock-outs. Out of the single cell clones created, a few were tested for validation (namely the clones number 8, 10 and 11 produced from R211 and the clones number 2, 3 and 5 produced from B191), first by a western-blot for analysis of BRD4 protein expression, then via PCR for the BRD4 gene.

BRD4's predicted band is 152 kDa, but it was observed at around 200 kDa. As is visible in Figure 25, all samples expressed many unspecific bands and a very large protein above 200kDa. In this first western Blot, the negative control was missing, but Huh7 was used as a positive control. After many similar attempts (with negative control included), the polymerase chain reaction method was chosen to continue the selection for knock-outs.

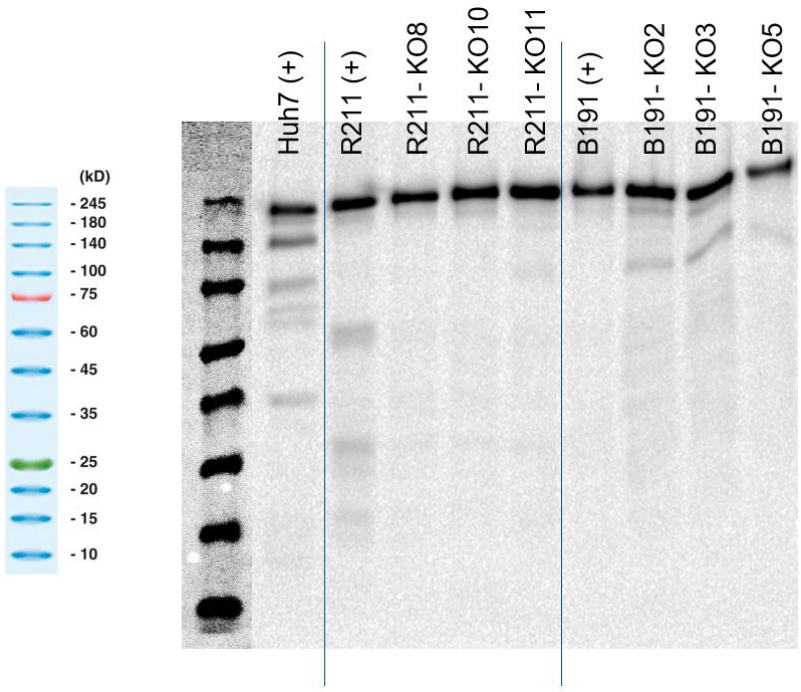

Figure 25: Western blot gels for BRD4 (around 200kDa).

In Figure 26, the PCR products of two reactions are shown, the first one (A) with two sets of primers targeting different sequences within the bromodomain target, was missing an important positive control band for the original cell line R211. The presence of a band was a confirmation of the expression of BRD4, while its absence meant no BRD4 was expressed (as expected from the "KO" cell lines). In this set, R211-KO10 was positive for BRD4 in two repeated experiments, R211-KO11 was once negative, once positive, and B191-KO2 and 3 were also once positive, once negative. Only R211-KO8 was twice negative, as well as B191-KO5. As the primers for exon 3-1 seemed more efficient than for exon 3-2, the first was selected for another PCR.

The second PCR (B, using the primers for exon 3-1) showed all positive controls bands, but the results differed from the first set. Only two edited cell lines were constantly negative, R211-KO8 and B191-KO5: these were chosen for Sanger sequencing.

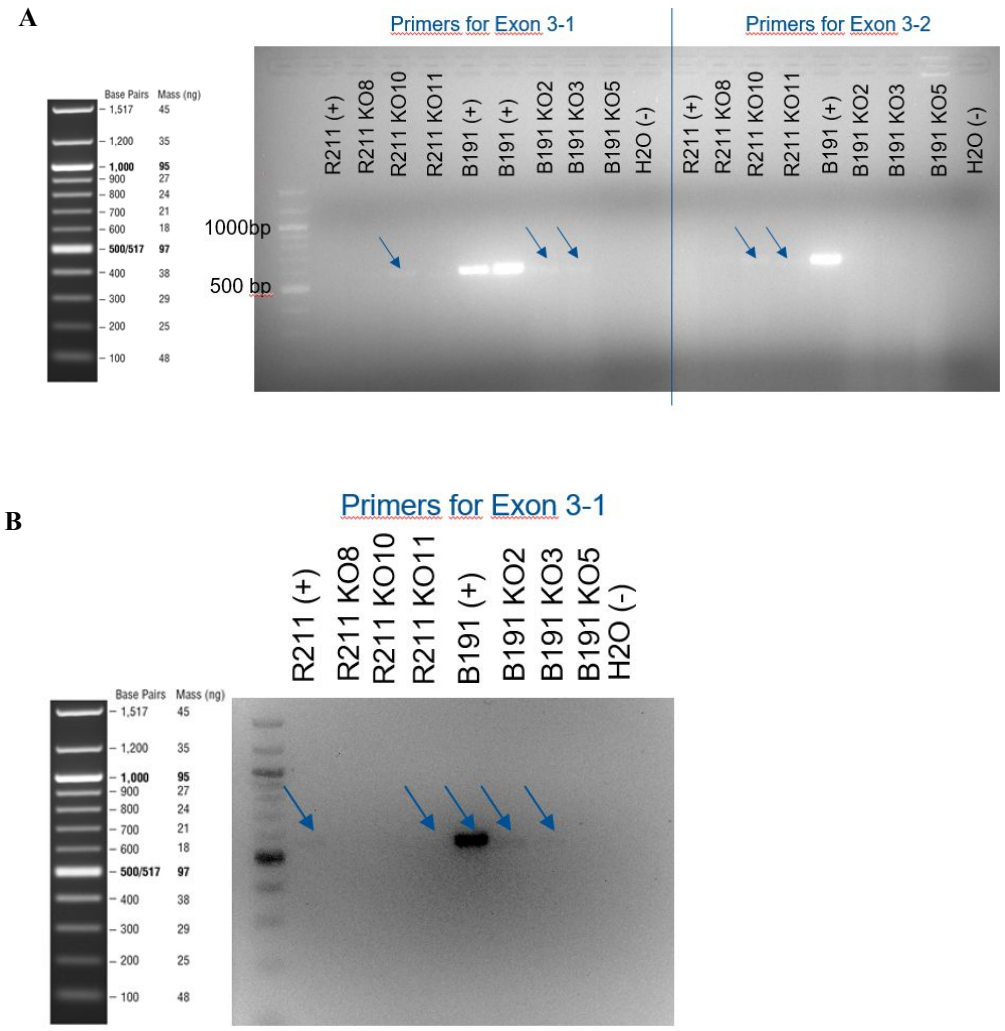

Figure 26: PCR for BRD4 expression. Exon 3-1: 563 bp, exon 3-2: 595 bp.Used as positive controls are the R211 and B191 samples, negative control is water. Both A and B experiments were repeated under the same conditions. (A) For exon 3-1, bands are visible only for R211-KO10, both B191 samples, B191-KO2, B191-KO3. For exon 3-2, bands are visible only for R211-KO10, R211-KO11 and B191. (B) For exon 3-1, bands are visible for both positive controls R211 and B191, and also R211-KO11, B191-KO2, B191-KO3.

The analysis tool from Synthego® enabled a confrontation of the original cell lines sequences with their edited versions (as seen in Figure 27). The knock-out score revealed the proportion of indels (insertions or deletions) indicating a frameshift, of over 21bp long (assuming all edits were in the coding region), while the model fit determined how well the proposed indel distribution fit the Sanger sequence data of the edited sample. In both cases, the model fit was high enough to trust the data. To sum up, the R211-KO8 cell line was identified as a knock-down: it was probably

not from a single cell clone as originally intended, and had only 63% indels differences from the original cell line. On the other hand, the B191-KO5 cell line was a real knock out, with 95% indels within the coding region, meaning that only 5% of the original sequence from B191 was conserved.

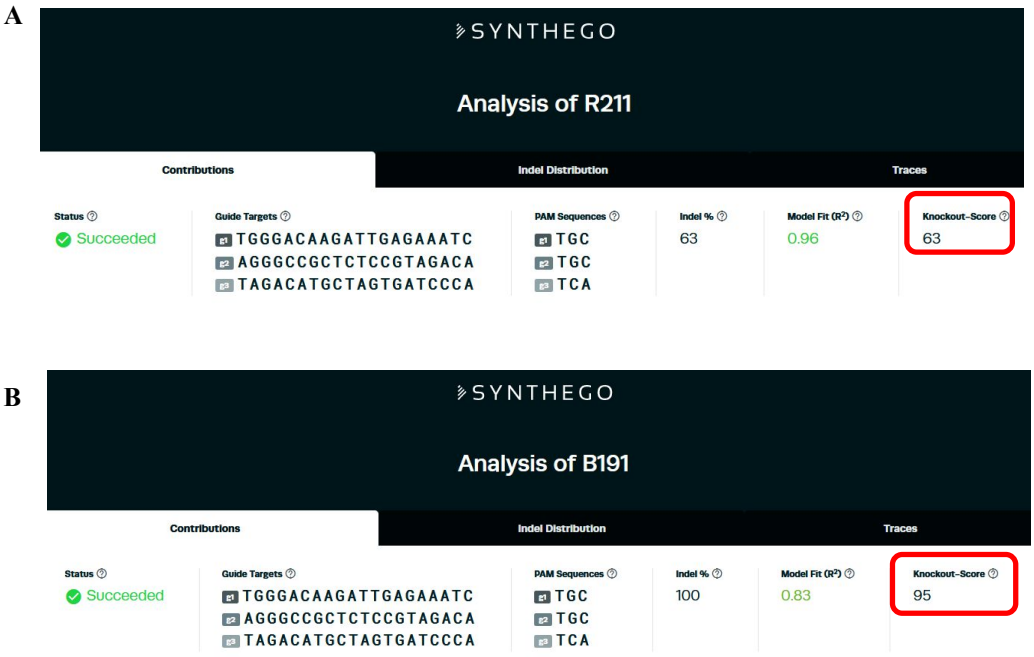

Figure 27: Comparison of the wildtype cell line with the clones in Synthego (A) R211 versus R211-KO8 (B) B191 versus B191-KO5.

Next, these edited cell lines were characterized *in vitro*, to see if they behaved like the original cell-lines under AZD5153-inhibition (results are available in Figure 28). Corresponding microscopic pictures with syncytia formation are shown in Figure 29.

First, the cell viability assay revealed that AZD5153 also had an effect at a concentration of 20nM in the edited cell lines. Surprisingly, the B191-KO5 cell line behaved almost identically to B191, with a single difference: the uninfected KO cell line was proportionally more inhibited in its growth than B191, at the same concentration. On the other hand, R211-KO8's viability remained almost

unaffected by the sole viral infection, but dropped when it was combined with AZD5153, though to levels higher than for the original cell line.

As for the viral titres, they confirmed the very analog behaviour of B191 and its knock-out: the replication attained similar values at 24 hours, and remained stable until 48 hours post-infection, with the only difference being a negligible decline at 48 hours for the uninhibited B191. On the other hand, R211-KO8, the incomplete KO cell line, behaved like R211 under inhibition at 24 hours. While virus titres in R211 cells were still rising at 48 hours post-infection (to $9x10^4$) in the absence of the AZD inhibitor, the peak titre was already reached at 24 hours when the infection occurred in the presence of the inhibitor. The noticeable difference was the steady titre increase of uninhibited R211 to reach its maximum value (higher than under inhibition or R211-KO8), while R211 with AZD5153, as well as R211-KO8 with AZD5153, were slowly declining. Interestingly, the highest titres from this experiment were achieved by R211-KO8 with inhibitor, with no drop observed between 24 and 48 hours.

In the end, the best replication was reached by the incomplete BRD4-KO cell line R211-KO8, under addition of AZD5153. This “incomplete KO” cell line performed similarly to the original cell line with 20nM inhibition on its own, which maybe corresponded to the dose where infections were more potent, but the uninfected cells’ density wasn’t affected. Also, a strong inhibition of BRD4 or a real KO, in an already highly susceptible cell line didn’t trigger a better replication.

These results also suggest a nonspecific mechanism of action from the BRD4 inhibitors, as their action couldn’t be reproduced by targeting the bromodomains only.

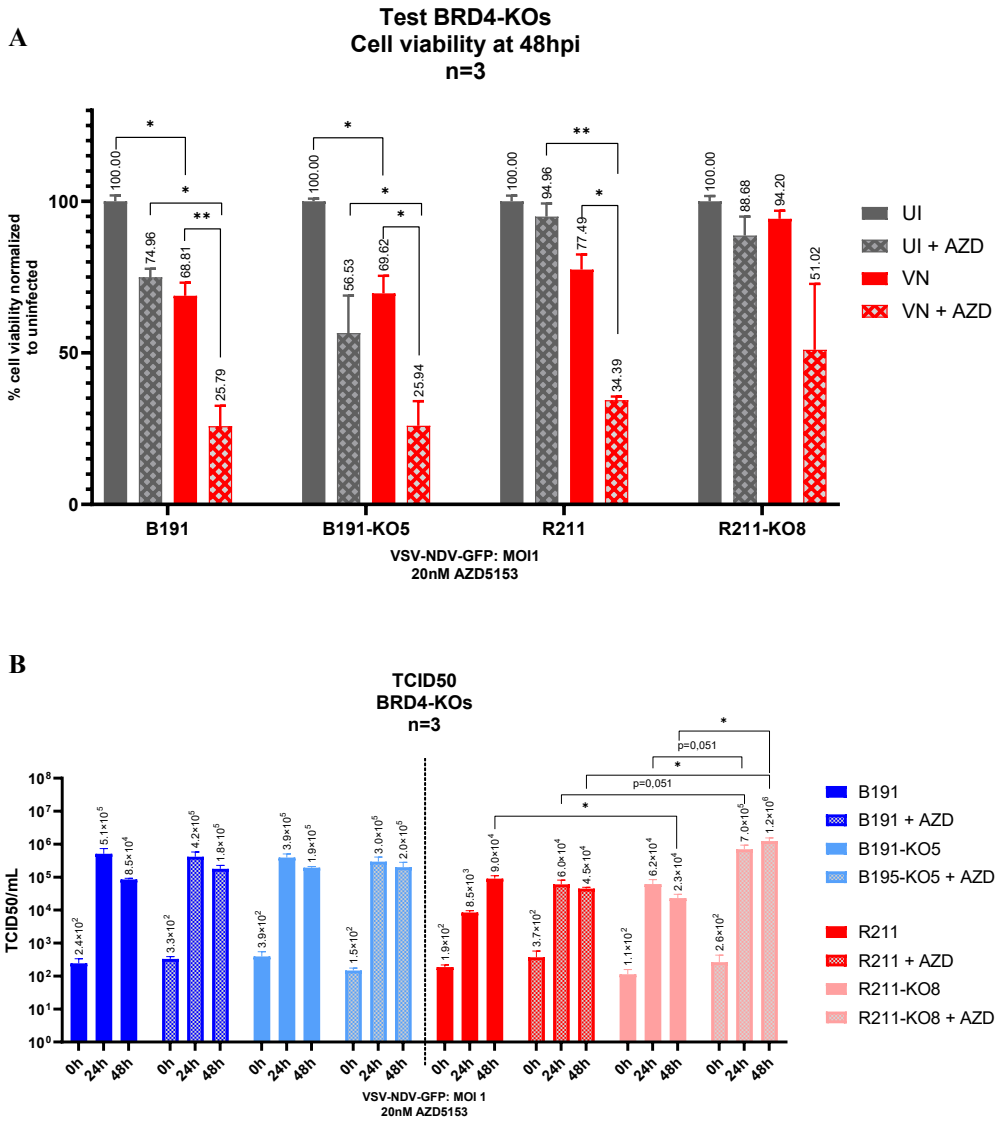
A
Test BRD4-KOs
Cell viability at 48hpi
n=3
% cell viability normalized to uninfected
100
50
0
100.00
74.96
68.81
25.79
100.00
56.53
69.62
25.94
100.00
94.96
77.49
34.39
100.00
88.68
94.20
51.02
B191
B191-KO5
R211
R211-KO8
VSV-NDV-GFP: MOI1
20nM AZD5153
UI
UI + AZD
VN
VN + AZD
B
TCID50
BRD4-KOs
n=3
TCID50/mL
p=0,051
p=0,051
0h
24h
48h
VSV-NDV-GFP: MOI 1
20nM AZD5153
B191
B191 + AZD
B191-KO5
B195-KO5 + AZD
R211
R211 + AZD
R211-KO8
R211-KO8 + AZD

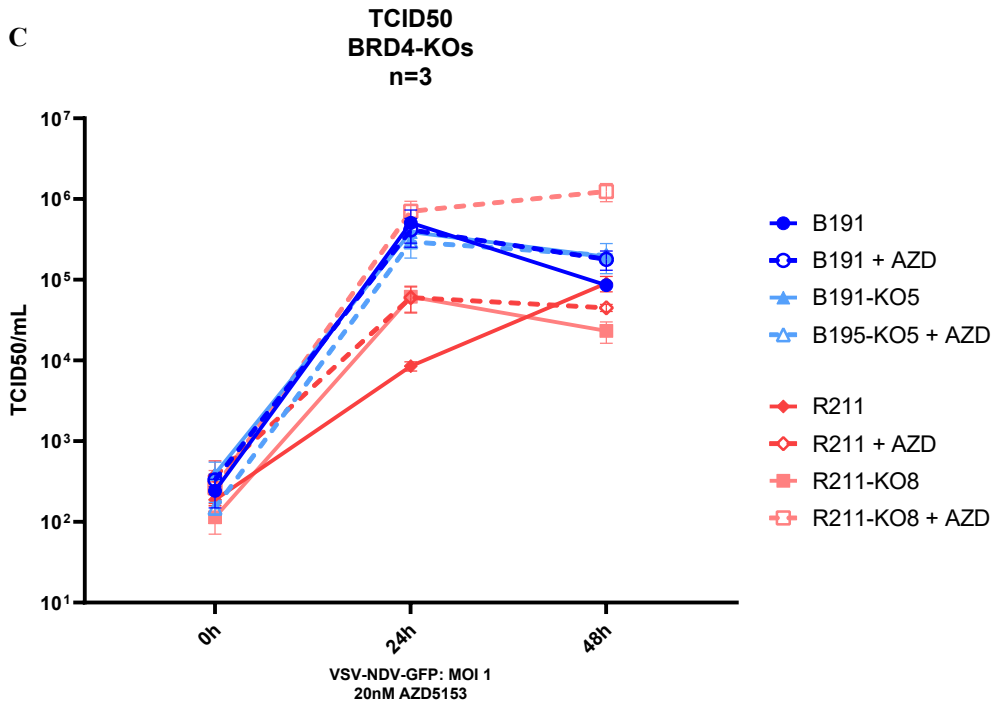

Figure 28: Comparison of the original PDAC cell lines B191 and R211 with their BRD4 knock-out versions, B191-KO5 and R211-KO8, under infection with VSV-NDV alone or in combination with AZD5153 (A) Cell viability assay at 48hours post-infection, by Cell Titer Glo (B, C) Growth curves for 0, 24 and 48 hours post-infection, determined by TCID50.

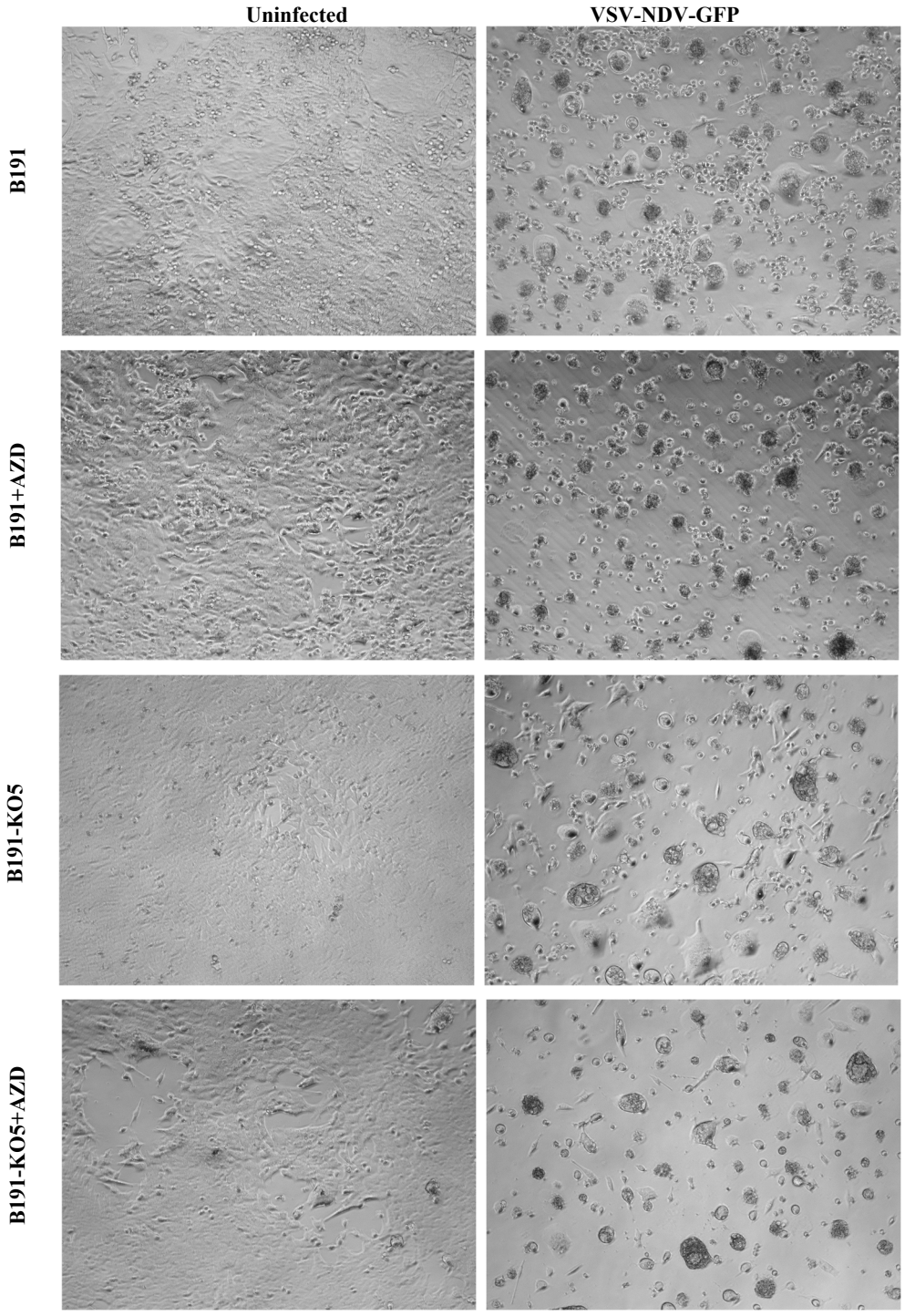
Uninfected
VSV-NDV-GFP
B191
B191+AZD
B191-KO5
B191-KO5+AZD

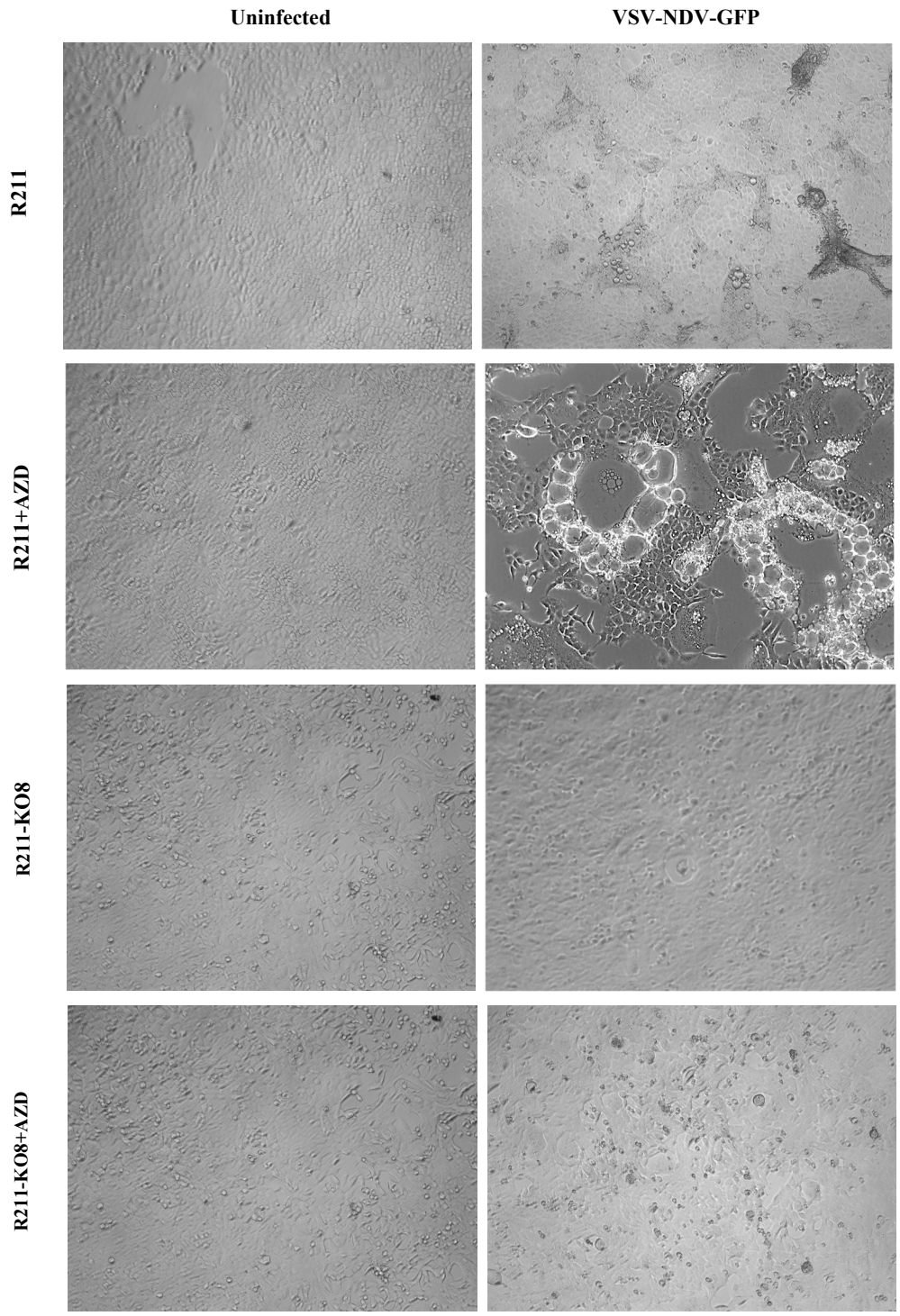

Figure 29: Representative pictures of the different cell lines, at 48 hours post-infection, 10x. All cells are represented in an uninfected state (left column), and infected with VSV-NDV-GFP at MOI 1 (right column).

5.2. *IN VIVO* EXPERIMENTS

5.2.1. Basic PDAC experiments

5.2.1.1. Orthotopic PDAC model establishment

In order to establish a predictive preclinical PDAC model, preliminary experiments, not detailed in this work, were conducted. They helped define which cell line would reliably grow in the mice: only R211, how many cells per mouse should be injected: 2500 cells, in which vehicle to inject the cells: PBS, and in which volume: 10 µL. To find the time-point for randomization of mice to treatment groups, a few mice were imaged at different time-points post-implantation. The results of these experiments indicated that the period between day 12 to 18 was the best, which is why day 14 was chosen. Figure 30 shows the development of an untreated tumour over a period of 23 days.

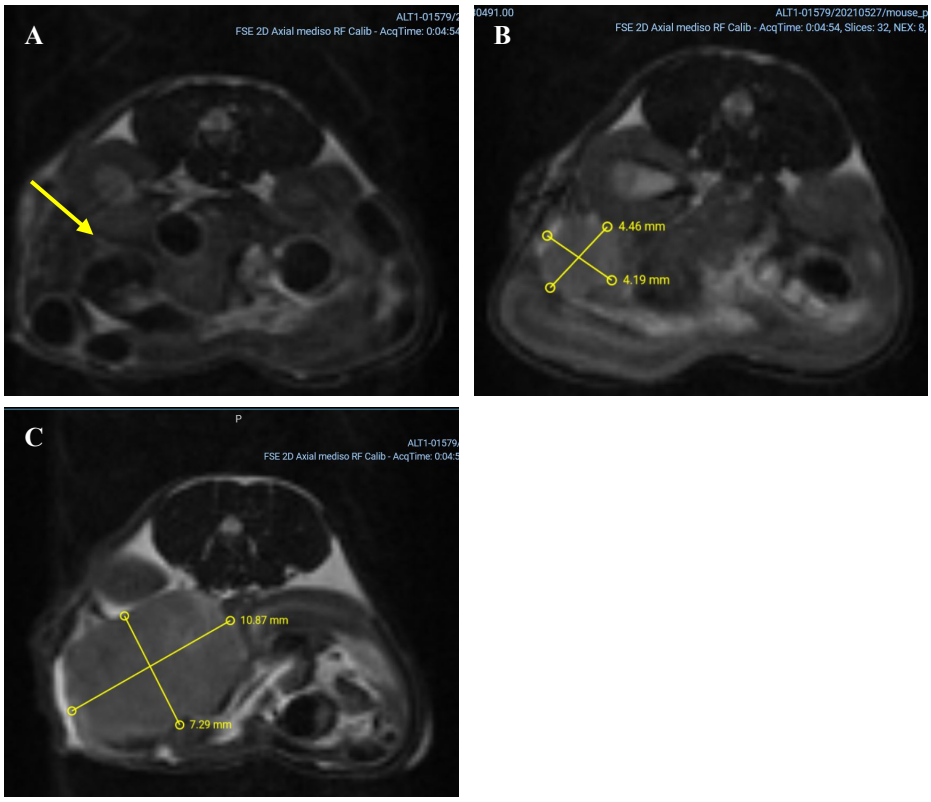

Figure 30: MRI of mice implanted in the pancreas with the 2500 cells of the PDAC cell line R211, in 10µL of PBS. A) tumour 9 days post-implantation B) tumour 17 days post-implantation C) tumour 23 days post-implantation.

5.2.1.2. Route-finding experiments

The experiment consisted in implanting Black 6 mice orthotopically with 2500 cells of the murine PDAC in PBS, then image the mice to confirm the presence of tumours and randomize them into groups. The treatment groups would be PBS against VSV-NDV at a concentration of 10^7 virions per mouse and per injection (on days 0, 3, 7 and 14), but most importantly, comparing intravenous (iv.) against intraperitoneal (ip.) injections. The aim was to define which systemic application would correlate with the longest survival.

Figure 31 A schematizes the timeline of the experiment, while Figure 31 B shows the Kaplan-Meier survival curve obtained. The data for the ip. groups are merged from 2 experiments, while the data for iv. groups come from one experiment. The intravenous regimen showed a median survival of 29 days for the virus-treated group (5 mice) compared with 20 days for the mock-treatment group (5 mice), while the intraperitoneal group yielded a median survival of 37 days for the virus-treated mice (N = 10) versus 31,5 days for the PBS-treated mice (N = 6). The mice were sacrificed between day 13 and day 49 post-treatment, upon reaching the exclusion criteria.

This route-finding experiment did not provide a satisfying answer to the question of which route would be the best delivery mode for the virus, although it was encouraging to see a trend towards prolonged survival in response to VSV-NDV treatment via either route. Three facts influenced the final decision. First, the intravenous route was the only one to be consistent between the groups, showing a treatment benefit with the virus. Second, the group had already witnessed success in an orthotopic rat hepatocarcinoma model via the intravenous route[102], so it was known that the virus could still be potent after circulation in the blood. Third, the intravenous route was considered the most elegant delivery for potential subsequential clinical trials. Thus, subsequent *in vivo* experiments all used tail vein injection as a delivery mode.

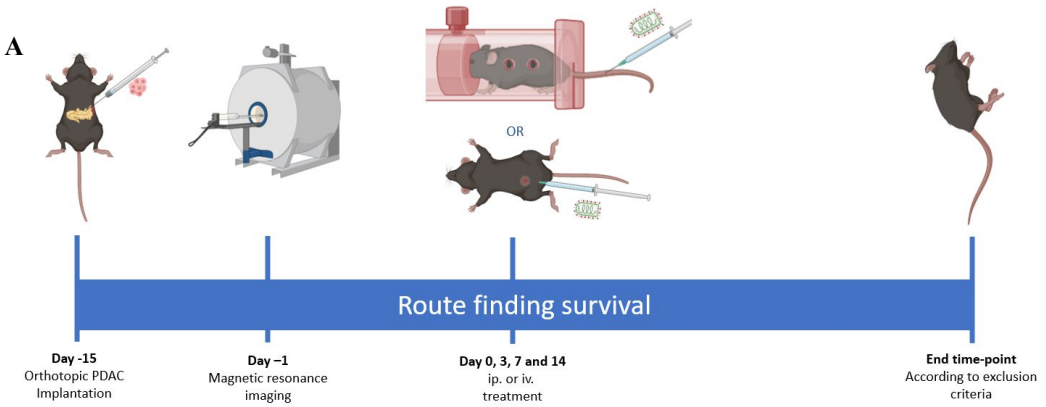

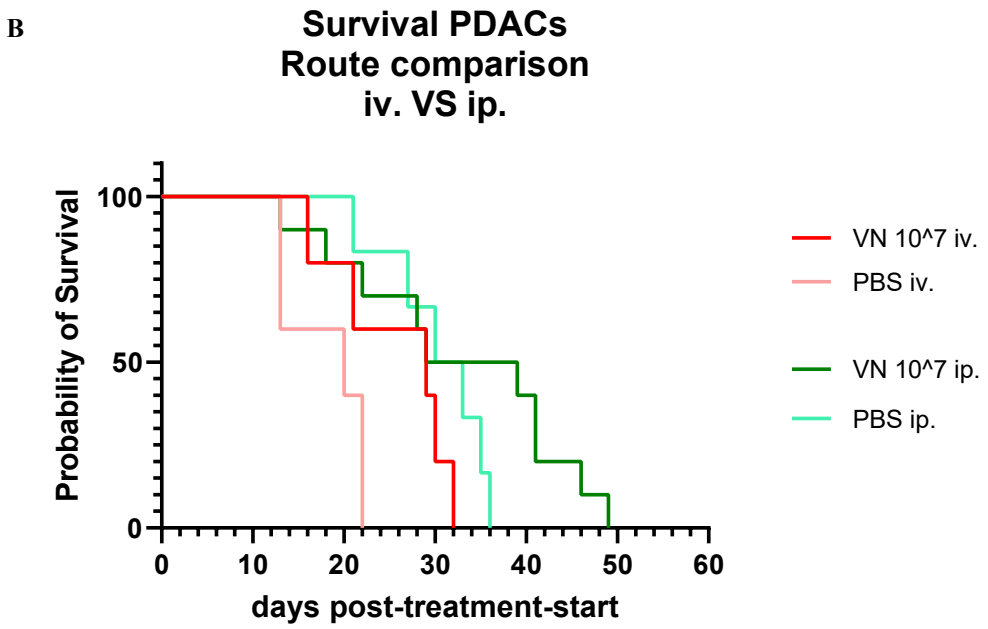

Figure 31: Route-finding survival experiment (A) Time-line: C57/BL6J mice received a pancreatic implantation of 2500 R211 cells at the age of 8 to 9 weeks, were imaged by magnetic resonance imaging (MRI) and randomized to treatment groups, to receive VSV-NDV (10^7 virions) or PBS, either intravenously or intraperitoneally, and sacrificed at humane endpoints. *Created with Biorender.com* (B) Kaplan-Meier survival curve for the 4 groups: intravenous against peritoneal injections, PBS against VSV-NDV. There were 5 mice in each iv. group, 10 mice for the PBS ip. group, and 6 mice for the PBS ip. group.

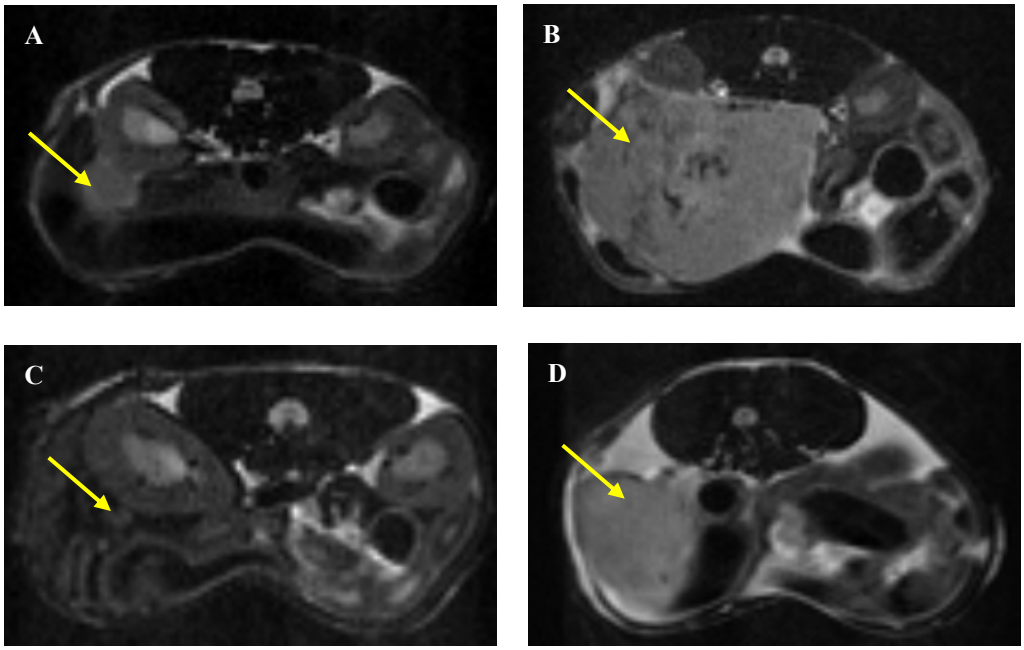

Figure 32: examples of magnetic resonance images from PDAC mice at two times points**.** (A) PBS injected ip. mouse at day 16 post-implantation (B) same PBS ip. mouse at day 36 post-implantation (C) VSV-NDV treated ip. mouse at day 16 post-implantation (D) same VSV-NDV ip. treated mouse at day 36 post-implantation.

5.2.1.3. Determination of optimal dose of VSV-NDV in orthotopic implanted PDAC mice

After having chosen the iv. route for further investigations, the next step was to determine whether the viral dose had an impact on the effectiveness of the treatment. Therefore, a comparison was conducted between $1x10^7$ and $1x10^8$ TCID50 (infectious virions) per injection, with PBS as a control. Figure 33 A) schematized the experimental steps, while B) showed the results in a survival curve.

The median survival for the PBS mice (n = 7) was 18 days, while it reached 29 days for the 10^7 group (5 mice) and 24 days for the 10^8 TCID50 dose (5 mice). Despite the longer median survival in the lower dose group, this did not achieve statistical significance (p = 0.56) compared to PBS with the small group size, the higher dose achieved statistical significance, with p=0,024. The comparison of survival between treatment doses was not statistically significant. Almost all mice died

between day 11 and day 32, with the exception of one VSV-NDV 10^8 mouse, who died on day 70 post-treatment. Hence, the higher dose was deemed more efficient than the lower one, although the difference was likely determined by a single mouse.

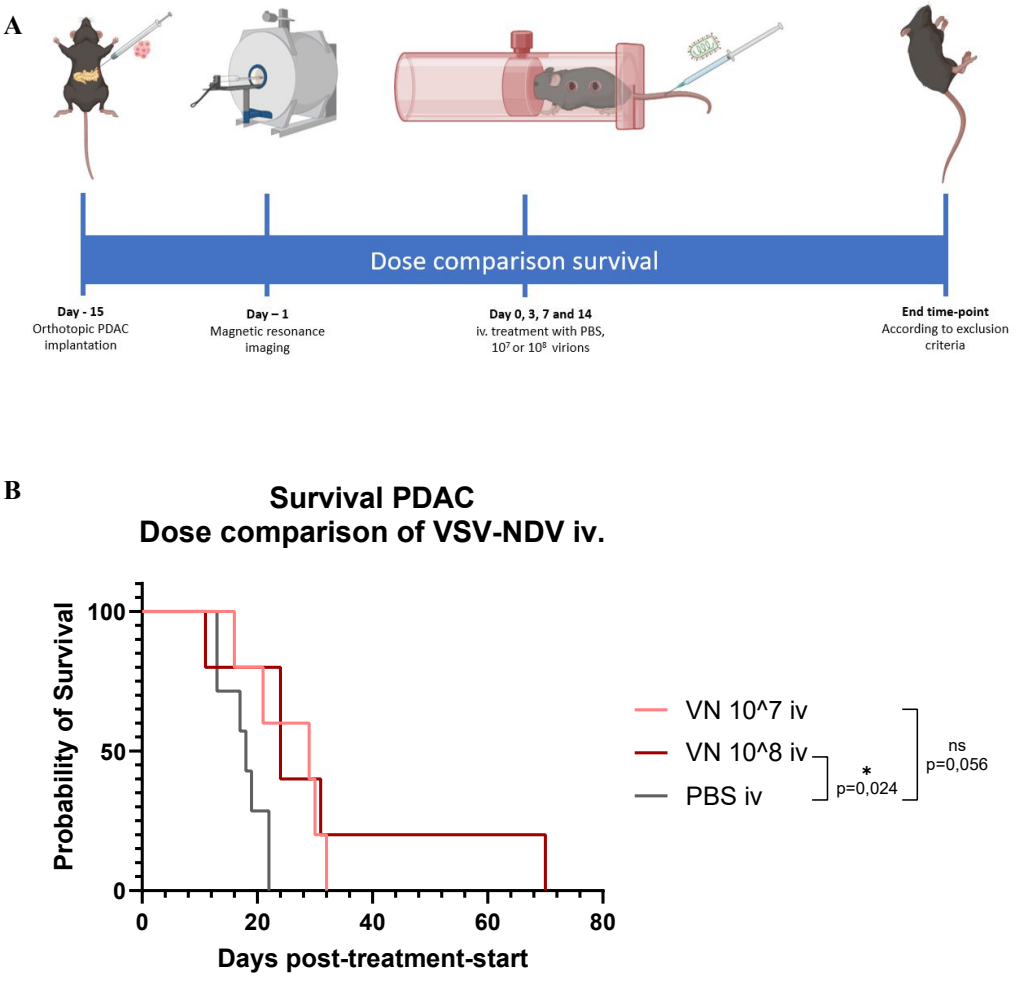

Figure 33: Dose-comparison experiment (A) Time-line: C57/BL6J mice received a pancreatic implantation of 2500 R211 cells at the age of 8 to 9 weeks, were imaged by magnetic resonance imaging (MRI) and randomized to treatment groups, to receive VSV-NDV (10^7 virions) or PBS intravenously, and sacrificed at humane endpoints. *Created with Biorender.com* (B) Kaplan-Meier survival curve for the 3 groups. There were 7 mice in the PBS group, 5 mice in the VSV-NDV (10^7 virions) group and 5 mice in the VSV-NDV (10^8 virions) group.

5.2.1.4. *In vivo* mechanistic studies

After the successful results obtained through simple intravenous therapy with VSV-NDV, a kinetics experiment was designed to uncover the timely mechanisms of the virotherapy at the beginning of the treatment, namely one day after each of the 3 treatment time-points on day 0, 3, and 7. Figure 34 presents the detailed timeline of this experiment.

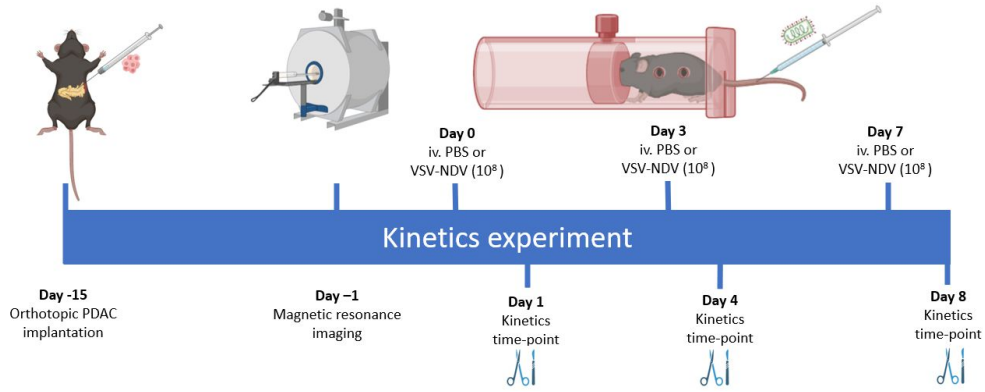

Figure 34: Timeline for the kinetics experiment**.** C57/BL6J mice received a pancreatic implantation of 2500 R211 cells at the age of 8 to 9 weeks, were imaged by magnetic resonance imaging (MRI) at day -1 and randomized to treatment groups, to receive VSV-NDV (10^8 virions) or PBS intravenously at days 0, 3 and 7, and sacrificed at days 1, 4 or 8. *Created with Biorender.com*

Three important organs (the tumours, the livers and the spleens) were extracted, weighed and prepared for flow-cytometry analysis. The antibody panels used for each organ revolve around 3 axes: the NK panel for the early innate response on days 1 and 4, the T-helper cells panel and the cytotoxic T cells panel for the adaptive immune answer, on days 4 and 8. There were attempts to analyse immune cells of the draining lymph nodes of the tumour ; however due to inconsistencies in the isolation and low cell counts, these data are not presented.

Immune cell data from the tumours are summarized in Figure 35.

As could be seen on the weights' representation, the tumours from Day 1 were much smaller than on the other time points, hence the impossibility to run many panels on them. The differences in immune cell compartments between the treatment groups were not statistically significant.

On day 4 however, differences between the virus-treated group and the control group were already prominent. The NK-cell population, an important component of innate immunity was significantly increased in the treated group than in the controls. As expected, interferon-gamma, secreted by NKs and responsible for the antiviral response, was highly expressed in intratumoural NK cells in the VSV-NDV group, compared to the PBS group. The percentage of CD69 positive NK-cells was highly upregulated in the virus group, as a sign of their enhanced cytotoxicity. Also, the Granzyme A positive cells, which secrete cytotoxic granules, were more numerous in the viral group. NKG2D-positive cells, sensors for viral infections and DNA damaged cells, as well as mediators of immune activation, were also more present in the virus group than in the mock.

The CD4 positive T-cells, or helper T-cells, found in the tumours on day 4, were slightly down-regulated (although not statistically significant) in the virus-treated group than in the mock-treated group, but this trend inverted on day 8. The specifically CD69 and PD-1 positive T-helpers cells showed an early activation for the virus group at day 4, with an exhaustion observed at day 8.

Similarly, the number of cytotoxic T-cells in the tumours at day 4 was similar in both treatment groups, while the number was significantly higher in the VSV-NDV-treated mice on day 8. Presumably, by day 8 the priming and proliferation had taken place in the tumour, or with new CD8+ T cells arriving into the tumour. For the two activation markers depicted here, CD69 and PD-1, we also noticed a general upward regulation over time, significantly stronger for the virus-treated group than the control. Over time, activation of CD69 can contribute to T cell exhaustion via upregulation of immune checkpoints, such as PD-1. While PD-1 is considered to be an activation marker at early time-points, it becomes a marker of exhaustion at later time-points.

These flow-cytometry data indicate that the immune cell infiltration of the tumours was higher in the mice treated intravenously with VSV-NDV than with PBS. The presence of the virus and of damaged cells through its replication leads to remodelling of the TME, probably via both, an antiviral and an antitumoural response. However, within the limitations of the included analyses, it is impossible to distinguish against what the identified immune responses were directed.

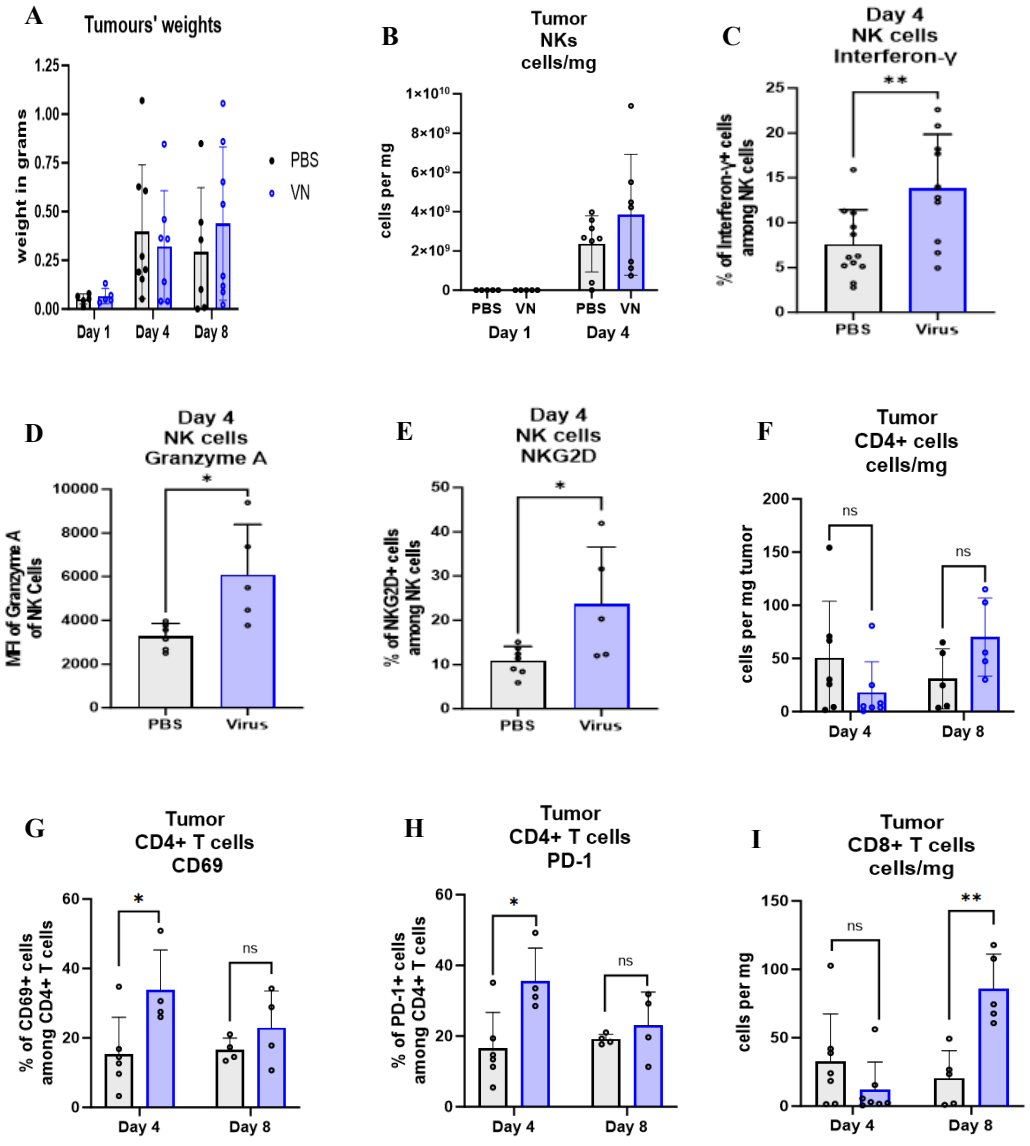

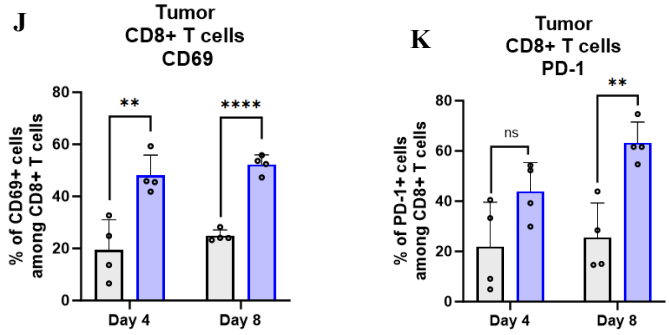

Figure 35: Flow-cytometry analysis for the tumours of days 1, 4 and 8. A) tumours weights in grams. (B to E) Natural killer cells panel (F to G) T-helper or CD4+ cell panel (H to K) Cytotoxic or CD8+ T cell panel.

To paint a more complete picture of the virotherapy in the mice, the livers and spleens of the mice were also analysed for systemic effects. The liver-based data are shown in Figure 36.

Because liver analysis was new to the group, there was an evolution in the methodology between day 1 and 4 and 8. On day 1, only one lobe of the livers was taken and directly processed, while on days 4 and 8, the whole livers were perfused with PBS and fully processed, which explained the major weight difference. In general, there was no significant weight difference between the groups.

As was mentioned earlier, the liver exerts the important role of immunosurveillance, as it drains blood from the portal vein. Hence, the number of ***activated*** immune cells (NK cells, T-helpers and Cytotoxic T cells) found into the livers was persistently more elevated for the virus treated mice, than the controls.

The absolute number of NK cells detected within the livers augmented between day 1 and 4, and they were recruited more strongly for the viral treated mice (in an extremely significant manner on day 4). NKG2D positive NK cells remained more present within the virus group than in the control, as their mission is to sense viral and DNA damages in the cells correlating with the higher number of Granzyme A secreting NK cells detected in the virally exposed livers by day 4. The activation and senescence marker KLRG1 on day 4 signals an exhaustion of the NK cells.

The absolute number of T-helper cells was equivalent between the groups, and both reached exhaustion between day 4 and 8. On day 4, there wasn't much difference in the CD69 and PD-1 markers, but by day 8, these two markers were significantly elevated for the virus exposed group. CD69 in CD4+ cells is associated with tissue residency[150], while PD-a is a common marker for immune downregulation and is widely expressed in the liver.

Conversely, the numbers of CD8 + T-cells kept on increasing for the virus group, but decreased in the control group: maybe a sign of beginning immune tolerance from the PBS treated animals. Again, part of the intrahepatic CD69+ CD8+ T cells detected might be tissue resident, with reduced effector functions[151]. However, the increase in cell numbers suggests the recruitment of more T cells, potentially "normally" primed. The PD-1+ helper cells remained more numerous in the virus group than in the PBS, just like the senescent KLRG1 positive T-cells: these were signs of the continuing immune response, heading towards exhaustion.

In the end, the general trend was a stronger immune cell response at day 8 than at day 4, which seemed normal, given the percent of cells present on these days. Considering the immune tolerant nature of the liver, the fact that the virus group shows activation is another proof of the immunogenicity of VSV-NDV.

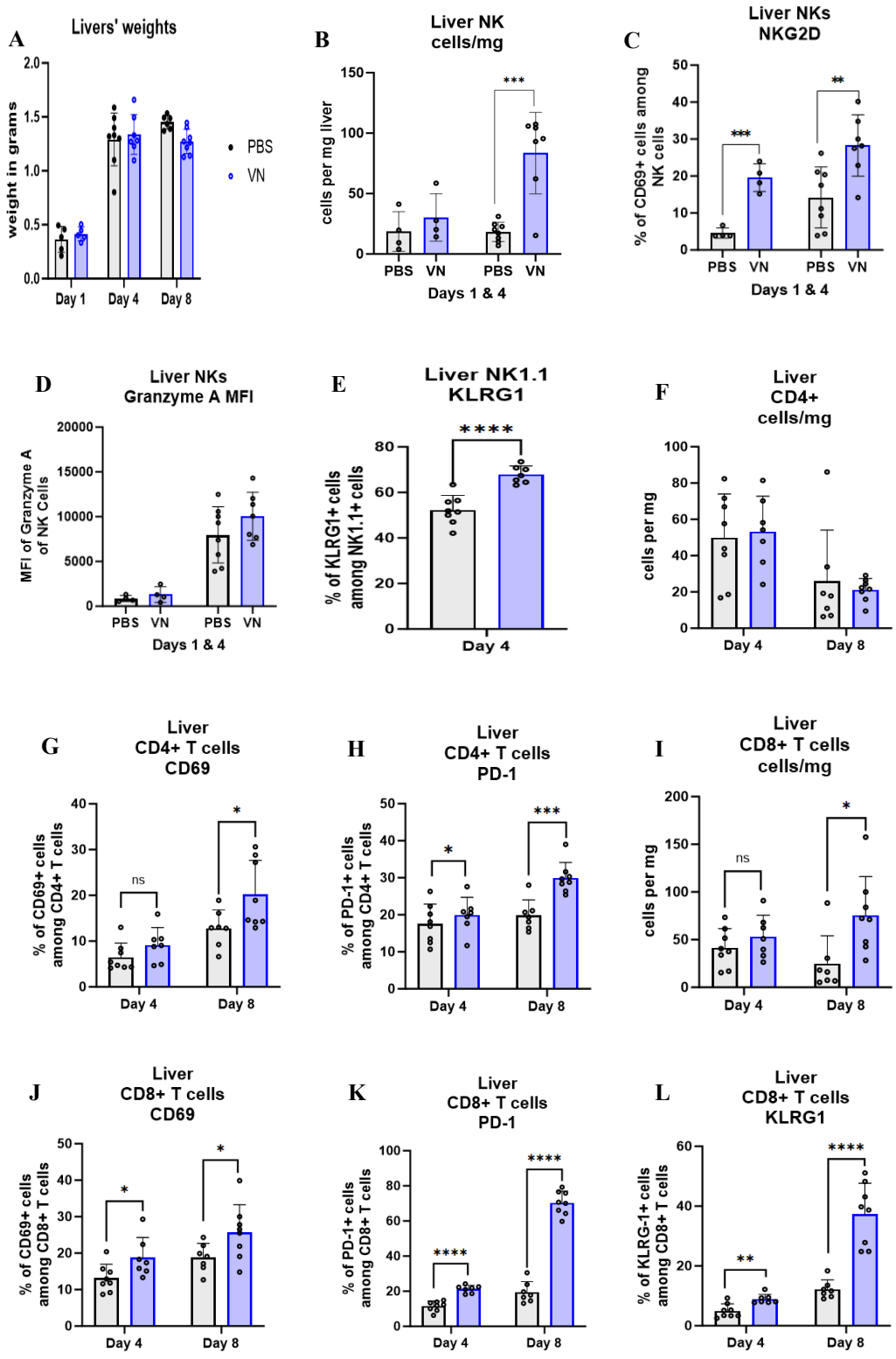

Figure 36: Flow-cytometry analysis for the livers on days 1, 4 and 8. A) liver weights in grams. (B to E) Natural killer cells panel (F to H) T-helper or CD4+ cell panel (I to L) Cytotoxic or CD8+ T cell panel.

Finally, the main secondary lymphoid organ of the body was analysed for its immune cells population (Figure 37). The spleen's systemic response to the virus was the most impressive: there was a significant increase in the weight of the VSV-NDV mice compared to the controls on day 4 and 8, a strong indication that the immune cells are proliferating.

On day 1, there is a very significant depletion of the NK cells for the virus group, which worsened until day 4, where both groups had very low levels of NKs. Nevertheless, analysis of NK activation markers (CD69, IFN- γ, granzyme A, and NKG2D) demonstrated significant activation on days 1 and 4 post-treatment with VSV-NDV compared to PBS. There were generally more activated NK cells (CD69), more antiviral, antitumour sensing (NKG2D) and signalling (IFNγ), more direct cytotoxicity (Granzyme A). This observation also applied to the CD4+ and CD8+ cells, both displaying more activation and proliferation within the viral group: CD69 (activation), PD-1 (activation and regulation), and KLRG1 were upregulated. Logically, the activation of KLRG1, the senescence marker, was delayed compared to the other markers.

The spleen was fulfilling its functions of privileged priming and proliferation site for the circulating immune cells, as an answer to the viral presence, the release of the tumour antigens, and the damaged cells resulting from the infection. The immune system stimulated by the oncolytic virus showed a more potent activation than the PBS controls.

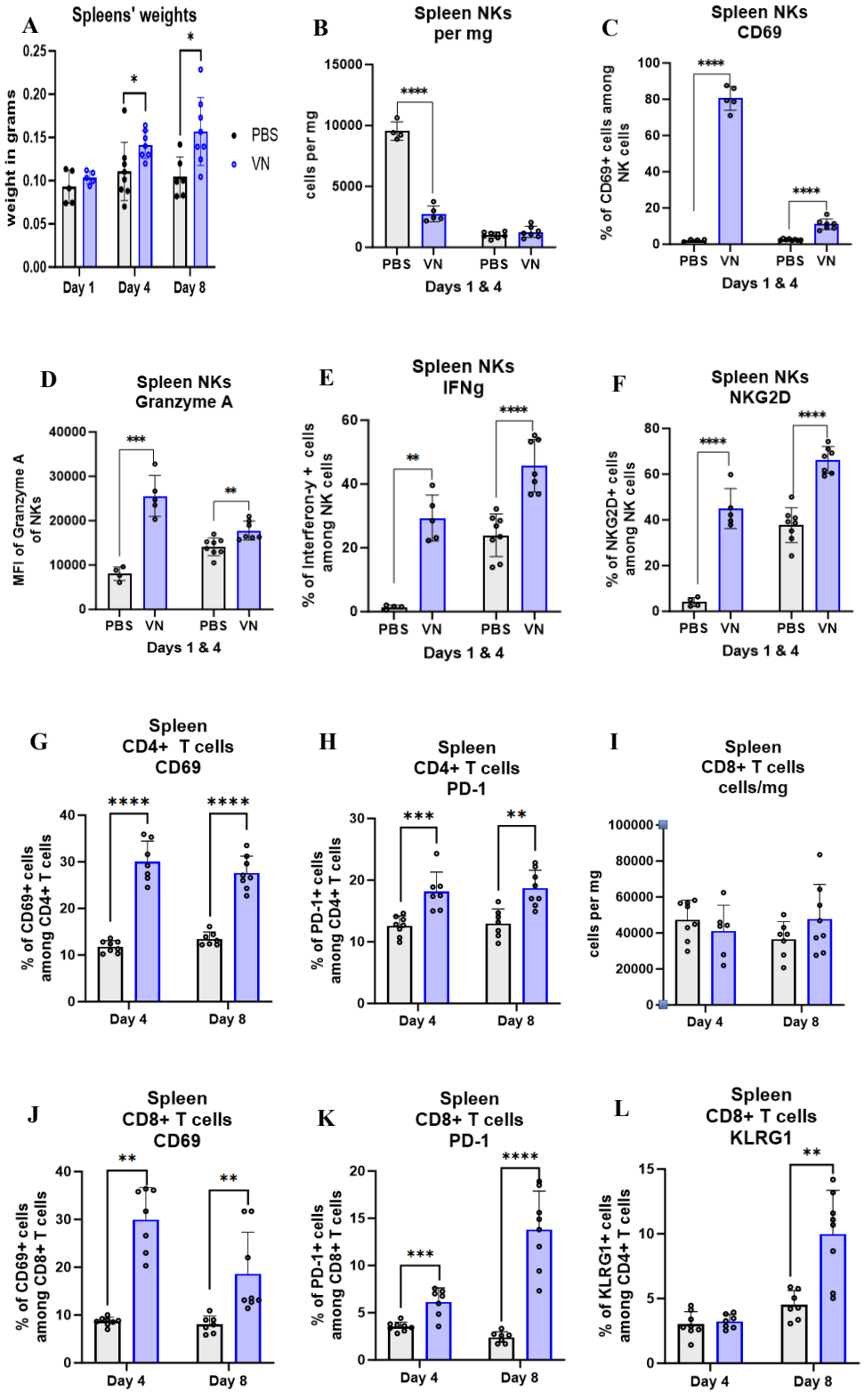

Figure 37: Flow-cytometry analysis for the spleens on days 1, 4 and 8. A) liver weights in grams. (B to F) Natural killer cells panel (G to H) T-helper or CD4+ cell panel (I to L) Cytotoxic or CD8+ T cell panel.

To sum up, evidence of an enhanced immune cell infiltration, proliferation, and activation could be observed in the tumour, liver, and spleen in response to oncolytic VSV-NDV therapy, indicating both a local and systemic immune response that was likely, at least partially, directed against the tumour.

5.2.2. Extracellular matrix experiments

With the VSV-NDV infection demonstrating effects on the life-span and immune cell infiltration of the mice, we were motivated to investigate whether the ECM-degrading viruses could potentially improve these effects by further targeting the predominant PDAC stroma.

The tumour implantation and randomization were performed as described in the dose-finding study, with the exception being the treatment groups: VSV-NDV, VSV-NDV-SPAM1, -MMP8, and -RLN2, all injected intravenously at a dose of 10^7 TCID50 per animal on days 0, 3, 7, and 14. Unfortunately, due to the attenuation of the viruses *in vitro*, production of some of the ECM-degrading viruses at a sufficient concentration to achieve a higher dose of 10^8 TCID50 was not realisable.

As can be seen in the survival curve of Figure 38 below, there was no significant difference between any of the groups. From the *in vitro* experiments, it was known that the ECM-degrading viruses were attenuated, and the “low” treatment dose may have further limited their potency. Surprisingly, the VSV-NDV-SPAM1 group had the shortest median survival with 12,5 days and died earlier on average than the PBS group, with 14 days, although this is not statistically significant. The VSV-NDV-RLN2 virus performed very similarly to the PBS group, while the VSV-NDV-MMP8 group lived a median of 18 days, nearly overlapping with the VSV-NDV survival curve, and VSV-NDV-RLN2 a median of 15 days. The first mouse died on day 8 after treatment start, the last ones on day 29 post-treatment.

Overall, this experiment failed, as even the VSV-NDV group did not perform better than the untreated mice group. Thus, no clear conclusion can be drawn regarding the relative efficacies of the ECM-degrading viruses in comparison to parental VSV-NDV based on this pilot experiment. The experiment should be repeated with higher viral concentrations and larger group sizes. Furthermore, initiating treatment at a time-point in which the tumours are less advanced might allow for improved treatment outcomes and potentially, a setting in which it is easier to discern therapeutic differences among the viral vectors.

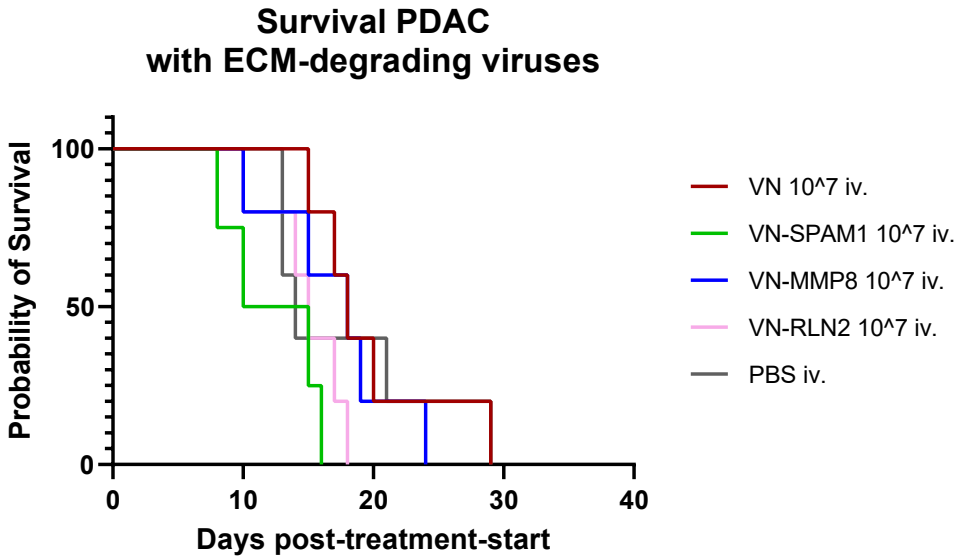

Figure 38: Kaplan-Meier curve for the ECM-degrading viruses survival experiment. C57/BL6J mice received a pancreatic implantation of 2500 R211 cells at the age of 8 to 9 weeks, were imaged by magnetic resonance imaging (MRI) and randomized to treatment groups, to receive 10^7 virions per injection of VSV-NDV, VSV-NDV-SPAM1, VSV-NDV-MMP8, VSV-NDV-RLN2 or PBS intravenously, at days 0,3,7 and 14. The mice were sacrificed at humane endpoints. (B) Kaplan-Meier survival curve for the 3 groups. There were 5 mice in the VSV-NDV group, 4 mice in the VSV-NDV-SPAM group, 5 mice in the VSV-NDV-MMP8 group, 5 mice in the VSV-NDV-RLN2 group, and 5 mice in the PBS group.

5.3.3. *In vivo* virotherapy of VSV-NDV in combination with a BRD4 inhibitor: AZD5153

In order to investigate the action of the BRD4-inhibitor AZD5153 on PDAC tumours *in vivo* in combination with VSV-NDV, the previously described orthotopic PDAC model was employed. After randomization, 10^8 TCID50 of VSV-NDV or PBS was injected intravenously on days 0, 3, 7, and 14 in addition to 30mg/kg of AZD5153 or control vehicle administered by oral gavage 3 times per week, over 21 days, starting on day 0. A schematic representation of the timeline is visible in Figure 39 A).

Unfortunately, as depicted in Figure 39 B), all of the groups showed a very similar survival trend, with a median survival of VSV-NDV with control gavage of 46 days, VSV-NDV with AZD5153: 42 days, PBS with control gavage: 45,5 days, PBS and AZD5153: 48,5 days. Intriguingly, the overall survival span was situated between 18 and 77 days.

This survival study, due to the unusually slow and heterogenous growth rate of the tumours, cannot allow for any conclusions to be drawn regarding the therapeutic efficacy of AZD5153 in combination with oncolytic VSV-NDV. Furthermore, the administered dose of AZD5153 was selected based on reports in literature for other solid tumours, and had not yet been tested in this orthotopic model. Therefore, prior dose testing of the inhibitor should be performed to adapt the concentration and maybe frequency of treatment, to then repeat the experiment.

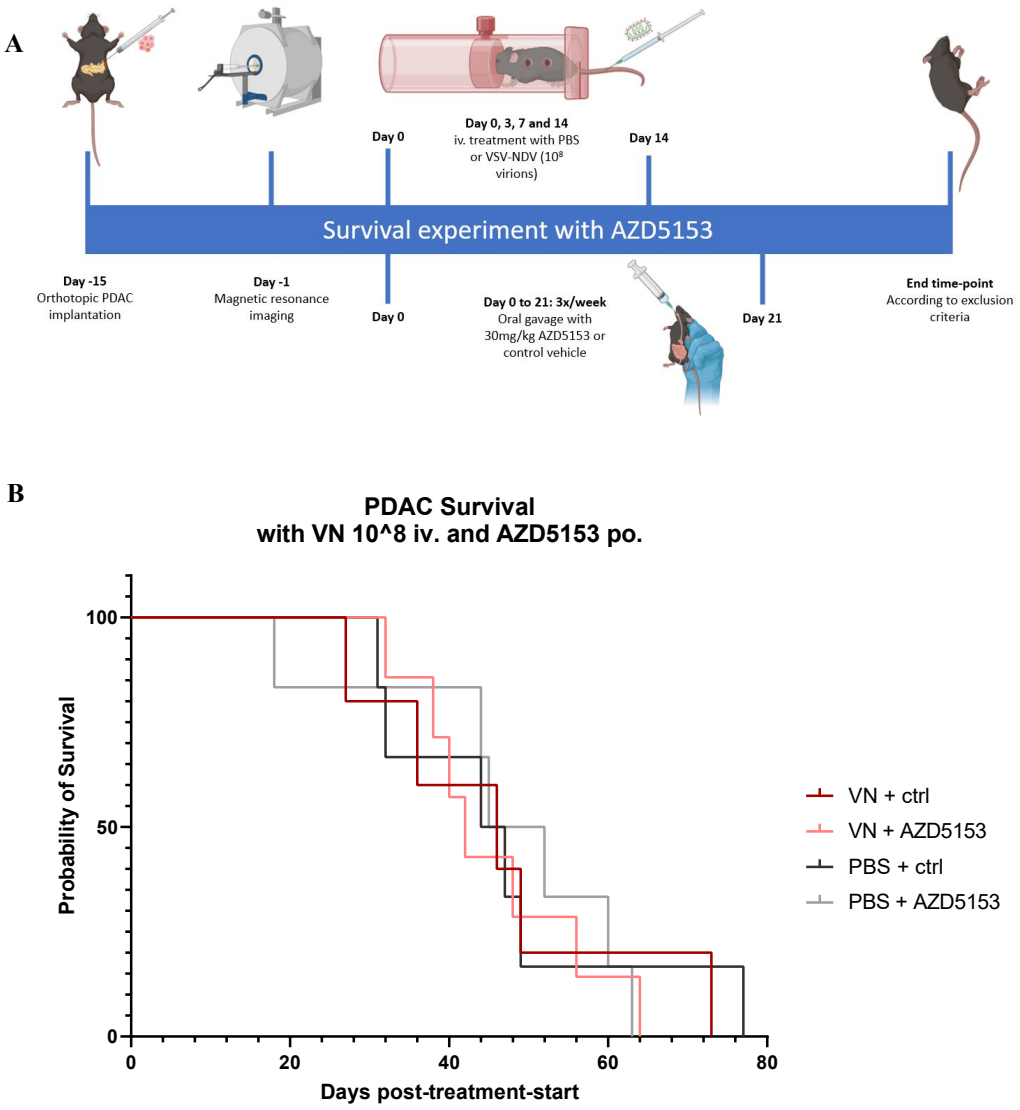

Figure 39: Timeline and survival curve for the survival experiment with VSV-NDV and AZD5153 (A) Time-line: C57/BL6J mice received a pancreatic implantation of 2500 R211 cells at the age of 8 to 9 weeks, were imaged by magnetic resonance imaging (MRI) and randomized to treatment groups, to receive VSV-NDV (10^8 virions) or PBS intravenously, in combination with oral gavage of either AZD5153 (30mg/kg) or control three times a week, from day 0 to day 21. The mice were sacrificed at humane endpoints. *Created with Biorender*. (B) Kaplan-Meier survival curve for the survival experiment combining VSV-NDV (10^8 virions per injection) and oral AZD5153 (30mg/kg.). The VSV-NDV + control group was composed of 5 mice, VSV-NDV + AZD5153 group of 7 mice, the PBS + control group of 6 mice, and the PBS + AZD5153 group of 6 mice.

6. DISCUSSION

Oncolytic therapy is a new possible treatment option for PDAC patients, especially when complete surgical resection is impossible, when the tumours are resistant to therapy, or in case of metastatic disease. Oncolytic viruses, through their ability to activate the immune system, turn "cold" tumours into "hot" ones, and target metastases (VSV-NDV itself was proven efficient on abscopal tumours[69]), represent great candidates. With the high mutation rate and resistances characteristic for PDAC, an effective monotherapeutic approach seems unlikely, which is why combination therapies and "armed" viruses are investigated in this work.

Various types of murine PDAC cell lines, epithelial or mesenchymal, were screened for their susceptibility to VSV-NDV infection. One of the profiles (KRAS-driven, epithelial type) was tendentially more infectible, although even among these cell types, the response to virus infection was rather heterogenous. As for the parent viruses, tested in two murine PDAC cell lines, VSV was the fastest virus, followed by NDV, and VSV-NDV. However, VSV-NDV proved efficient at lower titres than its parent viruses, in former publications[102]. The relative susceptibilities of the cell lines might be due a variety of mechanisms, including differences in virus-targeting receptor expression (thereby affecting entry), or other genotypic or phenotypic differences within the cells that effect virus replication and/or packaging efficiency. Ongoing work within our group revealed that the same heterogeneity was found in human PDAC cell lines, ranging from very susceptible to VSV-NDV infection to very resistant. A much wider cell panel testing and genomics, transcriptomics, or proteomics analysis may point in the direction of the relevant mutations or signalling pathways implicated in determining the permissiveness to VSV-NDV. This could ultimately allow for the pre-testing of patient's samples considering our therapy in the future.

With the *in vitro* experiments showing encouraging results for VSV-NDV infections, we decided to test the model *in vivo*. The effect of a VSV-NDV monotherapy at a repeated dose of 10^8 virions, injected intravenously has been

demonstrated in the survival experiment. The subsequent kinetics study of the mechanism demonstrated a heightened immune cell infiltration within the tumours in the virus treatment group, along with an indication of systemic activation of the immune system, as witnessed in the liver and spleen. However, due to limitations of these proof-of-concept studies presented here, one cannot distinguish between the immune reaction that is induced by the released tumour antigens (and thereby directed against the tumour) and the antiviral immune response. To address this question, additional studies are needed, including studies in non-tumour bearing mice, in order to evaluate the baseline immune response against the virus. In addition, survival studies, in which tumour-bearing mice are treated with immune cell-depleting antibodies, would allow for the evaluation of the respective immune cell contribution to the therapeutic effect. Furthermore, the introduction of a model antigen into the tumour cell line would enable the discrimination of antiviral versus antitumoural T-cell responses directed against this artificial antigen, by using FACS tetramers that are specific for TCRs targeting the model antigen versus a viral protein (N).

An important aspect to note is that, although virus-directed immune responses are often considered to be counter-productive to the therapy, they can, in fact, contribute indirectly to a potent therapeutic effect, since cytotoxic T cells specific for the virus antigens would efficiently home to the TME and kill infected tumour cells. Furthermore, the ability of OVs to efficiently prime T cell responses supports their use to overexpress predominant tumour antigens as a cancer vaccination approach. This is approach is currently under investigation in the group, using an oncolytic VSV-NDV expressing the OVA protein (ovalbumine) as a model antigen.

The studies presented here show us the limitations in the orthotopic model employed. Tumour growth was rather heterogenous, at least partially due to leakage of the injected tumour cells from the injection site during implantation in the pancreas, and the difficulty of assessing the tumour volume in the MRI scan, which may have influenced the group randomisation as well. As was seen in the *in vivo* experiments with ECM-degrading viruses and the combination experiment with AZD5153, the heterogeneity in tumour growth rate also plays an important role in

whether or not the treatment has a chance to prove its efficiency. Voluminous and aggressive tumours by treatment start are clearly more challenging than less advanced tumours, especially because of the desmoplastic microenvironment, with its collapsed vessels and prevailing immunosuppressive background. Also, larger tumours require a more effective debulking, and limit the time the treatment has to mediate its effects before the patient succumbs to the overwhelming tumour burden. In the future, the use of genetically engineered mouse PDAC model would be beneficial, to demonstrate the efficiency of our virotherapy in a more realistic pathologic context, and to come closer to clinical trials.

PDAC tumours are known for their ability to develop resistances during treatment, which is why the combination of different strategies through multi-chemotherapies such as FOLFIRINOX for instance, have proven more efficient. On the oncolytic virus side, first combination studies using various inhibitors have demonstrated the potential of such adjuvants, BRD4 inhibitors having distinguished themselves with other virus types, namely Herpes viruses[152]and Adenoviruses so far. Indeed, the simultaneous use of T VEC and BRD inhibitors lead to an enhanced therapeutical effect on NC carcinoma cells, *in vitro*. However, the authors considered these inhibitors mostly for their capacity to slow down the tumour growth, while not impeding the viral replication, until the oncolytic and immunologic effects of the virus would take over[152].

The BRD4 protein is present in the pancreas and almost all tissues[153]. It is also overexpressed in many PDAC lines, where it promotes tumour cell proliferation and can support resistance mechanisms against chemotherapeutics like Gemcitabine, via regulation of the sonic hedgehog (SHH) pathway[154,155].

More interestingly, in a PDAC context, a screening was performed to assess the replication of three Adenoviruses in combination with various small molecule inhibitors, all potentially facilitating viral replication: out of them, two BRD inhibitors, iBet-762 and OTX-015, were selected over EZH2 and Aurora inhibitors. With these Adenoviruses and BRD inhibitors combinations, infections in 3D cultures and *in vivo* xenografts showed more lysis and a better viral replication. These were attributed to increased viral gene expression, parallel to a decreased

expression of oncogenes as well as of interferon pathways. Noticeably, these combinations also rendered previously non-susceptible stellate cells more infectible[156].

The most commonly described mode of action for BRD4 inhibitors is the downregulation of the ubiquitous c-Myc pathway, which maintains the TME by regulating multiple intracellular and extracellular functions[157] such as cell proliferation, stromal modulation, the secretion of inflammatory cytokines (IL-6, CCL2[158]) or angiogenesis, ultimately responsible for tumour growth. JQ1 is able to downregulate ACTA2, leading CAFs to adopt a normal secretive state[158]. Endogenous c-Myc was proven essential for the maintenance of KRAS-driven lung tumours in a genetic mouse model[159] and in 2011, *Sodir et al* demonstrated that c-Myc inhibition had a negative effect on the vascularization of a pancreatic RIP1-Tag2 tumour model[157]. JQ1 was indeed able to block tumour development, c-Myc and inflammation in a KRAS driven PDAC model[160,161]. Curiously, the effects described by the inhibition of the SHH pathway mirror those of a c-Myc inhibition.

However, JQ1's in *vitro* effects are not always representative of its *in vivo* action, as was witnessed by *Yamamoto et al:* cell growth inhibition was negligible *in vitro*, and only evident *in vivo*. This, and the fact that their BRD4 knockdown only partially reproduced JQ1's effects, led them to hypothesize that extrinsic mechanisms must be involved in the inhibition's positive effects. They also noticed a reduced tumour infiltration of macrophages in JQ1 treated animals[158]. This is positive, as JQ1's synergistic actions may be enhanced *in vivo* compared to *in vitro*. Interestingly, BRD4 inhibitors like JQ1 were shown to attenuate BATF expression in CD8+ T cells, leading to a longer persistence and superior anti-tumour effects, as well as more differentiation into effector memory phenotype T-cells[162]. As we observed an increased immune cell infiltration in our kinetics experiments after virus treatment, it is tempting to speculate that BRD4 inhibition could increase the efficacy of activated T-cells, thereby contributing to the rationale for combining oncolytic VSV-NDV with BRD4 inhibition in cancer therapy.

Contrarily to oncolytic viruses, inhibitors also influence non-neoplastic cells, as mentioned earlier with the PDAC stellate cells. Hence, the systemic inhibition of

the c-Myc pathway with a BRD4 inhibitor, for both neoplastic and non-malignant cells, might be a valid approach against other types of KRAS-induced cancers, especially as stromal cells are more stable and less prone to mutations than cancer cells. Targeting them in order to unbalance the TME, which they support and maintain, could be a reliable strategy. In the end, as the whole tumour would be targeted, the combination effects might be greater.

Indeed, the stroma of PDAC tumour makes up for most of its volume, and CAFs have become a point of interest over the years, due to their various cancer sustaining functions. Crosstalk between CAFs and PDACs has been described in the context of a VSVΔ51 infection in PDAC[66]. In this case, the tumours cells, through secretion of TFG-β, mediated the production of fibroblast growth factor (FGF2) by the CAFs, which induced a downregulation of the RIG-I pathways in the cancer cells, sensitizing them to infection. This was observed *in vitro* and *in vivo* in a xenograft model. In the project presented here, crosstalk between murine PDAC cells and one out of three tested CAF cell lines led to increased cytotoxicity of cancer cells indicating a similar role of CAFs during VSV-NDV infection. However, this effect could not be reproduced in the other two CAF cell lines analysed and susceptibility of CAF cells to VSV-NDV infection was low. It has to be noted that all three CAF cell lines analysed here were derived from an identical genetic background, but behave differently in face of a viral infection. More investigations into the detailed crosstalk may uncover differences between these cell lines, and help determine the responsible factors for enhanced infection: for instance, measuring TGF-β, FGF2, IFN levels or RIG-I expression. Another possible explanation for the different results could be the slower proliferation rate of PSC3 Prxx1, compared to PSC806/10 and FB704F3.

In a real PDAC tumour, different subpopulations of CAFs fulfil complementary roles[163], as described by *Öhlund et al, 2016.* The so-called inflammatory CAFs (iCAFs) grow in the periphery of the stroma, express lower α-SMA levels but secrete proinflammatory cytokines such as IL-6 and IL-11 which promote tumour expansion and invasion. On the other hand, the myofibroblastic CAFs (myCAFs), directly surrounding PDAC cells, are characterized by a high expression of α-SMA.

These myCAFs can physically protect cancer cells from outer threats, but also limit their expansion. Most importantly, CAFs can switch between an inactivated, or activated iCAF or myCAF state, depending on the signalling in their environment[163].

In the experiments presented here, the CAFs were always activated and in the direct coculture, in immediate contact with the PDAC cells, meaning that they adopted a myofibroblast phenotype. Hence, despite bringing this *in vitro* model closer to a real tumour setting, the intricate balance between the different CAF populations and stromal cell matrix compartments, as well as their respective crosstalk could not be recapitulated *in vitro*. One could argue that the conditioned media experiments were closer from an inflammatory CAF phenotype, but unidirectional. In the end, this *in vitro* setting allowed the indication of crosstalk occurring between the PDACs and myCAFs. It would be interesting to use more plastic CAFs, able to switch between an inactivated state, and the myCAF or iCAF activated phenotype, to see how the crosstalk evolves depending on the coculture chosen: direct with cell-cell contact, or indirect through transwells, as well as combined, and which effect the different subtypes of CAFs have on the oncolytic virus infection. This enhanced setup might also better predict a potential enhancement of OV infection mediated by BRD4 inhibition.

In this work, using an oncolytic virus to target the TME was an additional strategy that was investigated. The TME is largely composed of activated cancer fibroblasts[164], responsible for the typical PDAC desmoplasia. To circumvent this problem, a common strategy consists in depleting the microenvironment of its collagen, classically with collagen-degrading enzymes. The use of ECM-degrading enzymes to target the fibrotic tumour stroma showed encouraging preclinical results with the systemic application of hyaluronic acid combined with Gemcitabine[21], or with viruses expressing ECM-degrading enzymes, with VCN-01 even going to clinical trials[75]. On the contrary, the use of Relaxin (RLN) *in vivo* led to unexpected outcomes. RLN upregulates matrix metalloproteinases, leading to ECM degradation. In a colorectal cancer metastatic liver model, exposure to the peptide hormone promoted a quiescent phenotype of hepatic stellate cells, with reduced

contractility and diminished expression of fibrotic gene expression. At the same time, a better T-cell infiltration of the tumour was observed[165]. However, the effect of RLN on cancer cannot be considered exclusively from an ECM-degrading point of view, as the peptide also harbours cancer invasive properties, as reviewed by T*hanasupawat et al, 2019*. In fact, the systemic activation of the relaxin family peptide receptor 1 (RXFP1) pathway by RLN2 increased cell proliferation and matrix invasion in prostate, breast, osteosarcoma and endometrium cells lines, and also in patient's derived glioblastoma multiforme brain cancers *in vitro*[166]. Yet, as oncolytic viruses specifically target the tumour tissues, the systemic effects of RLN might not be relevant. Interestingly, improved survival was observed in a xenograft melanoma model treated with a RLN-armed adenovirus[167], as well as in a PDAC xenograft model treated in combination with Gemcitabine[118].

Ultimately, this work demonstrated that VSV-NDV has therapeutic potential for the treatment of PDAC as virotherapy prolonged survival *in vivo* and induced an enhanced immune response in the tumour as well as systemically. Furthermore, this project highlighted the importance of the TME in PDAC, and the alteration of CAFs and the desmoplasia surrounding the tumour might improve therapeutic outcome even further. Additionally, *in vitro* experiments showed the potential of BRD4 inhibition in combination with VSV-NDV treatment in PDAC cells and further *in vivo* studies are necessary to confirm this synergistic effect. To further investigate the therapeutic potential of VSV-NDV for PDAC, further combinations and comparison with the current gold standard treatment should also be conducted to identify promising combinatorial therapies for PDAC patients.

V. SUMMARY

In vivo characterization of an oncolytic virus for the treatment of pancreatic cancer

Therapies against pancreatic ductal adenocarcinoma are multiple, but so far, none of them has been able to really offer hope to diagnosed patients. With immunotherapies on the rise, and oncolytic viruses getting approval as cancer therapeutics around the world, we decided to test our hybrid virus VSV-NDV in pancreatic ductal adenocarcinoma tumours. Indeed, when injected systemically, oncolytic viruses have the ability to recognize and target cancer cells, including metastases, and to trigger an immune answer against the tumour cells by releasing antigens during replication, while sparing healthy cells. They can also be "armed" with novel properties, or used alongside other drugs, in a multimodal approach.

The virus was first applied to murine pancreatic adenocarcinoma cell lines, *in vitro*. Cells from different backgrounds were infected at different concentrations, and the viral replication and cytotoxic effects were assessed, revealed various levels of susceptibility to VSV-NDV, ranging from very infectible to very resistant.

To better reflect a real TME, different coculture set-ups were introduced to study the interaction between cancer-associated fibroblasts and pancreatic ductal adenocarcinoma cells and the impact on subsequent oncolytic viral infection. The co-culture involving the pancreatic stellate cells PSC3 Prxx1 showed promising results, with a better infection in direct contact coculture than for both cell lines cultured independently, suggesting a crosstalk between these cell types.

In parallel, the viral monotherapy was tested in an orthotopic implanted pancreatic model, using the R211 cell line in immunocompetent C57BL/6 mice. Survival benefits were observed when VSV-NDV was administered intravenously at a dose of 10^8 TCID50 in comparison to the PBS control. The corresponding kinetics experiment demonstrated an increased immune cell infiltration into the tumour, as well as systemic effects in the spleen and liver, via flow-cytometry measurements.

In approach to potentially enhance the oncolytic effects of our virus, various small molecule inhibitors were tested on the pancreatic ductal adenocarcinoma and the cancer-associated fibroblasts cell lines. Bromodomain 4 inhibitors showed promising synergistic results with VSV-NDV; however, Bromodomain 4 knock-out cell lines failed to reproduce the effects of the inhibitor, indicating that off-target effects of the Bromodomain 4 inhibitor were the likely responsible for the enhancement of VSV-NDV infection.

Following these encouraging *in vitro* results, a survival experiment involving oral administration of AZD5153 alongside intravenous treatment with VSV-NDV was conducted. Regrettably, the growth of the tumours was inexplicably heterogeneous and different from that observed in previous experiments, and no conclusive findings could be derived from this study. It is also possible that the dose of AZD5153 used in this experiment was sub-optimal.

Finally, in order to improve the tumour accessibility for treatment, experiments were conducted using three recombinant extracellular matrix-degrading viruses, engineered to express hyaluronidase, matrix-metalloproteinase 8, or relaxin 2. Unfortunately, the viruses showed attenuated properties *in vitro*, although these effects were compensated by the addition of a Bromodomain 4 inhibitor. The corresponding *in vivo* survival experiment was conducted using a low dose of virus and failed to demonstrate any clear treatment benefits compared to mock. However, a repetition with a higher virus dose, in combination with a synergistic Bromodomain 4 inhibitor could mediate improved therapeutic outcomes.

In the end, the implementation of the VSV-NDV oncolytic virus as a therapeutic for murine pancreatic ductal adenocarcinoma is a promising strategy, laying the foundations for further research.

VI. ZUSAMMENFASSUNG

In vivo Charakterisierung eines onkolytischen Virus für die Behandlung des pankreatisches Adenokarzinoms

Obwohl es zahlreiche Therapien gegen das duktale pankreatische Adenokarzinom gibt, bleibt bei den Patienten mit dieser Diagnose bisher wenig Hoffnung. Im Rahmen der sich weiterentwickelnden Immuntherapien, mit Zulassungen von onkolytischen Viren als Krebstherapeutika weltweit, haben wir unser Hybridvirus VSV-NDV in Pankreas-Adenokarzinom-Tumoren getestet. Onkolytische Viren haben nämlich die Fähigkeit, wenn systemisch verabreicht, Krebszellen, einschließlich Metastasen, zu erkennen und anzugreifen, um eine Immunantwort gegen die Tumorzellen auszulösen, indem sie während der Replikation Antigene freisetzen, wobei gesunde Zellen geschont bleiben. Onkolytische Viren können auch mit neuartigen Eigenschaften „ausgerüstet“ werden, oder als Teil einer multimodalen Therapie eingesetzt werden.

Zuerst wurde das Virus in vitro auf murine Pankreas-Adenokarzinom-Zelllinien angewendet. Zellen unterschiedlicher Herkunft wurden in unterschiedlichen Konzentrationen infiziert und die Virusreplikation, sowie die zytotoxischen Wirkungen bewertet. Dabei wurden unterschiedliche Grade der Anfälligkeit für VSV-NDV festgestellt, die von sehr sensitiv bis sehr resistent reichten. Um eine reale Tumormikroumgebung besser abzubilden, wurden verschiedene Co-Kultur Bedingungen eingeführt. Die Wechselwirkungen zwischen krebsassoziierten Fibroblasten und duktalen pankreatischen Adenokarzinomen Zellen, und deren Auswirkungen auf eine nachfolgende OV-Infektion wurden untersucht. Die Co-Kultur mit den PSC3 Prxx1 Pankreas-Sternzellen zeigte vielversprechende Ergebnisse, wobei die Infektion in der direkten Kontakt Co-Kultur effizienter war als für die jeweiligen Monokulturen, was auf einen Crosstalk hindeutet.

Parallel dazu wurde die virale Monotherapie in einem orthotopisch implantierten Pankreasmodell unter Verwendung der R211-Zelllinie in immunkompetenten C57BL/6-Mäusen getestet. Überlebensvorteile gegenüber der PBS-Kontrolle wurden beobachtet, wenn VSV-NDV intravenös in einer Dosis von 108 TCID50

verabreicht wurde. Das entsprechende Kinetikexperiment zeigte mittels Durchflusszytometriemessungen eine verstärkte Infiltration von Immunzellen in den Tumor, sowie systemische Effekte in der Milz und Leber.

Um die onkolytische Wirkung unseres Virus möglicherweise zu verstärken, wurden verschiedene sogenannte „small molecules"-Inhibitoren an den PDACs und den krebsassoziierten Fibroblasten-Zelllinien getestet. Inhibitoren der Bromodomäne 4 (BRD4) zeigten vielversprechende synergistische Effekte mit VSV-NDV; BRD4-Knockout-Zelllinien konnten die Wirkungen des Inhibitors jedoch nicht reproduzieren, was darauf hindeutet, dass Off-Target-Wirkungen des BRD4-Inhibitors wahrscheinlich für die Verstärkung der VSV-NDV-Infektion verantwortlich waren.

Aufgrund der ermutigenden *in-vitro* Ergebnisse wurde im Rahmen eines Überlebensexperiments eine Kombinationstherapie mit oraler Verabreichung von AZD5153 und intravenöser Behandlung mit VSV-NDV durchgeführt. Leider war das Wachstum der Tumore aus unerklärlichen Gründen heterogen und unterschied sich von dem, was in früheren Experimenten beobachtet wurde: aus dieser Studie konnten daher keine schlüssigen Ergebnisse abgeleitet werden. Möglich ist auch, dass die in diesem Experiment verwendete Dosis von AZD5153 nicht optimal war.

Um schließlich die Zugänglichkeit des Tumors für die Behandlung zu verbessern, wurden Experimente mit drei rekombinanten extrazellulären Matrix-abbauenden Viren durchgeführt, die so konstruiert wurden, dass sie Hyaluronidase, Matrix-Metalloproteinase 8 oder Relaxin 2 exprimieren. Bedauerlicherweise zeigten diese Viren abgeschwächte Eigenschaften *in vitro*, obwohl die Zugabe eines BRD4-Inhibitors diese niedrigeren Effekte kompensierte. Leider wurde das *in vivo*-Überlebensexperiment mit einer niedrigen Virusdosis durchgeführt und konnte keine eindeutigen Behandlungsvorteile im Vergleich zu den Kontrollgruppen nachweisen. Es besteht jedoch die Hoffnung, dass eine Wiederholung mit einer höheren Virusdosis in Kombination mit einem synergistischen BRD4-Inhibitor zu verbesserten Therapieergebnissen führen könnte.

Letztendlich ist die Implementierung des onkolytischen VSV-NDV-Virus als Therapeutikum für murines PDAC eine vielversprechende Strategie, die den Grundstein für weitere Forschung legt.

VII. REFERENCES

1. Sung, H. *et al.* Global Cancer Statistics 2020: GLOBOCAN Estimates of Incidence and Mortality Worldwide for 36 Cancers in 185 Countries. *CA Cancer J Clin* **71**, 209–249 (2021).

2. Accolla, R. S. *et al.* Immune Conversion of Tumor Microenvironment by Oncolytic Viruses: The Protoparvovirus H-1PV Case Study. *Frontiers in Immunology | www.frontiersin.org* **1**, 1848 (2019).

3. FDA Approves T-VEC to Treat Metastatic Melanoma - NCI. https://www.cancer.gov/news-events/cancer-currents-blog/2015/t-vec-melanoma.

4. Sun, J., Russell, C. C., Scarlett, C. J. & McCluskey, A. Small molecule inhibitors in pancreatic cancer. *RSC Medicinal Chemistry* vol. 11 164–183 Preprint at https://doi.org/10.1039/c9md00447e (2020).

5. Rawla, P., Sunkara, T. & Gaduputi, V. Epidemiology of Pancreatic Cancer: Global Trends, Etiology and Risk Factors. *Review World J Oncol* **10**, 10–27 (2019).

6. Pancreatic cancer incidence statistics | Cancer Research UK. https://www.cancerresearchuk.org/health-professional/cancer-statistics/statistics-by-cancer-type/pancreatic-cancer/incidence#heading-Two.

7. Rahib, L. *et al.* Projecting Cancer Incidence and Deaths to 2030: The Unexpected Burden of Thyroid, Liver, and Pancreas Cancers in the United States. doi:10.1158/0008-5472.CAN-14-0155.

8. Orth, M. *et al.* Pancreatic ductal adenocarcinoma: Biological hallmarks, current status, and future perspectives of combined modality treatment

approaches. *Radiation Oncology* vol. 14 1–20 Preprint at https://doi.org/10.1186/s13014-019-1345-6 (2019).

9. Wang, S. *et al.* The molecular biology of pancreatic adenocarcinoma: translational challenges and clinical perspectives. *Signal Transduction and Targeted Therapy* vol. 6 Preprint at https://doi.org/10.1038/s41392-021-00659-4 (2021).

10. Hu, H. feng *et al.* Mutations in key driver genes of pancreatic cancer: molecularly targeted therapies and other clinical implications. *Acta Pharmacologica Sinica* vol. 42 1725–1741 Preprint at https://doi.org/10.1038/s41401-020-00584-2 (2021).

11. McGuigan, A. *et al.* Pancreatic cancer: A review of clinical diagnosis, epidemiology, treatment and outcomes. *World Journal of Gastroenterology* vol. 24 4846–4861 Preprint at https://doi.org/10.3748/wjg.v24.i43.4846 (2018).

12. Kuehn, B. M. Looking to Long-term Survivors for Improved Pancreatic Cancer Treatment. *JAMA - Journal of the American Medical Association* vol. 324 2242–2244 Preprint at https://doi.org/10.1001/jama.2020.21717 (2020).

13. Von Hoff, D. D. *et al.* Increased Survival in Pancreatic Cancer with nab-Paclitaxel plus Gemcitabine. *New England Journal of Medicine* **369**, 1691–1703 (2013).

14. Klein-Brill, A., Amar-Farkash, S., Lawrence, G., Collisson, E. A. & Aran, D. Comparison of FOLFIRINOX vs Gemcitabine Plus Nab-Paclitaxel as First-Line Chemotherapy for Metastatic Pancreatic Ductal Adenocarcinoma + Supplemental content. *JAMA Netw Open* **5**, 2216199 (2022).

15. Huguet, F., Mukherjee, S. & Javle, M. Locally advanced pancreatic cancer: The role of definitive chemoradiotherapy. *Clin Oncol* **26**, 560–568 (2014).

16. Wang, D. *et al.* Effect of neoadjuvant radiotherapy on survival of non-metastatic pancreatic ductal adenocarcinoma: A SEER database analysis. *Radiation Oncology* **15**, 107 (2020).

17. Flier, J. S., Underhill, L. H. & Dvorak, H. F. Tumors: Wounds That Do Not Heal. *New England Journal of Medicine* **315**, 1650–1659 (1986).

18. Ho, W. J., Jaffee, E. M. & Zheng, L. The tumour microenvironment in pancreatic cancer — clinical challenges and opportunities. *Nature Reviews Clinical Oncology* vol. 17 527–540 Preprint at https://doi.org/10.1038/s41571-020-0363-5 (2020).

19. Ge, Y. *et al.* Stem Cell Lineage Infidelity Drives Wound Repair and Cancer. *Cell* **169**, 636-650.e14 (2017).

20. Dougan, S. K. The pancreatic cancer microenvironment. *Cancer Journal (United States)* vol. 23 321–325 Preprint at https://doi.org/10.1097/PPO.0000000000000288 (2017).

21. Provenzano, P. P. *et al.* Enzymatic Targeting of the Stroma Ablates Physical Barriers to Treatment of Pancreatic Ductal Adenocarcinoma. *Cancer Cell* **21**, 418–429 (2012).

22. Clark, C. E. *et al.* Dynamics of the immune reaction to pancreatic cancer from inception to invasion. *Cancer Res* **67**, 9518–9527 (2007).

23. Zhang, T., Ren, Y., Yang, P., Wang, J. & Zhou, H. Cancer-associated fibroblasts in pancreatic ductal adenocarcinoma. doi:10.1038/s41419-022-05351-1.

24. Chauhan, V. P. *et al.* ARTICLE Angiotensin inhibition enhances drug delivery and potentiates chemotherapy by decompressing tumour blood vessels. *Nat Commun* (2013) doi:10.1038/ncomms3516.

25. Doherty, G. J., Tempero, M. & Corrie, P. G. HALO-109-301: A Phase III trial of PEGPH20 (with gemcitabine and nab-paclitaxel) in hyaluronic acid-high stage IV pancreatic cancer. *Future Oncology* **14**, 13–22 (2018).

26. Ramanathan, R. K. *et al.* Phase IB/II randomized study of FOLFIRINOX plus pegylated recombinant human hyaluronidase versus FOLFIRINOX alone in patients with metastatic pancreatic adenocarcinoma: SWOG S1313. in *Journal of Clinical Oncology* vol. 37 1062–1069 (American Society of Clinical Oncology, 2019).

27. Gorchs, L. *et al.* The vitamin D analogue calcipotriol promotes an anti-tumorigenic phenotype of human pancreatic CAFs but reduces T cell mediated immunity. (2020) doi:10.1038/s41598-020-74368-3.

28. Garg, B. *et al.* NFκB in Pancreatic Stellate Cells Reduces Infiltration of Tumors by Cytotoxic T Cells and Killing of Cancer Cells, via Up-regulation of CXCL12. *Gastroenterology* **155**, 880-891.e8 (2018).

29. Grell, P. *et al.* Phase II study of the anti-TGF-β monoclonal antibody (mAb) NIS793 with and without the PD-1 inhibitor spartalizumab in combination with nab-paclitaxel/gemcitabine (NG) versus NG alone in patients (pts) with first-line metastatic pancreatic ductal adenocarcinoma (mPDAC). *Journal of Clinical Oncology* **39**, TPS4173–TPS4173 (2021).

30. Ducreux, M. *et al.* Systemic treatment of pancreatic cancer revisited. *Seminars in Oncology* vol. 46 28–38 Preprint at https://doi.org/10.1053/j.seminoncol.2018.12.003 (2019).

31. Pattern recognition receptor (PRRs) ligands | British Society for Immunology. https://www.immunology.org/public-

information/bitesized-immunology/receptors-molecules/pattern-recognition-receptor-prrs.

32. Physiology of Domestic Animals. 2nd edition - PMC. https://www.ncbi.nlm.nih.gov/pmc/articles/PMC3659450/.

33. Shen, J. *et al.* Anti-cancer therapy with <scp>TNF</scp> α and <scp>IFN</scp> γ: A comprehensive review. *Cell Prolif* **51**, e12441 (2018).

34. Lewis, S. M., Williams, A. & Eisenbarth, S. C. Structure and function of the immune system in the spleen. *Science Immunology* vol. 4 Preprint at https://doi.org/10.1126/sciimmunol.aau6085 (2019).

35. Swiecki, M. & Colonna, M. The multifaceted biology of plasmacytoid dendritic cells. *Nature Reviews Immunology* vol. 15 471–485 Preprint at https://doi.org/10.1038/nri3865 (2015).

36. Oda, M., Yokomori, H. & Han, J. Regulatory mechanisms of hepatic microcirculation. *Clin Hemorheol Microcirc* (2003).

37. Kubes, P., Jenne, C. & Snyder, J. Immune Responses in the Liver. *Annu Rev Immunol* 44 (2018) doi:10.1146/annurev-immunol.

38. Doherty, D. G. & O'Farrelly, C. Innate and adaptive lymphoid cells in the human liver. *Immunological Reviews* vol. 174 5–20 Preprint at https://doi.org/10.1034/j.1600-0528.2002.017416.x (2000).

39. Crispe, I. N. The liver as a lymphoid organ. *Annual Review of Immunology* vol. 27 147–163 Preprint at https://doi.org/10.1146/annurev.immunol.021908.132629 (2009).

40. Diehl, L. *et al.* Tolerogenic maturation of liver sinusoidal endothelial cells promotes B7-homolog 1-dependent CD8+ T cell tolerance. *Hepatology* **47**, 296–305 (2008).

41. Huang, L. R. *et al.* Intrahepatic myeloid-cell aggregates enable local proliferation of CD8 + T cells and successful immunotherapy against chronic viral liver infection. *Nat Immunol* **14**, 574–583 (2013).

42. Berg, M. *et al.* Cross-presentation of antigens from apoptotic tumor cells by liver sinusoidal endothelial cells leads to tumor-specific CD8+ T cell tolerance. *Eur J Immunol* **36**, 2960–2970 (2006).

43. Doherty, D. G. Immunity, tolerance and autoimmunity in the liver: A comprehensive review. *Journal of Autoimmunity* vol. 66 60–75 Preprint at https://doi.org/10.1016/j.jaut.2015.08.020 (2016).

44. Heymann, F. & Tacke, F. Immunology in the liver-from homeostasis to disease. *Nature Reviews Gastroenterology and Hepatology* vol. 13 88–110 Preprint at https://doi.org/10.1038/nrgastro.2015.200 (2016).

45. Pillarisetty, V. G., Katz, S. C., Bleier, J. I., Shah, A. B. & DeMatteo, R. P. Natural Killer Dendritic Cells Have Both Antigen Presenting and Lytic Function and in Response to CpG Produce IFN-γ via Autocrine IL-12. *The Journal of Immunology* **174**, 2612–2618 (2005).

46. Krieghoff-Henning, E., Folkerts, J., Penzkofer, A. & Weg-Remers, S. Cancer – an overview. *Med Monatsschr Pharm* **40**, 48–54 (2017).

47. Teng, M. W. L., Swann, J. B., Koebel, C. M., Schreiber, R. D. & Smyth, M. J. Immune-mediated dormancy: an equilibrium with cancer. *J Leukoc Biol* **84**, 988–993 (2008).

48. Balkwill, F. R., Capasso, M. & Hagemann, T. The tumor microenvironment at a glance. *J Cell Sci* **125**, 5591–5596 (2012).

49. Topalian, S. L., Drake, C. G. & Pardoll, D. M. Targeting the PD-1/B7-H1(PD-L1) pathway to activate anti-tumor immunity. *Current Opinion in Immunology* vol. 24 207–212 Preprint at https://doi.org/10.1016/j.coi.2011.12.009 (2012).

50. Chen, A. *et al.* Oncolytic measles virus enhances antitumour responses of adoptive CD8+NKG2D+ cells in hepatocellular carcinoma treatment. *Sci Rep* **7**, (2017).

51. Sugiura, A. & Rathmell, J. C. Metabolic Barriers to T Cell Function in Tumors. *The Journal of Immunology* **200**, 400–407 (2018).

52. Noser, J. A. *et al.* The RAS/Raf1/MEK/ERK signaling pathway facilitates VSV-mediated oncolysis: Implication for the defective interferon response in cancer cells. *Molecular Therapy* **15**, 1531–1536 (2007).

53. Chirmule, N., Jawa, V. & Meibohm, B. Immunogenicity to Therapeutic Proteins: Impact on PK/PD and Efficacy. (2012) doi:10.1208/s12248-012-9340-y.

54. Borrego, F., Robertson, M. J., Ritz, J., Peña, J. & Solana, R. CD69 is a stimulatory receptor for natural killer cell and its cytotoxic effect is blocked by CD94 inhibitory receptor. *Immunology* **97**, 159–165 (1999).

55. Koyama-Nasu, R. *et al.* The cellular and molecular basis of CD69 function in anti-tumor immunity. *International Immunology* vol. 34 555–561 Preprint at https://doi.org/10.1093/intimm/dxac024 (2022).

56. Murphy, K. & Weaver, C. *Janeway Immunologie*. *Janeway Immunologie* (Springer Berlin Heidelberg, 2018). doi:10.1007/978-3-662-56004-4.

57. Lieberman, J. Granzyme A activates another way to die. *Immunological Reviews* vol. 235 93–104 Preprint at https://doi.org/10.1111/j.0105-2896.2010.00902.x (2010).

58. Krepela. Granzyme B-induced apoptosis in cancer cells and its regulation (Review). *Int J Oncol* **37**, (2010).

59. Zafirova, B., Wensveen, F. M., Gulin, M. & Polić, B. Regulation of immune cell function and differentiation by the NKG2D receptor.

Cellular and Molecular Life Sciences vol. 68 3519–3529 Preprint at https://doi.org/10.1007/s00018-011-0797-0 (2011).

60. Schroder, K., Hertzog, P. J., Ravasi, T. & Hume, D. A. Interferon-γ: an overview of signals, mechanisms and functions. *J Leukoc Biol* **75**, 163–189 (2004).

61. Gründemann, C. *et al.* The NK receptor KLRG1 is dispensable for virus-induced NK and CD8 $^{+}$ T-cell differentiation and function *in vivo*. *Eur J Immunol* **40**, 1303–1314 (2010).

62. Kaufman, H. L., Kohlhapp, F. J. & Zloza, A. Oncolytic viruses: a new class of immunotherapy drugs. (2015) doi:10.1038/nrd4663.

63. Hastie, E. & Grdzelishvili, V. Z. Vesicular stomatitis virus as a flexible platform for oncolytic virotherapy against cancer. *Journal of General Virology* vol. 93 2529–2545 Preprint at https://doi.org/10.1099/vir.0.046672-0 (2012).

64. Conry, R. M., Westbrook, B., Mckee, S., Norwood, T. G. & Francis©, T. &. Human Vaccines & Immunotherapeutics Talimogene laherparepvec: First in class oncolytic virotherapy Talimogene laherparepvec: First in class oncolytic virotherapy. (2018) doi:10.1080/21645515.2017.1412896.

65. Lauer, U. M. & Beil, J. Oncolytic viruses: Challenges and considerations in an evolving clinical landscape. *Future Oncology* vol. 18 2713–2732 Preprint at https://doi.org/10.2217/fon-2022-0440 (2022).

66. Ilkow, C. S., Marguerie, M., Batenchuk, C., Lichty, B. D. & Bell, J. C. Reciprocal cellular cross-talk within the tumor microenvironment promotes oncolytic virus activity. *Nat Med* **21**, (2015).

67. Zhang, Y., Li, Y., Chen, K., Qian, L. & Wang, P. Oncolytic virotherapy against the tumor microenvironment and its potential in pancreatic

cancer. *Journal of Cancer Research and Therapeutics* vol. 18 1247–1255 Preprint at https://doi.org/10.4103/jcrt.jcrt_91_21 (2022).

68. Bilgiç, B., Dokuzeylül, B. & Or, M. E. Oncolytic virotherapy and the current approaches in veterinary medicine. *German Journal of Veterinary Research* **2**, 17–27 (2022).

69. Marek, J. *et al.* Oncolytic virotherapy with chimeric VSV-NDV synergistically supports RIG-I-dependent checkpoint inhibitor immunotherapy. *Mol Ther Oncolytics* **30**, 117–131 (2023).

70. Hirooka, Y. *et al.* A Phase I clinical trial of EUS-guided intratumoral injection of the oncolytic virus, HF10 for unresectable locally advanced pancreatic cancer. *BMC Cancer* **18**, 596 (2018).

71. Bazan-Peregrino, M. *et al.* VCN-01 disrupts pancreatic cancer stroma and exerts antitumor effects. *J Immunother Cancer* **9**, (2021).

72. Hill, C. & Carlisle, R. Expert Opinion on Drug Delivery Achieving systemic delivery of oncolytic viruses Achieving systemic delivery of oncolytic viruses. (2019) doi:10.1080/17425247.2019.1617269.

73. Li, L., Liu, S., Han, D., Tang, B. & Ma, J. Delivery and Biosafety of Oncolytic Virotherapy. *Frontiers in Oncology* vol. 10 Preprint at https://doi.org/10.3389/fonc.2020.00475 (2020).

74. Miller, A. *et al.* Perfusion pressure is a critical determinant of the intratumoral extravasation of oncolytic viruses. *Molecular Therapy* **24**, 306–317 (2016).

75. Garcia-Carbonero, R. *et al.* Phase I, multicenter, open-label study of intravenous VCN-01 oncolytic adenovirus with or without nab-paclitaxel plus gemcitabine in patients with advanced solid tumors. *J Immunother Cancer* **10**, 3255 (2022).

76. Fu, X., Tao, L., Li, M., Fisher, W. E. & Zhang, X. Effective treatment of pancreatic cancer xenografts with a conditionally replicating virus derived from type 2 herpes simplex virus. *Clinical Cancer Research* **12**, 3152–3157 (2006).

77. Chan, W. M. & McFadden, G. Oncolytic poxviruses. *Annu Rev Virol* **1**, 191–214 (2014).

78. Liu, G. *et al.* pathogens Vesicular Stomatitis Virus: From Agricultural Pathogen to Vaccine Vector. (2021) doi:10.3390/pathogens10091092.

79. Fields, B. N. & Hawkins, K. Human Infection with the Virus of Vesicular Stomatitis during an Epizootic. *New England Journal of Medicine* **277**, 989–994 (1967).

80. Rozo-Lopez, P., Drolet, B. S. & Londoño-Renteria, B. Vesicular stomatitis virus transmission: A comparison of incriminated vectors. *Insects* vol. 9 Preprint at https://doi.org/10.3390/insects9040190 (2018).

81. Diaz, R. M. *et al.* Oncolytic immunovirotherapy for melanoma using vesicular stomatitis virus. *Cancer Res* **67**, 2840–2848 (2007).

82. Wu, L. *et al.* rVSV(MΔ51)-M3 is an effective and safe oncolytic virus for cancer therapy. *Hum Gene Ther* **19**, 635–647 (2008).

83. Altomonte, J. *et al.* Exponential enhancement of oncolytic vesicular stomatitis virus potency by vector-mediated suppression of inflammatory responses in vivo. *Molecular Therapy* **16**, 146–153 (2008).

84. Qi, X. *et al.* VEGF-D-enhanced lymph node metastasis of ovarian cancer is reversed by vesicular stomatitis virus matrix protein. *Int J Oncol* **49**, 123–132 (2016).

85. Mahoney, D. J. *et al.* Virus-Tumor Interactome Screen Reveals ER Stress Response Can Reprogram Resistant Cancers for Oncolytic Virus-Triggered Caspase-2 Cell Death. *Cancer Cell* **20**, 443–456 (2011).

86. Fulber, J. P. C. & Kamen, A. A. Development and Scalable Production of Newcastle Disease Virus-Vectored Vaccines for Human and Veterinary Use. *Viruses* vol. 14 Preprint at https://doi.org/10.3390/v14050975 (2022).

87. Choi, K. S. Newcastle disease virus vectored vaccines as bivalent or antigen delivery vaccines. *Clinical and Experimental Vaccine Research* vol. 6 72–82 Preprint at https://doi.org/10.7774/cevr.2017.6.2.72 (2017).

88. Yu, X. *et al.* The glutamic residue at position 402 in the C-terminus of Newcastle disease virus nucleoprotein is critical for the virus. *Sci Rep* **7**, (2017).

89. Ganar, K., Das, M., Sinha, S. & Kumar, S. Newcastle disease virus: Current status and our understanding. *Virus Research* vol. 184 71–81 Preprint at https://doi.org/10.1016/j.virusres.2014.02.016 (2014).

90. Tagesu, T. & Abdisa, T. Review on Newcastle Disease of Poultry and its Public Health Importance. *J Vet Sci Technol* **8**, 441 (2017).

91. Manual of diagnostic tests and vaccines for terrestrial animals 2021 - 6ème èdition. https://www.woah.org/fileadmin/Home/eng/Health_standards/tahm/A_summry.htm.

92. Alexander, D. J. Newcastle disease and other avian paramyxoviruses. *OIE Revue Scientifique et Technique* **19**, 443–462 (2000).

93. Park, M.-S., García-Sastre, A., Cros, J. F., Basler, C. F. & Palese, P. Newcastle Disease Virus V Protein Is a Determinant of Host Range Restriction. *J Virol* **77**, 9522–9532 (2003).

94. Washburn, B. & Schirrmacher, V. Human tumor cell infection by Newcastle Disease Virus leads to upregulation of HLA and cell adhesion

molecules and to induction of interferons, chemokines and finally apoptosis. *Int J Oncol* **21**, 85–93 (2002).

95. Koks, C. A. *et al.* Newcastle disease virotherapy induces long-term survival and tumor-specific immune memory in orthotopic glioma through the induction of immunogenic cell death. *Int J Cancer* **136**, E313–E325 (2015).

96. Salsman, J., Top, D., Boutilier, J. & Duncan, R. Extensive Syncytium Formation Mediated by the Reovirus FAST Proteins Triggers Apoptosis-Induced Membrane Instability. *J Virol* **79**, 8090–8100 (2005).

97. Burman, B., Pesci, G. & Zamarin, D. Newcastle disease virus at the forefront of cancer immunotherapy. *Cancers* vol. 12 1–15 Preprint at https://doi.org/10.3390/cancers12123552 (2020).

98. Lin, D., Shen, Y. & Liang, T. Oncolytic virotherapy: basic principles, recent advances and future directions. *Signal Transduction and Targeted Therapy* vol. 8 1–29 Preprint at https://doi.org/10.1038/s41392-023-01407-6 (2023).

99. Sinkovics, J. G. & Howe, C. D. Superinfection of tumors with viruses. *Experientia* **25**, 733–734 (1969).

100. van den Pol, A. N., Dalton, K. P. & Rose, J. K. Relative Neurotropism of a Recombinant Rhabdovirus Expressing a Green Fluorescent Envelope Glycoprotein. *J Virol* **76**, 1309–1327 (2002).

101. Mire, C. E. *et al.* Recombinant vesicular stomatitis virus vaccine vectors expressing filovirus glycoproteins lack neurovirulence in nonhuman primates. *PLoS Negl Trop Dis* **6**, (2012).

102. Abdullahi, S. *et al.* A Novel Chimeric Oncolytic Virus Vector for Improved Safety and Efficacy as a Platform for the Treatment of

Hepatocellular Carcinoma VIRUS-CELL INTERACTIONS crossm Downloaded from. **92**, 1386–1404 (2018).

103. Kelly, E. J., Nace, R., Barber, G. N. & Russell, S. J. Attenuation of Vesicular Stomatitis Virus Encephalitis through MicroRNA Targeting. *J Virol* **84**, 1550–1562 (2010).

104. Schirrmacher, V. Clinical trials of antitumor vaccination with an autologous tumor cell vaccine modified by virus infection: Improvement of patient survival based on improved antitumor immune memory. in *Cancer Immunology, Immunotherapy* vol. 54 587–598 (Cancer Immunol Immunother, 2005).

105. Freeman, A. I. *et al.* Phase I/II trial of intravenous NDV-HUJ oncolytic virus in recurrent glioblastoma multiforme. *Molecular Therapy* **13**, 221–228 (2006).

106. Susta, L. *et al.* Pathogenicity evaluation of different Newcastle disease virus chimeras in 4-week-old chickens. *Trop Anim Health Prod* **42**, 1785–1795 (2010).

107. Huang, Z., Krishnamurthy, S., Panda, A. & Samal, S. K. Newcastle Disease Virus V Protein Is Associated with Viral Pathogenesis and Functions as an Alpha Interferon Antagonist. *J Virol* **77**, 8676–8685 (2003).

108. Ebert, O. *et al.* Syncytia Induction Enhances the Oncolytic Potential of Vesicular Stomatitis Virus in Virotherapy for Cancer. *Cancer Res* **64**, 3265–3270 (2004).

109. Sergel, T. A., McGinnes, L. W. & Morrison, T. G. A Single Amino Acid Change in the Newcastle Disease Virus Fusion Protein Alters the Requirement for HN Protein in Fusion. *J Virol* **74**, 5101–5107 (2000).

110. Bateman, A. R. *et al.* Viral fusogenic membrane glycoproteins kill solid tumor cells by nonapoptotic mechanisms that promote cross presentation of tumor antigens by dendritic cells. *Cancer Res* **62**, 6566–6578 (2002).

111. de Graaf, J. F., de Vor, L., Fouchier, R. A. M. & van den Hoogen, B. G. Armed oncolytic viruses: A kick-start for anti-tumor immunity. *Cytokine and Growth Factor Reviews* vol. 41 28–39 Preprint at https://doi.org/10.1016/j.cytogfr.2018.03.006 (2018).

112. Marelli, G., Howells, A., Lemoine, N. R. & Wang, Y. Oncolytic viral therapy and the immune system: A double-edged sword against cancer. *Frontiers in Immunology* vol. 9 Preprint at https://doi.org/10.3389/fimmu.2018.00866 (2018).

113. Wojton, J. & Kaur, B. Impact of tumor microenvironment on oncolytic viral therapy. *Cytokine and Growth Factor Reviews* vol. 21 127–134 Preprint at https://doi.org/10.1016/j.cytogfr.2010.02.014 (2010).

114. Gómez-Torres, M. J. *et al.* Sperm Adhesion Molecule 1 (SPAM1) Distribution in Selected Human Sperm by Hyaluronic Acid Test. *Biomedicines* **10**, (2022).

115. Study of Nab-Paclitaxel and Gemcitabine and Plus/Minus VCN-01 in Patients With Metastatic Pancreatic Cancer - Full Text View - ClinicalTrials.gov. https://classic.clinicaltrials.gov/ct2/show/NCT05673811.

116. Cheng, J. *et al.* Human matrix metalloproteinase-8 gene delivery increases the oncolytic activity of a replicating adenovirus. *Molecular Therapy* **15**, 1982–1990 (2007).

117. Samuel, C. S. *Relaxin: Antifibrotic Properties and Effects in Models of Disease*. *Clinical Medicine & Research* vol. 3 http://www.clinmedres.org.

118. Jung, K. H. *et al.* Oncolytic adenovirus expressing relaxin (YDC002) enhances therapeutic efficacy of gemcitabine against pancreatic cancer. *Cancer Lett* **396**, 155–166 (2017).

119. Mekinist | European Medicines Agency. https://www.ema.europa.eu/en/medicines/human/EPAR/mekinist.

120. Eser, S., Schnieke, A., Schneider, G. & Saur, D. Oncogenic KRAS signalling in pancreatic cancer. *Br J Cancer* **111**, 817–822 (2014).

121. Bommareddy, P. K., Aspromonte, S., Zloza, A., Rabkin, S. D. & Kaufman, H. L. MEK inhibition enhances oncolytic virus immunotherapy through increased tumor cell killing and T cell activation. *Sci Transl Med* **10**, (2018).

122. Lee, S. *et al.* Inhibition of MEK-ERK pathway enhances oncolytic vaccinia virus replication in doxorubicin-resistant ovarian cancer. *Mol Ther Oncolytics* **25**, 211–224 (2022).

123. Zhou, X. *et al.* Enhancing Therapeutic Efficacy of Oncolytic Herpes Simplex Virus with MEK Inhibitor Trametinib in Some BRAF or KRAS-Mutated Colorectal or Lung Carcinoma Models. (2021) doi:10.3390/v13091758.

124. Xiang, X. S., Li, P. C., Wang, W. Q. & Liu, L. Histone deacetylases: A novel class of therapeutic targets for pancreatic cancer. *Biochimica et Biophysica Acta - Reviews on Cancer* vol. 1877 188676 Preprint at https://doi.org/10.1016/j.bbcan.2022.188676 (2022).

125. Bolden, J. E., Peart, M. J. & Johnstone, R. W. Anticancer activities of histone deacetylase inhibitors. *Nature Reviews Drug Discovery* vol. 5 769–784 Preprint at https://doi.org/10.1038/nrd2133 (2006).

126. Singh Vijay Patel Deepak K Jain Preeti Patel Harish Rajak, A. K. Panobinostat as Pan-deacetylase Inhibitor for the Treatment of

Pancreatic Cancer: Recent Progress and Future Prospects. (2016) doi:10.1007/s40487-016-0023-1.

127. Farydak | European Medicines Agency. https://www.ema.europa.eu/en/medicines/human/EPAR/farydak.

128. Serial Measurements of Molecular and Architectural Responses to Therapy (SMMART) PRIME Trial - Full Text View - ClinicalTrials.gov. https://classic.clinicaltrials.gov/ct2/show/NCT03878524.

129. Wu, Y. *et al.* Histone Deacetylase Inhibitor Panobinostat Benefits the Therapeutic Efficacy of Oncolytic Herpes Simplex Virus Combined with PD-1/PD-L1 Blocking in Glioma and Squamous Cell Carcinoma Models. *Viruses* **14**, (2022).

130. Pili, R. *et al.* Phase I study of the histone deacetylase inhibitor entinostat in combination with 13-cis retinoic acid in patients with solid tumours. *Br J Cancer* **106**, 77–84 (2012).

131. Bridle, B. W. *et al.* HDAC inhibition suppresses primary immune responses, enhances secondary immune responses, and abrogates autoimmunity during tumor immunotherapy. *Molecular Therapy* **21**, 887–894 (2013).

132. Lien-Anh Nguyê, T. *et al. Chemical Targeting of the Innate Antiviral Response by Histone Deacetylase Inhibitors Renders Refractory Cancers Sensitive to Viral Oncolysis*. www.pnas.org/cgi/content/full/ (2008).

133. Bennett, R. L., Bele, A., Maji, S. & Licht, J. D. Epigenetic therapy. in *Encyclopedia of Cancer* 1–13 (Elsevier, 2018). doi:10.1016/B978-0-12-801238-3.65065-1.

134. EU/3/18/2004 | European Medicines Agency. https://www.ema.europa.eu/en/medicines/human/orphan-designations/eu-3-18-2004.

135. Dhalluin, C. *et al.* Structure and ligand of a histone acetyltransferase bromodomain. *Nature* **399**, 491–496 (1999).

136. Shi, J. & Vakoc, C. R. The Mechanisms behind the Therapeutic Activity of BET Bromodomain Inhibition. *Molecular Cell* vol. 54 728–736 Preprint at https://doi.org/10.1016/j.molcel.2014.05.016 (2014).

137. Delmore, J. E. *et al.* BET bromodomain inhibition as a therapeutic strategy to target c-Myc. *Cell* **146**, 904–917 (2011).

138. Bradbury, R. H. *et al.* Optimization of a Series of Bivalent Triazolopyridazine Based Bromodomain and Extraterminal Inhibitors: The Discovery of (3R)-4-[2-[4-[1-(3-Methoxy-[1,2,4]triazolo[4,3-b]pyridazin-6-yl)-4-piperidyl]phenoxy]ethyl]-1,3-dimethyl-piperazin-2-one (AZD5153). (2016) doi:10.1021/acs.jmedchem.6b00070.

139. Hölscher, A. S., Schulz, W. A., Pinkerneil, M., Niegisch, G. & Hoffmann, M. J. Combined inhibition of BET proteins and class I HDACs synergistically induces apoptosis in urothelial carcinoma cell lines. *Clin Epigenetics* **10**, (2018).

140. Zhang, P. *et al.* BRD4 Inhibitor AZD5153 Suppresses the Proliferation of Colorectal Cancer Cells and Sensitizes the Anticancer Effect of PARP Inhibitor. *Int. J. Biol. Sci* **15**, 1942–1954 (2019).

141. Nicodeme, E. *et al.* Suppression of inflammation by a synthetic histone mimic. *Nature* **468**, 1119–1123 (2010).

142. Miller, A. L. *et al.* The BET inhibitor JQ1 attenuates double-strand break repair and sensitizes models of pancreatic ductal adenocarcinoma to PARP inhibitors. *EBioMedicine* **44**, 419–430 (2019).

143. Hamilton, E. P. *et al.* First-in-Human Study of AZD5153, A Small Molecule Inhibitor of Bromodomain Protein 4, in Patients with

Relapsed/Refractory Malignant Solid Tumors and Lymphoma. *Mol Cancer Ther* **22**, (2023).

144. Vigil, A. *et al.* Use of reverse genetics to enhance the oncolytic properties of newcastle disease virus. *Cancer Res* **67**, 8285–8292 (2007).

145. Yin, M. *et al.* Potent BRD4 inhibitor suppresses cancer cell-macrophage interaction. *Nat Commun* **11**, (2020).

146. Sanjana, N. E., Shalem, O. & Zhang, F. Improved vectors and genome-wide libraries for CRISPR screening. *Nat Methods* **11**, 783 (2014).

147. Hsiau, T. *et al.* Inference of CRISPR Edits from Sanger Trace Data. doi:10.1101/251082.

148. Yushkevich, P. A. *et al.* User-guided 3D active contour segmentation of anatomical structures: Significantly improved efficiency and reliability. *Neuroimage* **31**, 1116–1128 (2006).

149. Feldmann, K. *et al.* Mesenchymal Plasticity Regulated by Prrx1 Drives Aggressive Pancreatic Cancer Biology. *Gastroenterology* **160**, 346-361.e24 (2021).

150. Poch, T. *et al.* Single-cell atlas of hepatic T cells reveals expansion of liver-resident naive-like CD4+ T cells in primary sclerosing cholangitis. *J Hepatol* **75**, 414–423 (2021).

151. Stelma, F. *et al.* Human intrahepatic CD69 + CD8+ T cells have a tissue resident memory T cell phenotype with reduced cytolytic capacity. *Sci Rep* **7**, 1–10 (2017).

152. Ohnesorge, P. V *et al.* Efficacy of Oncolytic Herpes Simplex Virus T-VEC Combined with BET Inhibitors as an Innovative Therapy Approach for NUT Carcinoma. *Cancers (Basel)* **2022**, 2761 (2761).

153. Belkina, A. C. & Denis, G. V. BET domain co-regulators in obesity, inflammation and cancer. *Nature Reviews Cancer* vol. 12 465–477 Preprint at https://doi.org/10.1038/nrc3256 (2012).

154. Wang, Y. H. *et al.* BRD4 promotes pancreatic ductal adenocarcinoma cell proliferation and enhances gemcitabine resistance. *Oncol Rep* **33**, 1699–1706 (2015).

155. Tang, Y. *et al.* Epigenetic targeting of Hedgehog pathway transcriptional output through BET bromodomain inhibition. *Nat Med* **20**, 732–740 (2014).

156. Miao, T. *et al.* Inhibition of Bromodomain Proteins Enhances Oncolytic HAdVC5 Replication and Efficacy in Pancreatic Ductal Adenocarcinoma (PDAC) Models. (2024) doi:10.3390/ijms25021265.

157. Sodir, N. M. *et al.* Endogenous Myc maintains the tumor microenvironment. doi:10.1101/gad.2038411.

158. Yamamoto, K. *et al. Stromal Remodeling by the BET Bromodomain Inhibitor JQ1 Suppresses the Progression of Human Pancreatic Cancer*. www.impactjournals.com/oncotarget/ (2016) doi:10.18632/oncotarget.11129.

159. Soucek, L. *et al.* Modelling Myc inhibition as a cancer therapy. *Nature* **455**, 679–683 (2008).

160. Mazur, P. K. *et al.* Combined inhibition of BET family proteins and histone deacetylases as a potential epigenetics-based therapy for pancreatic ductal adenocarcinoma. *Nat Med* **21**, 1163–1171 (2015).

161. Garcia, P. *et al.* The BET bromodomain inhibitor JQ1 suppresses growth of pancreatic ductal adenocarcinoma in patient-derived xenograft models. *Oncogene* **35**, 833–845 (2016).

162. Kagoya, Y. *et al.* BET bromodomain inhibition enhances T cell persistence and function in adoptive immunotherapy models. *Journal of Clinical Investigation* **126**, 3479–3494 (2016).

163. Öhlund, D. *et al.* Distinct populations of inflammatory fibroblasts and myofibroblasts in pancreatic cancer. *J Exp Med* **214**, 579–596 (2017).

164. Rasheed, Z. A., Matsui, W. & Maitra, A. *Pathology of Pancreatic Stroma in PDAC*. *Pancreatic Cancer and Tumor Microenvironment* (2012).

165. Rizvi, S. & Gores, G. J. The Two Faces of Relaxin in Cancer: Antitumor or Protumor? Exogenous stimulation with RLN promotes an antifibrogenic HSC phenotype by i) reduction of HSC contractility; ii) induction of an antifibrogenic gene expression profile in HSCs; and iii) enhanced intrahepatic NO signaling. 4 Accordingly, in the tumor HHS Public Access. *Hepatology* **71**, 1117–1119 (2020).

166. Thanasupawat, T. *et al.* Emerging roles for the relaxin/RXFP1 system in cancer therapy. *Molecular and Cellular Endocrinology* vol. 487 85–93 Preprint at https://doi.org/10.1016/j.mce.2019.02.001 (2019).

167. Kim, J. H. *et al.* Relaxin expression from tumor-targeting adenoviruses and its intratumoral spread, apoptosis induction, and efficacy. *J Natl Cancer Inst* **98**, 1482–1493 (2006).

VIII. AKNOWLEDGMENTS

I would like to thank PD Dr. rer. Nat. Jennifer Altomonte heartwarmingly for giving me the opportunity to complete this doctoral thesis in her laboratory, part of the Medical Clinic and Policlinic for internal medicine II, at Technical University of Munich's hospital Rechts der Isar. She introduced me to the fascinating world of research and drug pre-clinical testing with much competence and precious guidance. Her natural friendliness, support and availability along the project enabled the realization of this thesis.

I also express my gratitude to Uni.-Prof. Dr. Thomas Göbel for accepting to supervise this thesis for its submission at the Faculty for veterinary medicine of the Ludwig Maximilian's University of Munich. Through his availability, he facilitated a good communication and progress.

I am also grateful to all the members of the Altomonte laboratory, Post-Doctorates and PhD candidates for their assistance during the various phases of this doctoral work, the professional advices and also friendly moments. Our very enjoyable and amicable team made these years, rich in experiences and emotions, an experience I cherish.

My thankfulness also goes to my partner, Fabio Tenebruso. His love, trust, understanding and sense of humour carried me through these years.

Finally, I would like to thank my parents Michèle and Thang Ba Trung, my sister Arya-Marie, and Arès for their unwavering emotional support. They helped me to come this far.